Copyright Warning & Restrictions

The copyright law of the United States (Title 17, United States Code) governs the making of photocopies or other reproductions of copyrighted material.

Under certain conditions specified in the law, libraries and archives are authorized to furnish a photocopy or other reproduction. One of these specified conditions is that the photocopy or reproduction is not to be "used for any purpose other than private study, scholarship, or research." If a, user makes a request for, or later uses, a photocopy or reproduction for purposes in excess of "fair use" that user may be liable for copyright infringement,

This institution reserves the right to refuse to accept a copying order if, in its judgment, fulfillment of the order would involve violation of copyright law.

Please Note: The author retains the copyright while the New Jersey Institute of Technology reserves the right to distribute this thesis or dissertation

Printing note: If you do not wish to print this page, then select "Pages from: first page # to: last page #" on the print dialog screen

ABSTRACT

TRANSPORT MECHANISMS AND MODELING OF RISER REACTOR

by
Dawei Wang

Riser reactors are extensively employed in various industrial applications. In a riser reactor, the hydrodynamics is closely interacted with kinetic reactions. Common models for the performance prediction of riser reactors overlook this vital coupling effect, which not only miss the important reaction characteristics in the dense-phase transport regime of riser reactors but also misinterpret the kinetic properties via ad hoc adjustments. It is noted that the modeling of hydrodynamics in riser flows has major flaws in its predictability of phase transport in both dense-phase and accelerating regimes where most reactions occur. In addition, with the spray feeding of reactants at the bottom of a riser reactor, the catalytic reaction that coherently coupled with vapor-catalyst mixing in the spray vaporization process has never been investigated. Understanding of this reaction in the spray region is important because it provides the inlet conditions of phase transport to the follow-up reactions in the riser reactor. This dissertation hence is aimed at the development of mechanism-based parametric model that yields reliable prediction in transport and reaction characteristics in general catalytic riser reactors.

The dissertation consists of three integrated parts: 1) governing mechanisms and modeling of gas-solids transport in a riser, with special focuses on the solids transport in dense-phase and acceleration regimes; 2) interacting mechanisms between hydrodynamics and catalytic reactions in riser reactors, with special focuses on the modeling of the coupling of hydrodynamics with catalytic reactions and the

determination of reaction properties that are independent of hydrodynamics; 3) modeling of reaction in the spray mixing and vaporization process, with special focuses on the coupling among spray evaporation, vapor-catalyst mixing and catalytic reaction.

On the hydrodynamic model, we have discovered the new control mechanisms that govern the solids acceleration. Most importantly, an additional resistant force, due to inter-solids collision in the acceleration regime, must be added to the momentum equation of solids. The new developed model has successfully predicted the axial profiles of transport properties throughout the entire transport domain, including dense phase, acceleration, and dilute phase regimes. To further explore the flow heterogeneity in both radial and axial directions, an integral-differential hydrodynamics model with a general third-order polynomial across any riser cross-sections has been developed. The model not only predicts the radial and axial phase transport but also yields the much-needed information of the wall boundary layer and backflow mixing for the popular core-annulus models.

On the coupling of hydrodynamics and catalytic reaction, a new correlation has been proposed to link the local reaction rate to the local transport properties (such as concentrations of catalysts and reactants, reaction temperature, and transport velocities). The resulted model not only predicts the correct reaction characteristics against the plant data but also demonstrates the feasibility of adopting the same reaction properties of the same type of catalytic reactions in different riser reactors.

The coupling of hydrodynamics and catalytic reaction has also been extended to investigate the catalytic reaction in the spray region. The resulted changes in transport properties provide the inlet conditions for the follow-up reactions in the riser reactor.

TRANSPORT MECHANISMS AND MODELING OF RISER REACTOR

by
Dawei Wang

A Dissertation
Submitted to the Faculty of
New Jersey Institute of Technology
in Partial Fulfillment of the Requirements for the Degree of
Doctor of Philosophy in Mechanical Engineering

Department of Mechanical and Industrial Engineering

May 2010

APPROVAL PAGE

TRANSPORT MECHANISMS AND MODELING OF RISER REACTOR

Dawei Wang

Dr. Chao Zhu, Dissertation Advisor — Date
Professor of Mechanical Engineering, NJIT

Dr. Ernest Geskin, Committee Member — Date
Professor of Mechanical Engineering, NJIT

Dr. Teh C. Ho, Committee Member — Date
Corporate Strategic Research Laboratories
ExxonMobil Research and Engineering Corporation, Annandale, NJ

Dr. Anthony D. Rosato, Committee Member — Date
Professor of Mechanical Engineering, NJIT

Dr. Pushpendra Singh, Committee Member — Date
Professor of Mechanical Engineering, NJIT

BIOGRAPHICAL SKETCH

Author: Dawei Wang

Degree: Doctor of Philosophy

Date: May 2010

Undergraduate and Graduate Education:

- Doctor of Philosophy in Mechanical Engineering,
  New Jersey Institute of Technology, Newark, NJ, 2010
- Master of Science in Thermal Engineering,
  Huazhong University of Science & Technology, Wuhan, P. R. China, 2003
- Bachelor of Science in Thermal Engineering,
  China University of Petroleum, Dongying, Shandong, P. R. China, 2000

Major: Mechanical Engineering

Presentations and Publications:

Dawei Wang, Jun You, Chao Zhu, Modeling of core flow in a gas-solids riser, *Powder Technology*, 2010, 199 (1), pp 13-22.

Chao Zhu, Dawei Wang, Chao-Hsin Lin, Jet dispersion and deposition of charged particles in confined chambers, *Particuology*, 2010, Volume 8 No. 1, pp 28-36.

Jun You, Dawei Wang, Chao Zhu, Entrance Effects on Gas-Solid Riser Flow Structure, *Industrial & Engineering Chemistry Research*, 2009, 48 (1), pp 310–319.

Jun You, Rajesh Patel, Dawei Wang, Chao Zhu, Role of inter-particle collision on solids acceleration in riser, *Particuology*, Volume 8 No. 1, pp 13-18.

Dawei Wang, Jun You, Chao Zhu, Heterogeneous Flow Structure In Gas-Solid Risers: Continuous Modeling, *AIChE 2008 Annual Meeting in Philadelphia, Pennsylvania*, Nov. 16 -21, 2008.

Dawei Wang, Zheng Shen, Chao Zhu, Phase Transfer In a Droplet-Solid Sphere Collision, *AIChE 2008 Annual Meeting in Philadelphia, Pennsylvania*, Nov. 16 - 21, 2008.

Jun You, Dawei Wang, Chao Zhu, A New Generic Modeling Approach for Gas-Solids Riser Reactor, *AIChE 2008 Annual Meeting in Philadelphia, Pennsylvania*, Nov. 16 -21, 2008.

Jun You, Dawei Wang, Chao Zhu, L. S. Fan, Modeling on Heterogeneous Structure in Acceleration Regime of Gas-Solid Riser Flows, *Proceedings of Fluidization XII*, May 13-18, 2007, Harrison, British Columbia, Canada.

This dissertation is dedicated to my wife, Fei and my son, Kevin.

ACKNOWLEDGMENT

I would like to express my deepest appreciation to Dr. Chao Zhu, who gave me guidance, supervision and research intuition, but also is a sincere friend providing experience, support, encouragement, and reassurance throughout my life during my study at New Jersey Institute of Technology. I would also like to acknowledge Dr. Teh C. Ho, Dr. Ernest Geskin, Dr. Pushpendra Singh and Dr. Anthony D. Rosato for their active participation on my dissertation committee.

I would like to acknowledge the Teaching Assistantships from the Department of Mechanical Engineering of New Jersey Institute of Technology, ExxonMobil Research and Development Corporation, Boeing Commercial Airplanes and Petroleum Research Fund for their support. The friendship and cooperation of Dr. Muhammad M. R. Qureshi, Dr. Jun You, Mr. Rajesh Patel, Ms. Zheng Shen, Mr. Raviat, Mr. Pengfei He and Mr. Jiayi Tong in the Particulate Multiphase Flow Laboratory also deserve my special recognition.

I would like to express my endless gratitude to my parents and other family members, who have always supported my academic pursuits and helped me in every possible way. Last, I want to thank my lovely wife, Fei Yang, and my adorable son, Kevin Wang, for their love and encouragement throughout these years.

TABLE OF CONTENTS

Chapter	Page
1 INTRODUCTION	1
1.1 Background	1
1.2 Literature Survey	6
1.2.1 Mechanisms of Gas-Solids Flow	6
1.2.2 Reaction Mechanisms of Riser Reactor	11
1.2.3 Spray Characteristics of Feed Reactant	15
1.3 Dissertation Structure, Objectives and Approaches	18
2 TRASNSPORT MECHANISMS OF GAS-SOLIDS RISER FLOW	22
2.1 General Governing Equations	23
2.2 Gas-Solids Interactions	25
2.2.1 Force due to Pressure Gradient	25
2.2.2 Frictional Drag Force	26
2.3 Inter-Particle Collision	29
2.3.1 Role on Energy Dissipation	29
2.3.2 Role in Momentum Equation	32
2.3.3 Formulation of Collision Force	34
2.4 Results and Discussion	36
2.5 Conclusion	46
3 FLOW HETEROGENITY IN BOTH RADIAL AND AXIAL DIRECTIONS	47
3.1 General Modeling Methodology	48

TABLE OF CONTENTS
(Continued)

Chapter	Page
3.2 Continuous Modeling of Hydrodynamics	51
3.3 Results and Discussion	57
3.4 Conclusion	67
4 HYDRODYNAMICS AND REACTION COUPLING OF RISER REACTOR	68
4.1 Chemical Reaction Scheme in Riser Reactor	70
4.1.1 Single-Phase (Gas) Flow Model	71
4.1.2 Two-phase flow (Riser Flow) Model	73
4.2 Equations of Hydrodynamics	77
4.3 Input Conditions	83
4.4 Model Validation and Comparisons	84
4.5 Conclusion	96
5 EVAPORATION AND REACTION OF SPRAY FEED REACTANT	98
5.1 Governing Equations	99
5.1.1 Hydrodynamic Equations	100
5.1.2 Reaction Equations	106
5.2 Intrinsic Correlations	107
5.3 Problem Closure	111
5.4 Results and Discussion	112
5.5 Conclusion	118
6 SUMMARY AND PROPOSED STUDY	119

TABLE OF CONTENTS
(Continued)

Chapter **Page**

6.1 Summary 119

6.2 Suggested future study 122

REFERENCES 124

LIST OF TABLES

Table		Page
2.1	Experimental Parameters for Model Validation	36
3.1	Major Experimental Parameters	57
4.1	Operation Parameters and FCC Properties of Riser Reactors	84
4.2	Pre-exponential Factor, Activation Energy, and Reaction Heat	85
5.1	Major Input Parameters	113

LIST OF FIGURES

Figure		Page
1.1	Riser reactor in the whole cat cracker system	2
1.2	Typical flow structure in Riser Reactor	4
1.3	Typical conversion and yield pattern of FCC riser	5
2.1	Control volume of a gas-solids riser flow	23
2.2	Comparison of Richardson-Zaki Equation and experimental results	27
2.3	Drag force vs relative velocity in various riser regimes...	28
2.4	Energy portions of solids hold up, dissipation and solids acceleration	30
2.5	Partitions of solids hold up, collision force and solids acceleration along riser	34
2.6	Comparison of model predictions and experimental results of axial profile of solid volume fraction (Arena et al., 1985)	37
2.7	Comparison of model predictions and experimental results of axial pressure gradient profile (Pugsley and Berruti, 1996)	40
2.8	Effect of Gas Velocity on flow pattern (G_s= 382 kg/m^2.s)	42
2.9	Effect of Solid mass flux variation on flow pattern (U_g = 7 m/s)	45
3.1	Heterogeneous flow Structure in a gas-solids riser	49
3.2	Solids volume fraction distribution of glass beads (Arena et al., 1985)	58
3.3	Pressure drop in the riser for sand (Pugsley and Beruti, 1996) ...	59
3.4	Radial solids velocity distribution (Yang et al., 1992)	60
3.5	Radial Profile of dimensionless solids volume fraction (Herb et al., 1989)	61
3.6	Solids volume fractions at different height of riser	62
3.7	Dimensionless solids volume fractions at different height of riser	63

LIST OF FIGURES
(Continued)

Figure		Page
3.8	Radial profile of solids velocity at different height of riser	64
3.9	Radial profile of gas velocity at different height of riser	64
3.10	Dimensionless upwards flow boundary and area along the riser	65
3.11	Back-mixing ratio of solids along the riser	66
4.1	Four-lump model for gas oil cracking reactions (Lee et al., 1989)	71
4.2	Flow Structure in a gas-solids riser	79
4.3	Computational domain of core-flow model	80
4.4	Comparisons of models predictions with FCC plat data	87
4.5	Model predictions of phase velocity	88
4.6	Model prediction of riser temperature	89
4.7	Model prediction of riser pressure	90
4.8	Model prediction of lump molar concentration	91
4.9	Parametrical study of power index "n"	92
4.10	Parametric study of catalyst to oil ratio	93
4.11	Parametric study of inlet temperature	94
4.12	Comparison of gasoline selectivity between two-phase and single-phase flow models at riser exit	95
5.1	Schematic diagram of spray jet into gas-solids riser flow	100
5.2	Schematic diagram of control volume	101
5.3	Spray jet trajectory in fluidized bed	114

LIST OF FIGURES
(Continued)

Figure		Page
5.4	Temperatures of phases in spray region	115
5.5	Velocity profiles in spray region	116
5.6	Volume fractions of phases in spray region	117
5.7	Mass concentrations of components of gas phase in spray region	118

LIST OF SYMBOLS

A	area (m^2)
a_D	Acceleration partition of drag force
c_D	Collision partition of drag force
C	molar concentration of lump (mol/m^3)
c_p	specific heat (J/kg K)
D	riser diameter (m)
E_{ai}	activation energy of i^{th} conversion (kJ/mol)
F_D	Modified drag force of solids phase (N/m^3)
F_{Do}	Drag force of Richard-Zaki Equation (N/m^3)
F_c	Collision force (N/m^3)
g	gravitational acceleration (m/s^2)
G	mass flux rate (kg/m^2 s)
G_D	Gravity partition of drag force
G_s	Solids mass flux (kg/m^2.s)
k_1	Coefficient for wake effect
K_2	Coefficient for collision force
K_3	Coefficient for collision force
k_i	rate constant of i^{th} conversion (s^{-1})
l_w	Circumferential length of riser (m)
M	molecular weight (kg/mol)
P	Pressure (Pa)

LIST OF SYMBOLS
(Continued)

R	universal gas constant (J/mol K)
r_{ij}	mass rate change (Kg/m^3 s)
T	temperature (K)
u_g	gas velocity (m/s)
u_s	solids velocity (m/s)
u_{pt}	Particle terminal seting velocity (m/s)
y_i	weight fraction of i^{th} lump
z	riser Height (m)
α_g	Gas volume fraction
α_s	Solid volume fraction
α_{sc}	Critical solid volume fraction for acceleration
Γ	Energy dissipation of gas-solids flow
Γ_ϕ	Energy dissipation due to inter-phase drag force
Γ_χ	Energy dissipation due to inter-particle collisions
ρ_d	Droplet density (kg/m^3)
ρ_g	Gas density (kg/m^3)
ρ_s	Particle density (kg/m^3)
$\tau_{\sigma\omega}$	Wall shear stress of particle (N/m^2)
ΔH_i	heat of reaction from i^{th} component (J/kg)

CHAPTER 1

INTRODUCTION AND LITERATURE SURVEY

1.1 Background

Riser Reactors are widely adopted in various important industries, such as polymerization, coal combustion and petroleum refinery system. In these applications, the riser reactors normally play a key role on the production of the system. Such as in the fluid catalytic cracking (FCC) system which is schematically described in Figure 1.1, the riser reactor is the heart part of the unit with most products produced in it. Although the usages for these applications are completely different, the dominating mechanisms inside riser reactors are the same. Such as, the riser flows are gas-solids two-phase flows with the flow structures determined by gas-solids inter-phase interaction and particle-particle collision. The processes inside riser reactors normally involve in complicated chemical reactions. The intensities of these chemical reactions normally are closed coupled with local hydrodynamic conditions. In a lot of applications, the reactants are injected into the bottom of the riser in the form of gas-droplet spray. There, the reactants encounter intensive mass, momentum and heat transfer from environmental gas-solids flow and are evaporated. In the spray region, the vapor phase normally has intensive chemical reactions. Thus, although the application background in the following description of our research topics and modeling approaches is fluid catalytic cracking process, the modeling methodology is a generic approach and can be applied to most applications involving gas-solids riser reactor.

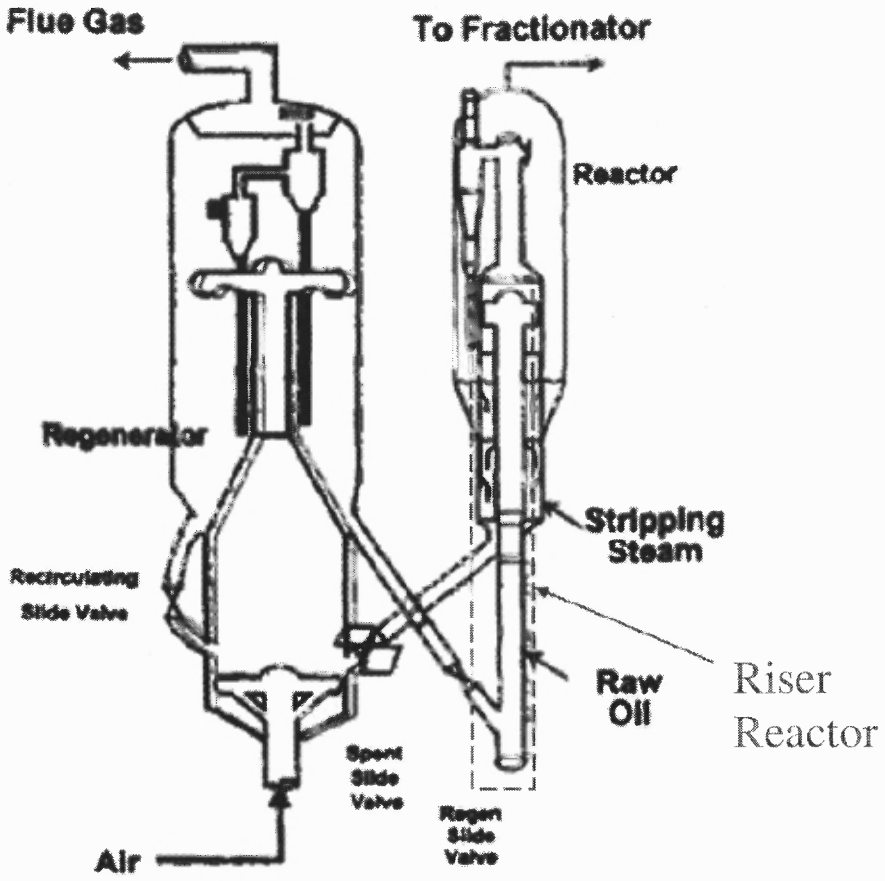

Figure 1.1 Riser reactor in the whole cat cracker system.
Source: Reza Sadeghbeigi, Fluid Catalytic Cracking Handbook, 2nd ed. (Gulf Publishing Company, Houston, Texas, 2000) pp 3.

Fluid catalytic cracking (FCC) process, with riser reactor-regenerator as its heart facilities, continues to play a key role in the conversion of crude oil, which use integrated refinery as its primary conversion process. In year of 2006, there are 400 petroleum refineries worldwide using FCC units. About one-third of the crude oil in these facilities is processed into high-octane gasoline and fuel oils. During 2007, the FCC units in the United States give a product amount of 5,300,000 barrels per day of feedstock, and worldwide the amount is about twice (Speight, 2006). Although there are several differences of mechanical configuration for different FCC units provided by different

operator, the common objective of FCC unit is to upgrade low-value feedstock to more valuable products. For many refiners, the key to make profit from crude oil refinery is the cat cracker whose successful operation determines the competitiveness of the company in today's market.

The feed of crude oil which is normally preheated to a temperature of 260°c to 370°c enters the riser near the bottom where it contacts the regenerated catalyst with a temperature ranging between 677°c to 732°c and evaporates into vapor phase with the thermal energy provided by hot catalytic particles. The catalytic reactions occur as well as the vapor phase occurs. The expanding volume of the vapor that is generated is the main driving force to carry the catalyst up the riser.

Efficient contacting of the feed and catalyst is critical for achieving the desired cracking reactions. Steam is commonly used to atomize the feed. Smaller oil droplets increase the availability of feed at the reactive acid sites on the catalyst. With high-activity catalyst, all the cracking reactions take place in as fast as three seconds or less. Risers are normally designed for an outlet vapor velocity of 15-23 m/s. The average hydrocarbon residence time is about two seconds. As a consequence of the cracking reactions, a hydrogen-deficient material called coke is deposited on the catalyst, reducing catalyst activity (Reza Sadeghbeigi, 2002). Figure 1.2 briefly describes the flow structure of a riser reactor.

Efforts are continuously made to improve the process in order to increase the productivity of the refinery industry and also to reduce pollutant emissions to the environment. During the course of the improvement of the process, cracking reaction time

in the FCC unit has become much shorter and hence, flow hydrodynamic effects on cracking processes have a greater impact on product yields. These effects make the

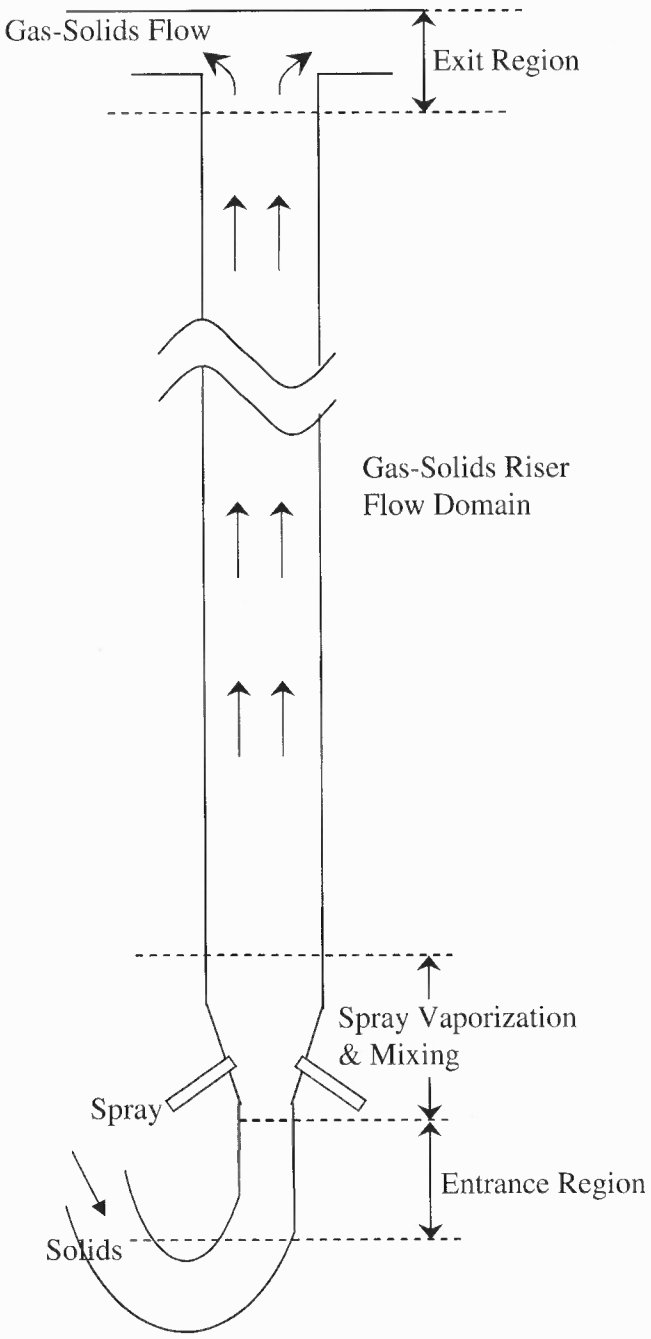

Figure 1.2 Typical flow structure in riser reactor.

understanding of the performance of the riser reactor much more difficult. As shown in Figure 1.3, although tremendous efforts have already been done on the simulating of the riser reactor performance, there is still a very large distance before correctly predicting the conversion trend of crude oil along the riser direction.

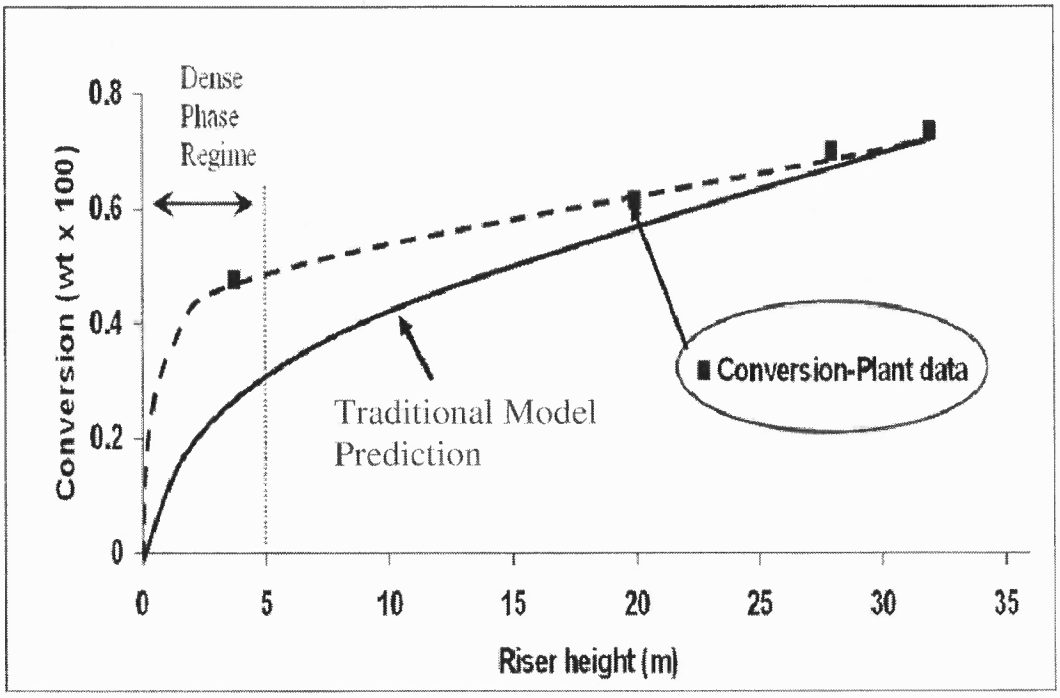

Figure 1.3 Typical conversion & yield pattern of FCC riser.
* Plant data from Derouin et al, 1997.

In the riser reactor, the hydrodynamics are normally closely coupled with chemical reactions. The traditional way to predict the performance of the riser reactor overlooked the importance of the coupling effect of the hydrodynamics and the chemical reactions. The performance of the riser reactor shall also be impacted by the inlet conditions which are normally determined by the spray characteristics. To better understand the performance of the riser reactors, the information and mechanism of the

following three aspects shall be obtained, 1) mechanisms for solids transport in riser; 2) chemical reaction scheme inside the riser reactor; 3) spray evaporation and reaction characteristics in spray region.

1.2 Literature Survey

1.2.1 Mechanisms of Gas-Solids Riser Flow

It is well known that the phase transport properties such as solids holdup and solids velocity are non-uniformly distributed along a riser, typically with a dense-phase transport in the lower part of the riser and lean-phase transport in the upper part of the riser (Li and Kwauk, 1980). The non-uniformity in axial phase distributions depends strongly on the operation conditions including the overall transport mass flux of solids and superficial gas velocity. From the point of view of energy balance, the solids acceleration and energy dissipations consume some portion of the pressure drop in the riser flow. Hence, strictly speaking, the traditional approach of equating the local solids holdup to the pressure drop in a riser will lead to an overestimation of local solids holdup. This overestimation can be quite large in the acceleration and dense phase transport regions where the effect of solids acceleration and the effect of energy dissipations due to interfacial friction between gas and solids phases and inter-particle collisions are expected to be significant. The following is a brief review of related modeling efforts and remaining challenges.

The actual flow structure of gas and solids in a riser flow is very complex, with multidimensional variations in axial, radial and even azimuthal directions (such as near a bend or asymmetric gas-solids feeder inlet); multidirectional flows in core, annulus and

wall regions; multi-scaled phase interactions (such as interactions among dispersed solids, clusters, turbulent eddies and pipe wall surfaces in different flow regimes); and other complications from solids cohesion and electrostatic charges. A simple mechanistic model of such a complicated system inevitably requires many assumptions for simplification. In order to evaluate the effects of solids acceleration and energy dissipations on the pressure drop in a riser flow, the simplest and most convenient analysis approach is based on cross-section averaged axial flow models.

Cross-sectional averaged solids holdup in a riser flow can be roughly estimated from pressure drop measurements by equating the gravitational force from local solids holdup to the local axial gradient of pressure with or without modifications of gas-solid flow frictions on pipe walls (Geldart and Rhodes, 1986; Bader et al. 1988; Rautiainen et al. 1999). Due to the neglect of effects of solids acceleration and phase friction, the converted volumetric solids holdup is conceptually different from the actual solids holdup and hence termed as apparent solids fraction or apparent solids concentration (Sun et al. 1999; Schlichthaerle and Werther, 1999).

While the above method of solids holdup estimation works reasonably well for gas-solid flows in the dilute transport regime, many studies suggest that the effect of solids acceleration should not be omitted in the estimation of solids holdup from the pressure drop measurements in the solids acceleration region (Weinstein and Li, 1989; Pugsley and Berruti, 1996; Sabbaghan et al. 2004). In most of these models, the modeling of solids acceleration is based on the drag forces on individual particles or clusters in fluids with semi-empirical correlations of the effective drag coefficients. The Richardson-Zaki equation is used as a basis for the drag force modification in gas-solids fluidization.

It is noted, however, that the Richardson-Zaki equation may not be adequate to describe the hydrodynamic forces on particle with net transport mass flux in the riser flows because the solids holdup is expected to be a function of both the gas and solids velocities rather than the gas velocity alone (He and Rudolph, 1996).

In the dense phase transport region, the experimental measurements based on γ-ray absorption or electric capacitance tomography shows that, while the detailed solids holdup distribution is very complex with a core-annulus-wall structure, the cross-sectional averaged solids volume concentration only varies slightly or virtually remains the same along the riser (Schlichthaerle and Werther, 1999; Du et al. 2004). The pressure drop measurements in the dense phase transport region however yield apparent solids concentrations much higher than the actual solids concentrations. These measurements strongly show that the solids acceleration is very much damped and significant energy dissipations occur in the dense phase transport region, possibly due to the strong particle collisions and inter-phase frictions.

Modeling efforts to interpret the effect of inter-particle collisions on the solids flow distributions are mostly based on the kinetic theory of granular flows and two-fluid model with apparent viscosity in solids phase (Louge et al. 1991; Miller and Gidaspow, 1992; Büssing and Reh, 2001). The application of the kinetic theory modeling approach to the gas-solid riser flows, however, has many inherent limitations due to its basic assumptions of center-to-center particle collisions in vacuum. The energy dissipation module in the kinetic theory modeling only depends on the restitution coefficient, a non-material property whose prediction in an arbitrary center-to-center collision of a pair of solid particles is still a mystery. In a fluidization, the dominant module of inter-particle

collisions is off-center or oblique collision where the energy dissipation not only depends on the loss from normal-component of collision (restitution coefficient) but also depends on the loss due to sliding and micro-slip friction in tangential and rolling contacts (Fan and Zhu, 1998). This inadequate description of collision-induced energy dissipation in kinetic theory modeling can also be reflected in the poor predictions of pressure drops in the dense phase transport region and the large uncertainties in the selections of restitution coefficients for the modeling of gas-solids fluidization.

The kinetic energy dissipation into heat is due to a combined effect of interfacial friction between interstitial gas and suspended solids, inter-solid collisions and solids wall friction. A preliminary analysis on detailed energy distributions shows that the portion of inter-solid collisions is quite significant in the acceleration and dense phase transport regions (Zhu and You, 2007).

It is realized that the conservation equation of kinetic energy is an integrated form of the corresponding momentum equation. Therefore, any non-zero terms in the energy equation have their corresponding terms in the momentum equation. The discovery of the significant energy dissipation by inter-particle collisions clearly indicates the existence of an axial force in the solids momentum equation (Zhu and You, 2007), whose function is to limit the degree of acceleration of a solid particle in a swamp of fluidized particles. It should be pointed out that this significant energy dissipation by collision may not be sufficiently explained by the existing kinetic theory of granular flow whose theoretical basis is on center-to-center and near-elastic collisions (Miller and Gidaspow, 1992). The restitution coefficient of solids, used in the theory to account for the kinetic energy loss by normal impaction, is typically only a few percentages, a value too low to reflect the

actual loss. In a dense phase fluidized state of solids, most inter-particle collisions are off-center or oblique, and the energy dissipation not only depends on the loss of normal component collision but also depends on the loss due to sliding and micro-slip friction in tangential and rolling contacts. Both the increase in transport velocity solids and the decrease in solids concentration along the riser are likely to make the bulk characteristics of collision stress unbalanced along the riser, which may provide a mechanistic explanation of the originality of this collision force in the axial direction.

Although Zhu and You (2007) pointed out the existence of collision force that was deduced from kinetic energy conservation of riser flow, their analysis had to rely on the experimental measurements of axial distribution of pressure as an input in the energy equation. Consequently the proposed approach is unable to independently to predict axial distributions of both pressure and solids concentration.

It is also noticed that, due to the radial heterogeneous structure, the one-dimensional approach may not be adequate to describe the hydrodynamics of gas-solids riser flow. The hydrodynamic characteristics of core and annulus (wall) areas are so different that it is not suitable to combine these two regions into a uniform region as the solids volume fraction in the wall region may be quit high and be equal to that at the minimum fluidization condition of the bed (zhou et al., 1994), and the flow direction of solids is downwards instead of upwards. Some researches on heterogeneous flow structure predefined the cross-section of the riser into two zones, say core-annulus (wall) flow structure (Bolton and Davidson, (1988); Rhodes and Geldart, (1987); Horio et al, (1988); Senior and Brereton, (1992)), which typically consider a dilute uniform core flow, and a dense wall flow along the riser. A 3-zone model is recently presented to

simulate the heterogeneous structure of the riser flow (Zhu et al. (2007)). The model yields a reasonable explanation not only for "core-annulus (wall)" flow structure but also the "core-annulus-wall" flow structure in riser flows. While, these models artificially divide the riser into 2 or 3 different zones and uses averaged values to describe the characteristics of the flow in each zone, thus it can not reveal the intrinsic mechanism and relationship of solids mass transport of each place. To make the problem to be closed, the models have to use pre-defined mass and momentum transfer relationships between zones. The detailed mechanism of hydrodynamic evolution from upwards flow in the center to the downwards flow near the wall is not investigated.

Although there are some efforts on investigation of radial solids concentration distributions (Schlichhaerle, Werther, (1999); Harris et al (2002)), the effects of this non-uniform distribution on radial mass and momentum transfer, upwards flow area, back-mixing ratio of solids phase, and thus the performance of riser are not investigated.

1.2.2 Reaction Mechanisms of Riser Reactor

Fluid catalytic cracking (FCC) is the primary conversion process in the petroleum refinery industry. A FCC riser reactor is designed to use acidic catalysts to decompose heavy oil, such as vacuum gas oil, into more valuable lighter hydrocarbons. The hydrocarbon feed enters into the riser reactor through feed atomizing nozzles and comes in contact with the hot catalysts coming from the regenerator which leads to vaporization of gas oil. The vaporized gas oil feed cracks down to the lighter molecules, as it travels upwards along with the catalysts against gravity in the riser. As a result of vaporization and cracking, the vapor expands and leading to gradually increase in velocities of both vapor and catalysts along the riser. The increase in catalyst velocity causes a decrease in

volumetric fraction of catalysts and hence, a decrease in catalyst-to-oil (CTO) ratio. In the meantime, coke, a key byproduct of cracking reactions, gets deposited on the catalyst surface, which causes the catalyst to loose its activity on cracking. The cracked hydrocarbons vapor is separated from the deactivated catalyst in a separator, after exiting from the riser reactor.

Efforts have been made to improve the process productivity since the invention of the FCC process over a half century ago. However, from the modeling point of view, a mechanistic understanding of FCC process in a riser reactor is far from complete. There are multiple challenges to overcome, including the complicity of catalytic cracking reactions which involves various simultaneous reactions of multi-component feed, the dynamic heterogeneity in vapor-catalyst transport in risers, and the inherent coupling of cracking reactions and hydrodynamics.

Most of the previous FCC modeling have employed oil vapor in a few lumps of various products (e.g., four-lump, ten-lump, fourteen-lump, *etc.*). Weekman & Nace (1970) proposed a three-lump cracking model to study the gasoline production in a FCC unit. The three lumps referred to gas oil, gasoline, and a combined group of light gases and coke. The three lumps was later on modified by Yen *et al.* (1987), proposing a more sound approach with four lumps, where coke and light gases were considered as separate lumps. Considering different feed properties in addition to boiling point range, Jacob *et al.* (1976) developed a more detailed ten-lump kinetic model. Liguras & Allen (1989a; 1989b) proposed a lumped kinetic model to utilize the pure components cracking data for the catalytic cracking of oil mixtures, and subsequently divided the petroleum feedstock into a number of pseudo-components. Pitault *et al.* (1994) proposed a kinetic model,

which is based on a molecular approach and experiments with a small fixed bed reactor (micro activity test). Even though the FCC process in a riser has been intensively investigated over the last few decades, most of the models are based on de-coupled isothermal plug flow hydrodynamics and the reaction model whose reaction rates are only related to the overall CTO of the entire riser.

Recent studies (e.g., Han & Chung, 2001; Subramanya *et al.*, 2005; Gupta *et al.*, 2007) show a growing interest on coupling the multiphase flow hydrodynamics into the FCC reaction process. However, on one hand, the complicated flow structure and hydrodynamics of gas-solid riser flow has not been fully described. Most important physical mechanisms including the inter-particle collision forces, gas/solid interfacial forces and wall boundary effects, which are among the most important aspects of the flow hydrodynamics, have not been properly addressed in those works. On the other hand, the interaction between the flow hydrodynamics and reaction kinetics has not been completely investigated, since in above literatures, only one way coupling has been presented in which only the influence from cracking reaction on flow hydrodynamics has been considered. The influence of flow hydrodynamics on cracking reaction, however, has not been coupled into the modeling. In our previous research, the modeling on flow hydrodynamics of gas-solid riser flow without reaction has been significantly improved, especially for the characterization of accelerating solids in the accelerating or solids diluting regime (You *et al.*, 2008; You *et al.*, 2009a; 2009b). With the inclusion of the proposed correlation of collision force in the solids momentum equation, our hydrodynamic model was able to produce reasonable phase distributions of gas-solid

flows, which has laid a solid basis for further exploring the inter-coupling between the flow hydrodynamics and reaction kinetics.

With the rapid advancement of computational fluid dynamics (CFD) techniques and computing capacity, a full-scale numerical simulation of gas–solid riser flows becomes possible to understand the FCC process. Most of the reported studies are based on the multi-fluid continuum modeling approach (Eulerian–Eulerian models), where the carrying gas and dispersed solid particles are treated as interpenetrating continuum (e.g., Theologos & Markatos, 1999; Das *et al.*, 2004). The kinetic theory of granular flows is introduced to account for inter-particle collisions (e.g., Mathesian *et al.*, 2000; Neri & Gidaspow, 2000; Van Wachem *et al.*, 2001). However, these models may inadequately simulate the complex gas–solid flows at high solids flux (Ranade, 2002). Eulerian–Lagrangian approach is another common modeling method of gas-solid flows, in which the dynamic motions of all particles are tracked by solving Lagrangian equation of motion for each group of particles in the system with a prescribed set of initial conditions (e.g., Zhao *et al.*, 2007). This method may offer a convenient way to simulate complex processes that require historic information of particle dynamics or chemical reactions. However, this approach faces difficulties in handling inter-particle collisions and other interactions in dense phase transport of solids, in addition to a significantly increased requirement on computational resources. Due to the limitations in computing capacity any full-scale CFD simulations are inconvenient to a quick and reliable parametric study that is commonly required in practical designs and operations

In summary, for a quick and reliable parametric evaluation, there is a need of developing a generic mechanistic model for FCC processes in riser reactors. Such an

approach requires not only the predictability of non-uniform characteristics of hydrodynamics and reactions along the riser but also the reasonable description of mechanistic coupling of multiphase flow hydrodynamics and the cracking kinetics. The aim of this paper is thus focused on developing a modeling framework to simultaneously simulate the multiphase flow hydrodynamics, cracking reaction, and the coupling characteristics in FCC riser reactors. In order to avoid the mathematical complexities, a simplified four-lump kinetic scheme is adopted into our model.

1.2.3 Spray Characteristics of Feed Reactant

Many important industrial applications, such as gas-phase polymerization reactions, the aniline synthesis, the production of polyethylene in the super-condensed mode, fluid catalytic cracking and fluid coking operations, involve gas-liquid spray jet into fluidized beds of fine particles. The sprays of gas-droplet are injected into fluidized bed with a relatively high momentum and interact with the gas and particles entrained from the environmental fluidized bed. The momentum of gas phase from the nozzle was dissipated by the mixing with the entrained gas and accelerating the entrained dry solids particles. The droplets which have high velocity collide with the entrained particles and take place intensive momentum and energy transfers which lead to the intensive evaporation of droplet into vapor phase. The collision efficiency between droplets and solids is directly related to the local velocities, sizes, volume fractions of both droplet and solids phases. The chemical reactions take place as long as the vapor phase occurs. The intensity of the chemical reaction highly depends on the local hydrodynamics in the spray jet region, which include the temperatures, velocities and volume fractions of gas, solids and droplet phases as well as the chemical reaction characteristics of the reactants and catalyst.

Extensive researches are made on the characteristics of gas jets into fluidized beds. A lot of correlations have been developed to predict the penetration lengths of gas jets, both in sub-sonic and sonic regimes, into gas-solids fluidized beds (Merry, 1971; Yates et al., 1988; Benjelloun et al., 1995; Hong et al, 1997). The effects of multiple key operating parameters, such as jet velocity, nozzle diameter, particle size and density, solids volume fraction of the fluidized bed are extensively conducted (Merry, 1975; Roach, 1993; Vaccaro et al., 1997; Musmarra, 2000; Matthew Dawe, 2008). The Expansion angles of gas jets in fluidized beds have also been investigated widely (hinze, 1975; Filla et al., 1983; Cleaver et al., 1995; Vaccaro, 1997).

Compared to the injection of reactants in gaseous form, the gas-liquid spray injection is used more widely as it provides many advantages such as high density to allow smaller nozzle and to save storage costs, latent heat of evaporation to avoid hot-spot near the feed nozzle, high momentum allowing deeper penetration to the center of fluidized bed. Many fluidized-bed reactors are operated at higher temperatures where the injected spray jets are heated and evaporated very soon after injected into reactors. Evaporating gas-liquid jets into fluidized beds are obtained wide interesting by the researchers. Liquid nitrogen is normally used as a test liquid in experimental studies for its rapidly evaporating characteristics. It is confirmed by different research groups (Gu et al, 1996;Maronga, 1997;skouby, 1999; Newton, 2001) that there exist an evaporation zone within the riser but there is no instantaneous evaporation at the nozzle exit which was often assumed in the early stages of modeling efforts on the liquid injection into fluidized bed reactors. Modeling approaches are also conducted to predict evaporation rates, jetting length, boundaries and other parameters of evaporative gas-liquid spray jet

into fluidized bed with various operational conditions (Fan, 2001; Zhu, 2000).

As for those fluidized bed where the mean temperature is near or below the boiling point of the injected liquid, the spray entrains solids into the jet from surrounding fluidized bed and the droplets collide with entrained solids to form a liquid layer on the particles' surface from where the liquid is evaporated and dried (Heinrich, 1999; Becher, 1997). A spraying zone near the nozzle exit was observed with the aid of X-ray imaging and Thermocouple matrix (Smith, 1982, Maronga, 1997).

Ariyapadi et al systematically investigate the horizontal gas-liquid spray jets into incipient gas-solids fluidized beds using X-ray imaging and thermocouples (Ariyapadi et al, 2003a; 2003b; 2004.). The results indicate that the jet expansion (half-angle) is considerably reduced for a gas-liquid jet (5-7 degrees) when compared to that of a gas jet (10-15 degrees). The gas-liquid jet also appears to penetrate more than a gas jet with the same momentum. The solids entrainment rate of the spray jet was also measured with the aid of a so-called "draft tube" (Felli, V., 2002; Ariyapadi et al, 2005;). They proposed a correlation of jet penetration length with the effect of nozzle size, Air-to-Liquid Ratio (ALR), bed conditions, nozzle conditions and a dimensionless coefficient called "Geometry Effect" which can only be determined by experimental studies for each of given nozzle geometry (Ariyapadi et al, 2004).

Compared with the relatively abundant researches on the hydrodynamics of spray jet into gas-solids flow, the chemical reaction characteristics in this region have not attracted much attention, although the chemical reaction of reactant in this region shall be very important and be closely coupled with the hydrodynamics.

1.3 Dissertation Objectives, Structure and Approaches

In summary, existing models for the performance prediction of riser reactors overlooked the vital coupling effect of the kinetic reactions and the hydrodynamics. The modeling approaches not only missed the important reaction characteristics in the dense-phase transport regime of riser reactors but also misinterpreted the kinetic properties via ad hoc adjustments. It is noted that the existing models of hydrodynamics in riser flows have major flaws in their predictability of phase transport in both dense-phase and accelerating regimes where most reactions occur. In addition, the mechanisms of the catalytic reaction that coherently coupled with vapor-catalyst mixing in the spray vaporization process have never been investigated when the reactants are sprayed into the bottom of a riser reactor. It is important to understand the mechanisms of this reaction as it provides the inlet conditions of phase transport to the follow-up reactions in the riser reactor. The aims of this dissertation are set to developing mechanism-based parametric models that yield reliable predictions in transport and reaction characteristics in general catalytic riser reactors.

The dissertation is composed of three parts: 1) governing mechanisms and modeling of gas-solids transport in riser reactors, which is specially focused on the solids transport in dense-phase and acceleration regimes; 2) interacting mechanisms between hydrodynamics and catalytic reactions in riser reactors, with special focuses on the coupling mechanisms of hydrodynamics and catalytic reactions, and the determination of reaction properties that are independent of hydrodynamics; 3) modeling of reaction in the spray mixing and vaporization process, with special focuses on the coupling among spray evaporation, vapor-catalyst mixing and catalytic reaction.

Specifically, on hydrodynamic part, the traditional approach of equating the local solids holdup to the axial pressure drop overlooked the role of particle-particle collision on the solids acceleration, thus failed in predicting the phase transport in dense phase and acceleration regimes of the riser. Jun You (2008) is the first researcher who introduces this mechanism on radial transport predictions of the riser. While, due to the lack of the detailed mechanisms of particle-particle collision, the impact of the collision on solids acceleration had to rely on the experimental measurements of axial pressure gradient. In the model, the pressure gradient has to be provided as an input. Consequently, his approach is unable to independently predict both pressure gradient and solids transport simultaneously. A better formulation of this impact, which is based on the mechanism of particle-particle collision, is much needed. Besides, the Richard-Zaki equation, which is popularly adopted for the formulation of frictional drag force, is derived from the measurement of dense-phase fluidized bed and is not suitable for the riser reactor. There is a need for the new drag force formulation. In addition, due to the lack of radial transport mechanisms, the researchers on the radial heterogeneity of riser flows artificially divided the riser cross-section into two regions with their boundaries and backflow mixing determined by empirical correlations. Hence, a better understanding on the radial transport mechanisms is needed for the prediction of radial heterogeneity of the riser reactor.

On catalytic reaction part, Jun You (2008) proposed a modeling approach for the coupling effect of the kinetic reactions and the hydrodynamics. However, in his model, the orders of the reactions are mis-formulated. Due to the wrong orders of the reactions, the definitions of reaction kinetic properties are problematic. A better understanding on

the catalytic reactions is essential. Furthermore, his approach is heavily limited by the flaws of hydrodynamic model. Contributed to the advances of hydrodynamic modeling made in the first part, it is possible to develop a better coupling model of hydrodynamics and reaction.

The models predicting the performance of the riser reactor normally assumed a non-pre-reaction and uniformed inlet condition, which is untested. This assumption is not only oversimplified but also unrealistic. Understanding the coupling mechanisms among spray evaporation, vapor-catalyst mixing and reaction in spray region is very important as it provides the inlet conditions of phase transport to the follow-up reactions. Parametric models of evaporating spray jet into gas-solids flows without chemical reaction are extensively developed (Xiaohua Wang, 2002; Guangliang Liu, 2003; Muhammad Rafique, 2006). However, the coupling of spray evaporation, vapor-catalyst mixing with chemical reaction is still needed.

In this dissertation, Chapter 2 dealt with the major intrinsic transport mechanisms. A new 1-D model was developed with the re-formulation of frictional drag force and detailed analysis of impact of particle-particle collision on kinetic energy dissipation as well as the solids acceleration. The model yields the correct prediction of axial transport profiles throughout the riser, including dense, acceleration and dilute phase regime. Chapter 3 described a continuous modeling approach for further exploring the flow heterogeneity in both radial and axial directions. An integral-differential hydrodynamics model with a general third-order polynomial across any riser cross-sections has been developed. The model not only predicts the radial and axial phase transport but also yields the much-needed information of the wall boundary layer and backflow mixing for

the popular core-annulus models. Chapter 4 dealt with the coupling of hydrodynamics and catalytic reaction. A new correlation has been proposed to link the local reaction rate to the local transport properties (such as concentrations of catalysts and reactants, reaction temperature, and transport velocities). The resulted model not only predicts the correct reaction characteristics against the plant data but also demonstrates the feasibility of adopting the same reaction properties of the same type of catalytic reactions in different riser reactors. Chapter 5 investigated the catalytic reaction in the spray region, the coupling mechanisms of hydrodynamics and catalytic reaction are applied to the characteristics of evaporating reactive spray jet in gas-solids fluidized bed. The resulted changes in transport properties provide the inlet conditions for the follow-up reactions in the riser reactor.

At the end of the dissertation, some possible future studies are suggested.

CHAPTER 2

TRASNSPORT MECHANISMS OF GAS-SOLIDS RISER FLOW

In a gas-solids riser flow, the solids are accelerated against gravity by a carrying gas flow in a vertical column. Due to the solids acceleration and consequently its concentration dilution, flow regimes vary through a dense phase, a strong acceleration phase and a dilute phase from the bottom entrance to the top exit of a riser. The hydrodynamic power to drive such a flow can be equated to the product of a pressure drop along the riser and the flow rate of carrying gas. This driving power, from a point of view of hydrodynamic energy conservation, is consumed into three consequences in phase transport: (1) the increase in potential energy of gas and solids against gravity, (2) the change in kinetic energy of gas and solids, and (3) the heat generation by dissipation of kinetic energy (He and Rudolph, 1996). During this process, there are complex gas-solids interphase and interparticle interactions. To fully understand and correctly model the gas-solids riser flow, these mechanisms shall be analyzed carefully and modeled correctly.

In this chapter, the general governing equations of gas-solids riser flow for a 1-D model is firstly developed based on mass and momentum conservations. The gas-solids interphase interaction is then expressed by drag force and pressure force. The detailed expressions are separately analyzed. A detailed analysis of the role of the collision force on the flow structure of gas-solids riser is then made by its effect on the energy and momentum conservation of the system. A simple formulation of the collision force is thus proposed to bear a similar format of drag force, with regard to the dependence upon local solids properties. With the inclusion of the proposed correlation of collision force in the

solids momentum equation, the model can yield phase distributions of gas-solid flows, which can be reasonably validated, in a bulk range, against available measurements of solids volume fraction and axial gradient of pressure.

2.1 General Governing Equations

Consider a steady, isothermal gas-solids riser flow and ignore the exit effect at the end of the riser. The 1-D hydrodynamic equations for the gas-solids riser flow can be obtained by applying conservation laws of gas and solids phases on a small increment of riser height dz as shown in Figure 2.1. In these equations, all phase variables are pre-averaged over the cross-section of the core region, hence, are functions of axial coordinate only. The friction loss of wall boundary is ignored.

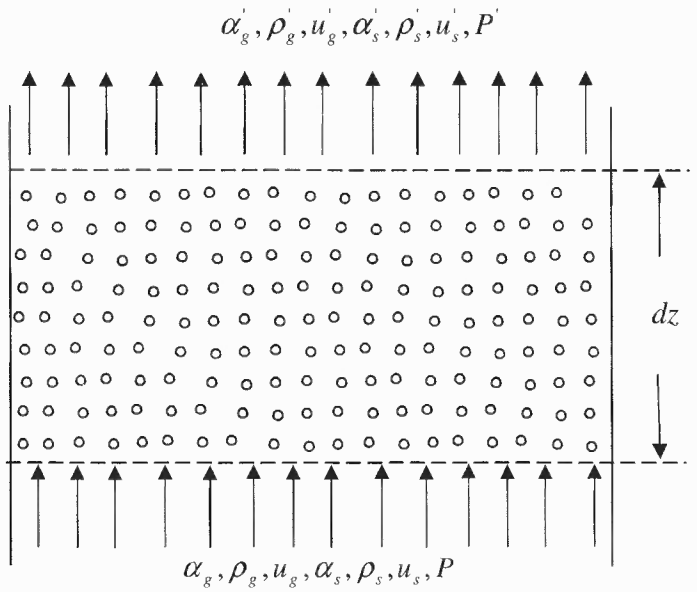

Figure 2.1 Control volume of a gas-solids riser flow.

According to the mass conservations, the mass continuity equations of gas and solids can thus be expressed by:

$$\frac{d(\alpha_g \rho_g u_g)}{dz} = 0 \tag{2.1}$$

$$\frac{d(\alpha_s \rho_s u_s)}{dz} = 0 \tag{2.2}$$

The momentum equation of gas and solids phases can be obtained by analyzing the momentum balance of each phase in the control volume,

$$\left[(P' - P) - \alpha_g \rho_g g dz - F_{gs} dz\right] A dt = \alpha_g' \rho_g' u_g'^2 A dt - \alpha_g \rho_g u_g^2 A dt \tag{2.3}$$

$$(F_{gs} - \alpha_s \rho_s g - F_c) dz A dt = \alpha_s' \rho_s' u_s'^2 A dt - \alpha_s \rho_s u_s^2 A dt \tag{2.4}$$

Divide the both sides of above equations by Adzdt, and remind the conservations of mass for gas and solids phases, we shall have,

$$-\frac{dP}{dz} = \alpha_g \rho_g u_g \frac{du_g}{dz} + \alpha_g \rho_g g dz + F_{gs} \tag{2.5}$$

$$F_{gs} = \alpha_s \rho_s g + F_c + \alpha_s \rho_s u_s \frac{du_s}{dz} \tag{2.6}$$

In above equations, F_{gs} represents the gas-solids inter-phase interactions, which include the frictional drag force and force due to pressure gradient of gas phase along riser height direction; F_c represets possible forces arose due to the particle-particle interaction such as collisions and frictions. Providing the sub-models of these intrinsic mechanisms,

the coupled equations ((2.1), (2.2), (2.5) and (2.6)) can be solved to find four coupled variables, namely pressure (P), solids volume fraction (α_s), gas velocity (u_g) and solids velocity (u_s), which are the essential parameters to understand a gas-solids riser flow.

2.2 Gas-Solids Interactions

The interactions between gas and solids phases can be divided into two parts, the drag force due to slip velocity and friction (F_D), and the fore due to pressure gradient (F_P).

2.2.1 Force due to Pressure Gradient

The pressure of gas inside a riser decreases gradually. The energy is consumed by gas and solids lifting up and other energy dissipations due to collision and friction. When there is a pressure gradient of fluid around a sphere particle, an additional force will act on the sphere. Using the axisymetric condition, the total force due to pressure gradient of fluid on a spherical particle shall be

$$f_p = -2\pi\left(\frac{d_s}{2}\right)^3 \int_0^{\pi} \frac{dP}{dz} \sin\theta \cos^2\theta d\theta = -\frac{dP}{dz}\frac{\pi d_s^3}{6} \tag{2.7}$$

where the minus sign means the force is in the opposite direction of the pressure gradient of the fluid phase.

Thus, the total force due to pressure gradient of gas on solids phase can be obtained,

$$F_p = n_s f_p = \frac{\alpha_s}{\pi d_s^3 / 6} f_s = -\alpha_s \frac{dP}{dz} \tag{2.8}$$

Put equation 2.7 into the general governing equations and make necessary rearrangement, we shall have

$$-\alpha_g \frac{dP}{dz} = \alpha_g \rho_g u_g \frac{du_g}{dz} + \alpha_g \rho_g g dz + F_D \tag{2.9}$$

$$-\alpha_s \frac{dP}{dz} = \alpha_s \rho_s g + F_c + \alpha_s \rho_s u_s \frac{du_s}{dz} - F_D \tag{2.10}$$

2.2.2 Frictional Drag Force

The inter-phase momentum transfer between gas and solids in fluidization is commonly termed as drag force, although the academic definition of drag force on an object refers to the momentum transfer of an isolated object in unbounded, uniform and non-accelerating flow. A commonly-adopted method of formulating the inter-phase drag force between gas and solids is based on the Richardson-Zaki equation [Richardson and Zaki, 1954], whose basic form can be expressed as

$$F_D = \frac{18\mu}{d_s^2} \cdot \frac{\alpha_s}{(1-\alpha_s)^n} \cdot \left(u_g - u_s\right) \tag{2.11}$$

It should be pointed that the Richardson-Zaki equation was originally obtained from a simple force balance of a single particle settling at terminal velocity among a swamp of neighboring particles in the creeping flow regime (i.e., particle Reynolds number is less or near one). Such an approach has been successful for the applications of dense-phase fluidized beds where the cross-sectional averaged solids transport is null and the averaged particle Reynolds number is typically less than one. However, in riser flows,

the averaged solids transport mass flux is not only non-zero but also varies along the riser. The particle Reynolds number can be far above one in the dense and acceleration regimes, where the hydrodynamic forces may exceed the gravitational force by a large margin, as schematically illustrated in Figure 2.2. Thus using a simple extension of Richardson-Zaki equation to formulate the hydrodynamic forces in riser flows can be quite problematic in accounting for the solids acceleration in these regimes.

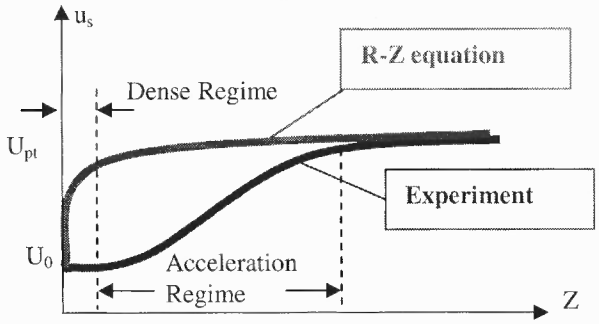

Figure 2.2 Comparison of Richardson-Zaki Equation and experimental results.

An alternative approach to formulate the drag force could be based on that of a single particle among a swamp of neighboring particles in a gas flow that can be far beyond the creeping flow regime. The drag force of an isolated particle in an unbounded, non-accelerating and uniform gas flow is given by

$$F_{D0} = C_D \frac{\pi}{8} \rho_g d_s^2 (u_g - u_s)^2 \tag{2.12}$$

where C_D is the drag coefficient expressed as a function of Reynolds number by

$$C_D = \begin{cases} \dfrac{24}{Re} & Re < 2 \\ \dfrac{18.5}{Re^{0.6}} & 2 < Re < 500 \\ 0.44 & 500 < Re < 2\times10^5 \end{cases} \tag{2.13}$$

Figure 2.3 clearly shows that the drag force is a non-linear function of slip velocity at dense regime where the Reynolds number is much higher than 1. At the acceleration regime, the drag force is located in a transition range from non-linear to linear function of slip velocity. In the dilute regime, as the slip velocity approaching to the particle terminal settling velocity, the drag force could be a linear function of slip velocity.

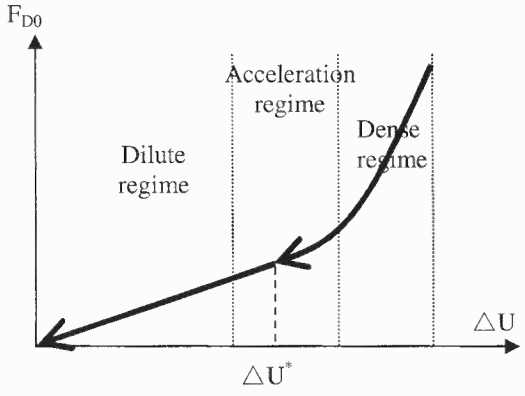

Figure 2.3 Drag force vs relative velocity in various riser regimes.

Effect of neighboring particles may be represented by the wake effect of interactive particles, which can lead to a significant reduction in drag force of affected particle [Zhu et al., 1994]. Hence the drag force may be modified, by considering effect of multiple neighboring particles, as

$$F_D = k_1 n_s F_{D0} \tag{2.14}$$

where n_s is the number density of solids particles, and k_1 is the reduction coefficient of wake effect of two-interactive particles, which is a function of solids volume fraction by [Zhu et al., 1994],

$$k_1 = 1-(1-A)\exp\left\{B\cdot\left(\sqrt[3]{\frac{\pi}{6\alpha_s}}-1\right)\right\} \tag{2.15}$$

A and B are empirical coefficients that are functions of Reynolds number as

$$\begin{cases} A = 1-\exp(-0.483+3.45\times10^{-3}\,\mathrm{Re}-1.07\times10^{-5}\,\mathrm{Re}^2) \\ B = -0.115-8.75\times10^{-4}\,\mathrm{Re}+5.61\times10^{-7}\,\mathrm{Re}^2 \end{cases} \tag{2.16}$$

2.3 Inter-particle collision

It is known that the intensive inter-particle collision in the gas-solids riser, especially at the bottom region of riser, causes a large amount of energy dissipation which may be a major factor for the existence of dense regime of gas-solids riser [Zhu and You, 2007]. The inter-particle collision is the major factor that causes the dense phase regime at the bottom region of riser. While, its roles on the momentum equation of solids phase and its correct modeling are not yet fully understood and analyzed.

2.3.1 Role on Energy Dissipation

The important effect of inter-particle collision on the energy transfer along the riser can be analyzed by kinetic energy equations of the system. The conservation of total kinetic energy yields

$$-\frac{dp}{dz}u_g = (\alpha_g u_g \rho_g + \alpha_s u_s \rho_s)g + \frac{d}{dz}(\alpha_g \rho_g u_g^2 + \alpha_s \rho_s u_s^2) + \Gamma \tag{2.17}$$

The left hand side of equation (2.17) is the total kinetic energy input, characterized by the product of gas velocity and axial gradient of pressure. The terms of right hand side represent the energy consumptions due to, respectively, solids lift up against gravity, the gain of kinetic energy by phase acceleration, and the energy dissipation. The intrinsic relationships among them can be illustrated by Figure 2.4. It is clearly that, in the dilute

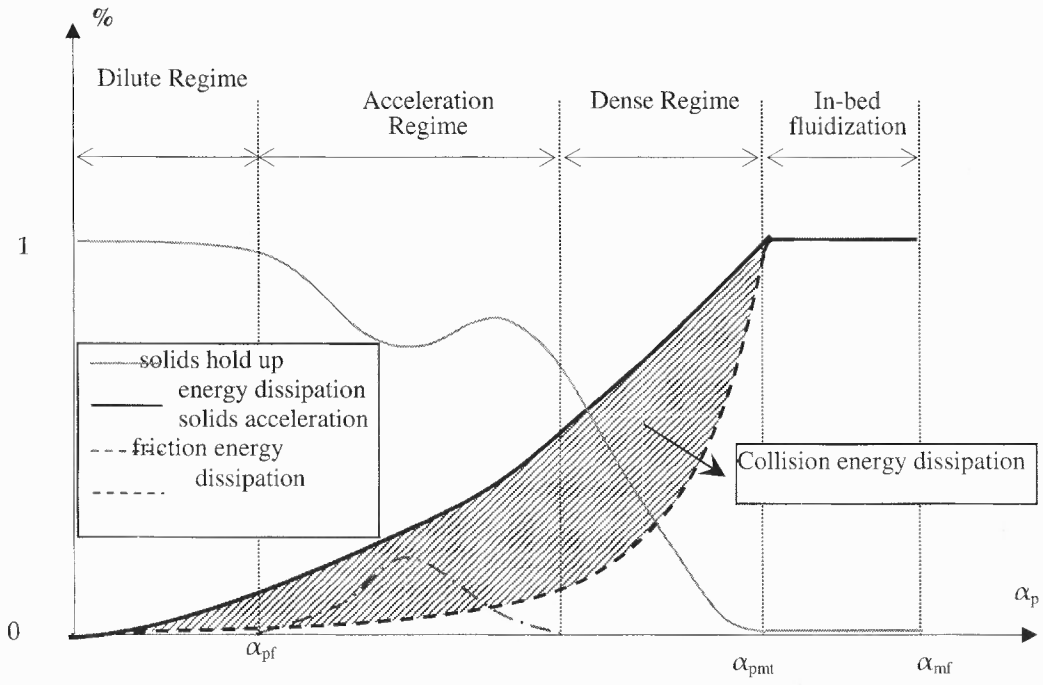

Figure 2.4 Energy portions of solids hold up, dissipation and solids acceleration.

phase transport region, the energy dissipation and kinetic energy increase by phase acceleration are nearly zero and most of energy consumption is due to the solids lift up. In the dense phase transport region, however, the energy consumption by phase acceleration is neglectable with all the energy consumptions are due to solids lift up and energy dissipation. In the dense phase in-bed fluidization, the energy consumption by solids lift up and phase acceleration are zero with all the energy consumption by energy dissipation. In the acceleration region, each of the three kinds of energy consumptions takes a non-neglectable portion of total energy input.

In above analysis, the energy dissipation can be further divided into two parts due to different mechanisms, namely, friction energy dissipation by inter-phase friction and collision energy dissipation due to inter-particle collisions. The relationship of these two parts can be analyzed from the kinetic energy equation of each phase.

The kinetic energy equation of gas can be written as

$$-\alpha_g \frac{dp}{dz} u_g = \frac{\tau_w l_w u_g}{A_R} + \alpha_g u_g \rho_g g + \frac{d}{dz}(\alpha_g \rho_g u_g^2) + F_D u_g \tag{2.18}$$

Similarly, the kinetic energy equation of solids phase becomes

$$-\alpha_s \frac{dP}{dz} u_s = -F_D u_s + \frac{\tau_{sw} l_w u_s}{A_R} + \alpha_s u_s \rho_s g + \frac{d}{dz}(\alpha_s \rho_s u_s^2) + \Gamma_c \tag{2.19}$$

Combining Equations (2.18) and (2.19), and comparing the resulted equation against Equation (2.17), the following equation can be obtained,

$$\Gamma = F_D(u_g - u_s) + \Gamma_c = \Gamma_f + \Gamma_c \tag{2.20}$$

where the left hand side of the equation is the total energy dissipation per volume of gas-solids riser flow, the two terms of right hand side are the frictional energy dissipation characterized by the product of drag force and slip velocity between gas and solids phases, and the collision energy dissipation. The portions of this two energy dissipations in the different regimes of a riser is shown in Figure 2.4. It is clear that, in the dense regime, the collision energy dissipation and friction energy dissipation both take large portions of total energy dissipation; in the acceleration regime, the portion of collision energy dissipation gradually decreases as the solids volume fraction decreases along the riser; in the dilute regime, with the further decrease of collision energy dissipation, the energy dissipation is mainly due to the friction loss until under the condition of particle terminal velocity, collision energy dissipation reach to zero.

2.3.2 Role in Momentum Equation

Due to the inter-particle collision, the momentum transfer in the system of a gas-solids riser would also be influenced. From an analysis of kinetic energy conservations in a riser flow, it can be logically deduced that there exists an axially non-balanced force by solids collision [Zhu and You, 2007]. Divide the both sides of solids kinetic energy Equation (2.19) with solids velocity, the kinetic energy equation of solids phase can be deduced into momentum equation, which is expressed as,

$$-\alpha_s \frac{dP}{dz} + F_D = \alpha_s \rho_s g + G_s \frac{du_s}{dz} + F_c \tag{2.21}$$

It is clearly shown that a source term in the momentum equation of solids phase, which is denoted as collision force F_c and characterized by the collision energy dissipation divided by solids velocity, shall be included to account for the influence of inter-particle collision on solids momentum change along the riser. This collision force may be contributed by any of or a combination of collision modes that yield the kinetic energy loss, including the inelastic normal compression and rebounding, sliding, non-sliding micro-slip and rolling effects among fluidized particles. It may also be realized that the collision behavior in axially-accelerating flow of solids is unbalance along the axial direction. The sum of these complex effects creates an axially unbalanced force on solids phase, which plays an important role in momentum equation of solids, especially in the dense and acceleration regimes where the particle-particle collision is significant.

It should be noted that the importance of gravitational force, solids acceleration and collision force, which are represented by the three terms at the right hand side of Equation (2.21), varies at the different regimes along the riser. Their intrinsic relationships can be further analyzed. Divide the both sides of Equation (2.21) with inter-phase interaction force, F_{gs}, and define

$$c_D = \frac{F_c}{F_{gs}}; \qquad G_D = \frac{\alpha_s \rho_s g}{F_{gs}} \qquad a_D = \frac{G_s \frac{du_s}{dz}}{F_{gs}} \tag{2.22}$$

The equation of partition functions of drag force could be obtained as,

$$c_D + G_D + a_D = 1 \tag{2.23}$$

Here the c_D, G_D and α_D are the partitions of drag force, respectively, to balance collision force, gravitational force and for the solids acceleration. It is clear that, in the dilute regime, $G_D \approx 1$ with $\alpha_D \approx 0$ and $c_D \approx 0$; in the dense regime, however, $c_D + G_D \approx 1$ with $\alpha_D \approx 0$; while, in the acceleration regime, all the three partitions have important influences. The relationships among them are shown in Figure 2.5.

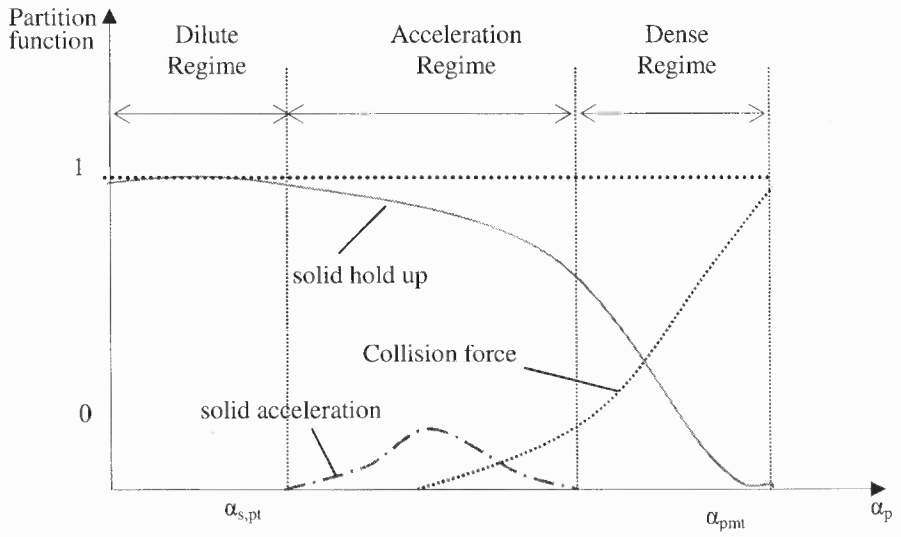

Figure 2.5 Partitions of solids hold up, collision force and solids acceleration along riser.

2.3.3 Formulation of Collision Force

According to above analysis, the collision force is subjected to some limiting conditions and its formulation could be constructed from the linkage of collision force with the actions of inter-phase drag force and gravitational force under these limiting conditions. It is shown above that at the dense phase regime, the solids acceleration can be neglected, which leads to,

$$F_c \approx F_D - \alpha_s \rho_s g \tag{2.24}$$

Since in the dense regime, slip velocity is much higher than particle terminal velocity (at least 20 times), and solids volume fraction is in a range of 0.25~0.45, the drag force is much higher than solids gravitational force (at least 100 times). Thus, the drag force is mainly balanced by the collision force in the dense phase and they have same magnitude. Second, the solids acceleration is expected to be a large partition and can not be ignored in the acceleration regime. Third, assuming a very long riser where solids velocity eventually approaches to the particle terminal velocity in the dilute regime, the drag force should be basically balanced by the gravity without collisions and acceleration. Thus, a semi-empirical correlation of collision force on inter-phase drag force could be expressed as,

$$F_c = (1 - k_2 k_3) F_D - (1 - k_3) \alpha_s \rho_s g \tag{2.25}$$

where k_2 and k_3 are coefficients and can be expressed, representatively, by

$$k_2 = \left[1 - \exp\left(-\left(\frac{\alpha_s + 0.2}{\alpha_{sc}} \right)^2 \right) \right] \tag{2.26}$$

$$k_3 = \frac{0.3}{\pi} \tan^{-1}\left(26 - 100 \cdot \alpha_s\right) + 0.15 \tag{2.27}$$

It is noted that k2 represents an S-shaped axial profile for cross-section averaged voidage in riser (Li and Kwauk, 1980)

2.4 Results and Discussion

In this section the proposed model is first validated by directly comparing the model predictions with available experimental data and those of previously published models which did not or incompletely consider the influence of collision force on solids hydrodynamics. Then, the partitions of energy dissipation and momentum transfer induced by particle-particle collision are presented and discussed.

In order to validate the proposed model, the model predictions of solid volume fraction and axial distribution of pressure are directly compared with the experimental data of different research groups (Arena et al.; 1985 and Pugsley and Berruti, 1996). In order to examine the model robustness and rationality of working conditions, the relevant parameters of experiments were purposely chosen in a wide range for particle type (including glass beads, FCC particles, sand), gas velocity and solid mass flux. The detailed operating conditions of the experiments used for the comparison of the proposed model predictions are shown in Table 2.1.

Table 2.1 Experimental Parameters for Model Validation

References	Particle Type	d_s μm	G_s kg/m^2.s	U_g m/s	ρ_s kg/m^3	Z m	D m
Arena et al., 1985	Glass Beads	88	600	7	2600	6.4	0.041
Arena et al., 1985	Glass Beads	88	199	7	2600	6.4	0.041
Pugsley & Berruti, 1996	Sand	208	400	8.5	2580	5.0	0.05
Pugsley & Berruti, 1996	Sand	208	700	8.5	2580	5.0	0.05

As a part of the model validation, the model predictions of axial distribution of solids volume fraction are compared with two set of experimental data of (Arena et al., 1985) in which solid mass flux changes from 199 to 600 kg/m2s. Besides, all following figures are in dimensionless format to make the comparison more representative.

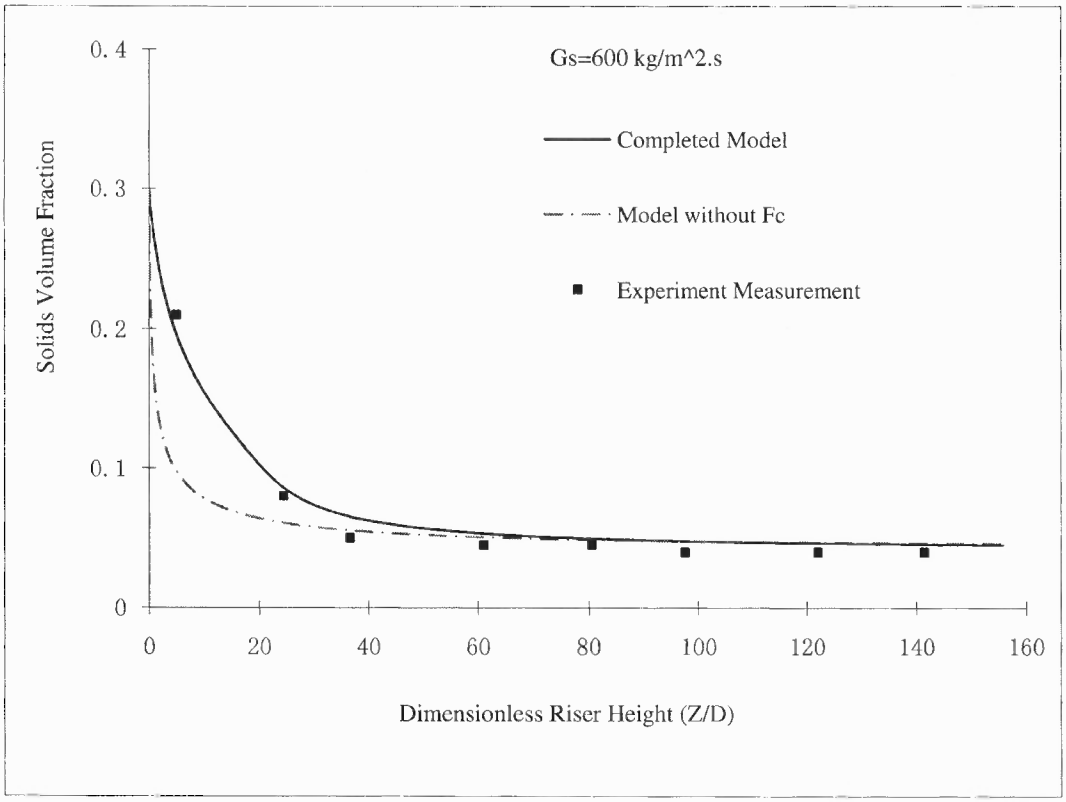

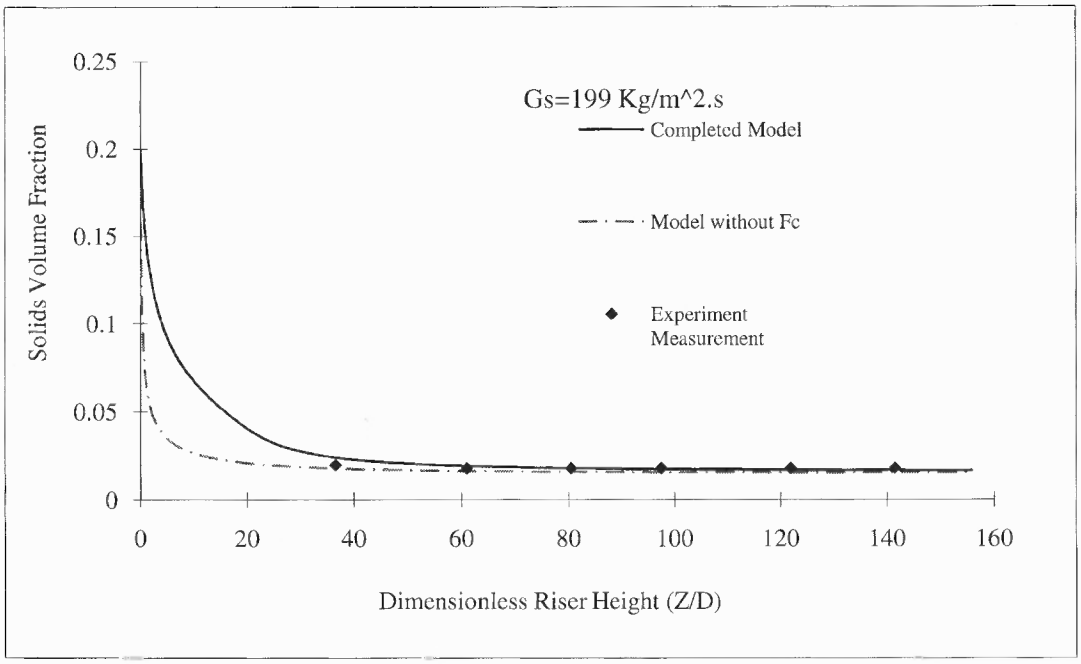

Figure 2.6 Comparison of model predictions and experimental results of axial profile of solid volume fraction (Arena et al., 1985).

As shown as both of cases in Figure 2.6, the model predictions for solid volume fraction fit the experimental data (Arena et al., 1985) satisfactorily along the riser height. Basically the distribution of solid volume fraction along riser height presents typical S-shape. It means that in the lower part of the riser, the flow is in the dense phase regime because of the low initial solids velocity. Then the solids are gradually accelerated under the interaction with gas phase, and finally reach the relatively steady and dilute regime at the upper part of riser. It is shown in Fig. 2.6 that, in the dilute phase transport regime, solid volume fraction remains constant in the rest of the riser height for both of the cases. The model predictions demonstrated the same trend for the solid volume fraction as experimental measurement and quantitatively matched with their values along the whole riser with reasonable accuracy. However, for very low solids mass flux, solids back-mixing will have significant influence on the overall flow structure, which can not be

neglected. Special attention should be given to the amount of solids back-mixing and variation of wall thickness. This part of study will be further covered in our next step study.

In Figure 2.6 we also compared the model prediction of solid volume fraction with/without the consideration of collision force. When the model did not consider the collision force, the solids phase picked up the velocity very fast and quickly reach the steady dilute phase. From the comparison, the function of the collision force can be described as placing certain limitation on the acceleration of the solid phase in a swamp of fluidized particles, especially in the dense and acceleration regions of the riser. In the dilute phase, due to the relatively large distance among particles, the collision force becomes very weak and its influence on the flow structure could be reasonably neglected.

Figure 2.7 shows reasonable agreements between model predictions and experimental data for axial gradient of pressure. As demonstrated in Figure 2.7, in the lower part of the riser, the axial gradients of pressure are much steeper than those in the upper part. In the lower part of the riser, gas-solid flow is in the dense phase regime, where violent inter-particle collision, normal compression, rebounding, sliding and non-sliding micro-slip rolling are the dominant factors for overall energy dissipation. This part of overall energy dissipation is much higher than those in the upper part of the riser, where the energy dissipation is mainly cased by friction loss and gravity. The solid phase is accelerated gradually with the increase of riser height and the dense gas-solid flow enters the acceleration transition regime and then dilute transport regime. The inter-particle spacing becomes larger in dilute phase transport regime and hence, the energy dissipation is dominated only by friction loss between gas/solid and wall, which leads to a quite steady axial pressure gradient in the upper part of the riser.

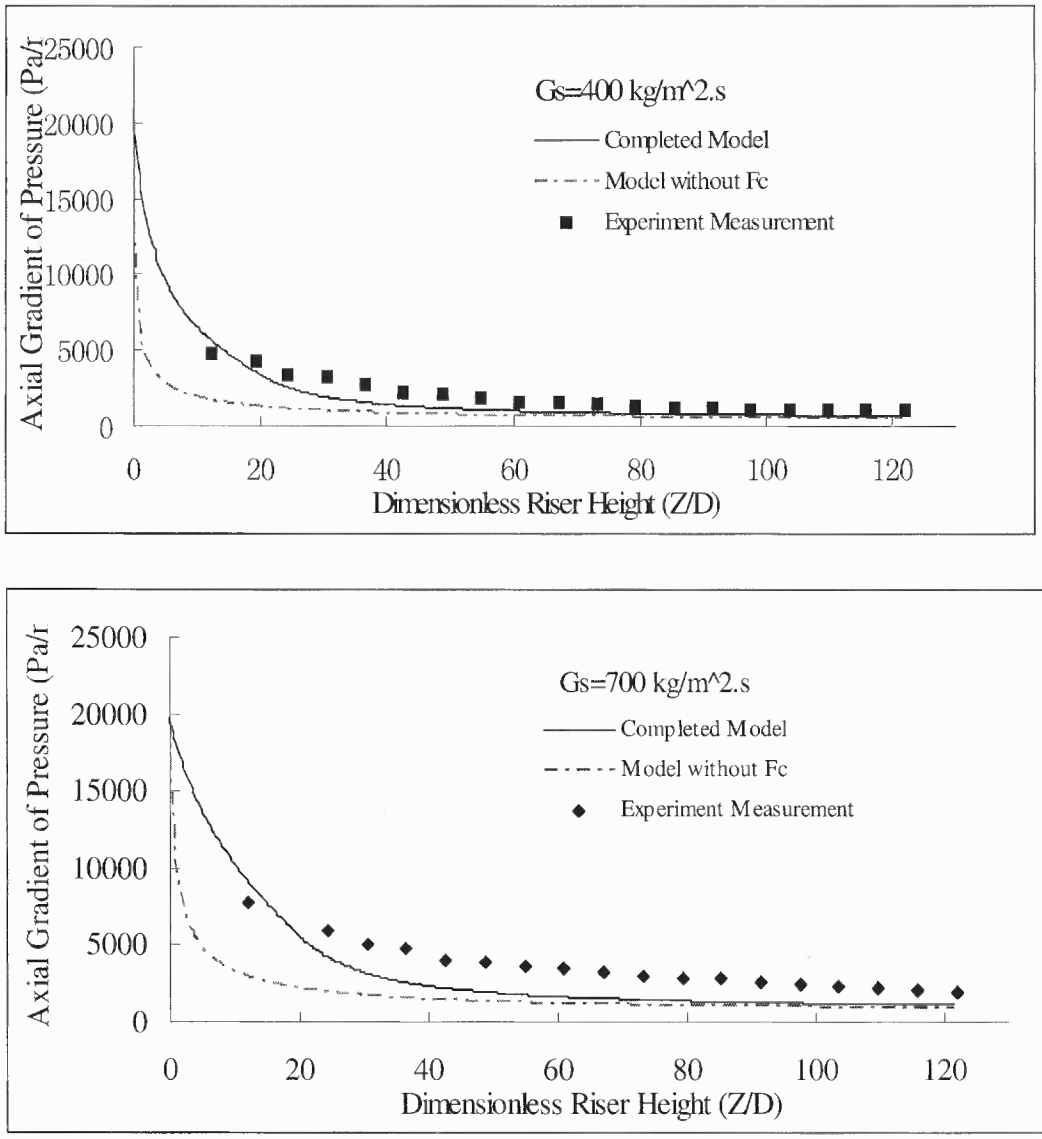

Figure 2.7 Comparison of model predictions and experimental results of axial pressure gradient profile (Pugsley and Berruti, 1996).

Similarly, the comparison of model prediction of axial pressure gradient w/o consideration of collision force is also shown in Figure 2.7. It was shown that when the collision force was not included in the model, the pressure drop gradient is much larger than the case when collision force was considered. From energy conservation point of view, some portion of the total mechanical energy will be consumed by the inter-particle

collision in the form of energy dissipation, as shown in the result of completed model prediction.

In order to extend the model applications beyond experimental conditions, a parametric study is carried out to study the effect of gas velocity and solids mass flux on axial gradient of pressure, solid volume fraction, and phase velocity. We tested the proposed model in conditions that the gas velocity changes from 6 to 20 m/s and solid mass flux changes up to 1000 kg/m2s.

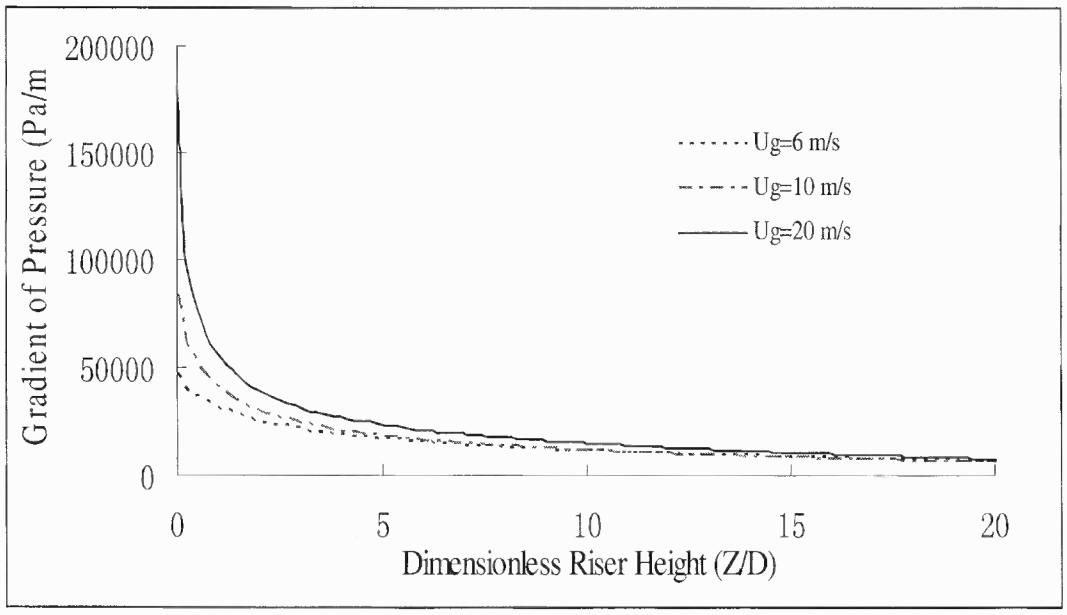

(a) Axial gradient of pressure

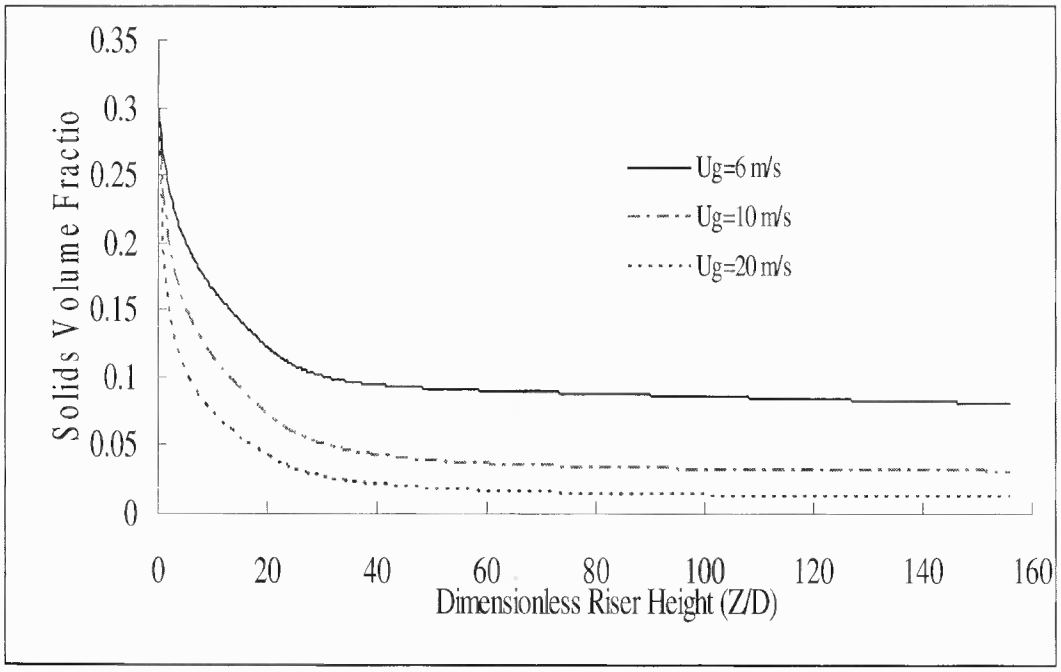

(b) Solid volume fraction

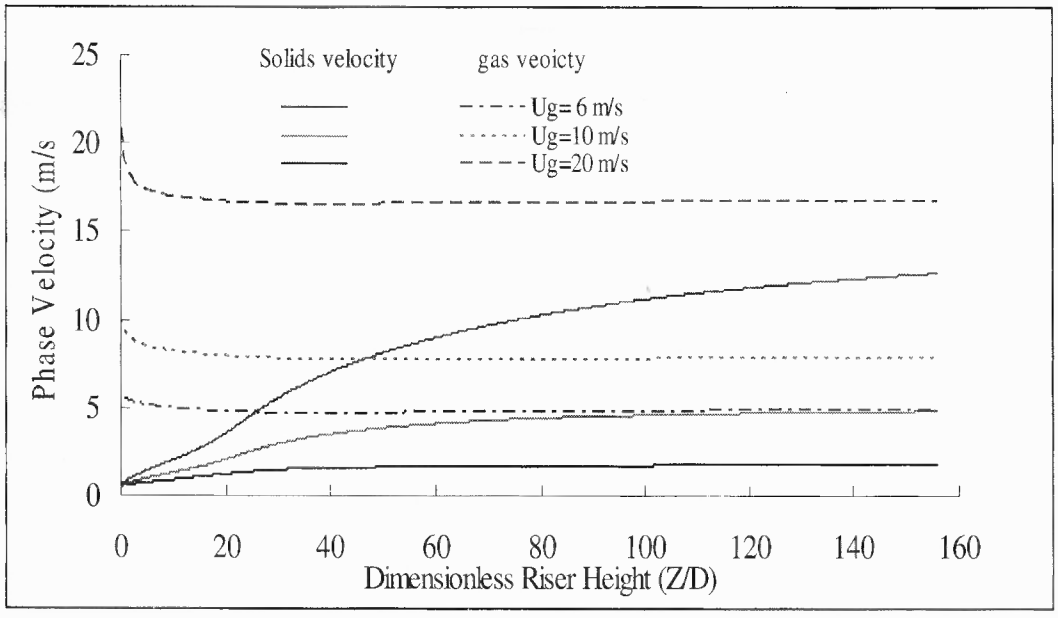

(c) Solid and Gas Velocity

Figure 2.8 Effect of Gas Velocity on flow pattern (Gs= 382 kg/m2.s).

Figure 2.8(a), 2.8(b) and 2.8(c) shows, the effect of gas velocity on axial gradient of pressure, solid volume fraction and solid velocity, when initial gas velocity changes from 6m/s to 20 m/s with constant solid mass flux at 382 kg/m2s.

It is seen from Figure 2.8(a) that, for given constant mass flux rate as the gas velocity is decreased, the total pressure drop also decreases along the whole riser, especially in the lower part of the riser. This is because more intensive energy dissipation due to inter-particle collision when the gas velocity is relatively high. However in the upper part of the riser, the pressure drop gradient is almost constant, because the major contribution to the pressure drop in this regime is due to friction loss and solid gravity, which don't change significantly with the change of gas velocity.

Figure 2.8(b) shows the effect of gas velocity on axial profile of solid volume fraction at constant solid mass flux. In the dense phase regime as the gas velocity increases the momentum gained by the solid phase leads to the decrease in solid volume fraction in this zone. While the flow is in the dilute transport regime, the solid volume fraction is almost remains constant, which indicates the fully developed solid-gas flow. However, for different initial gas velocity, the solid volume fraction in the dilute phase is quite different because the solid momentum gained from gas phase is different, so the final solid velocities are also different. With decrease in gas velocity, the solid volume fraction increases and pressure drop is almost remaining constant in fully developed transport region.

Figure 2.8(c) shows the axial solid and gas velocity profiles along the riser. It is interesting to notice that the solids velocity in dense phase region is almost constant, because the particles are packed and have no space for acceleration in dense phase region.

However in acceleration phase region, as the solid volume fraction decreases, the particles are unlocked above the minimum fluidization velocity and are free to accelerate so, the solids particle velocity increases in this region with increase of gas velocity. The solids velocity profiles follow the typical S-shape curve. As for the gas velocity profile, it is the combined effect of change of solid volume fraction and pressure drop, which present a little bit different patterns for different initial gas velocity.

Till now, Fig. 2.8(a), 2.8(b) and 2.8(c) have presented how the flow pattern, including axial pressure gradient profile, axial solid volume fraction, gas and solids velocity, will be influenced by the variation of initial gas velocity. In the next part, we will discuss the effect of variation of the solids mass flux on overall flow patterns.

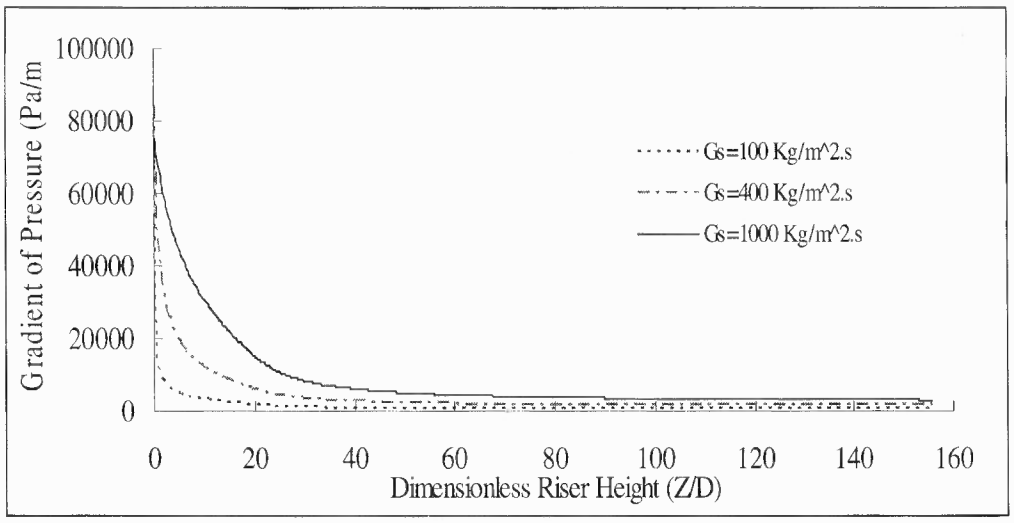

(a) Axial gradient of pressure

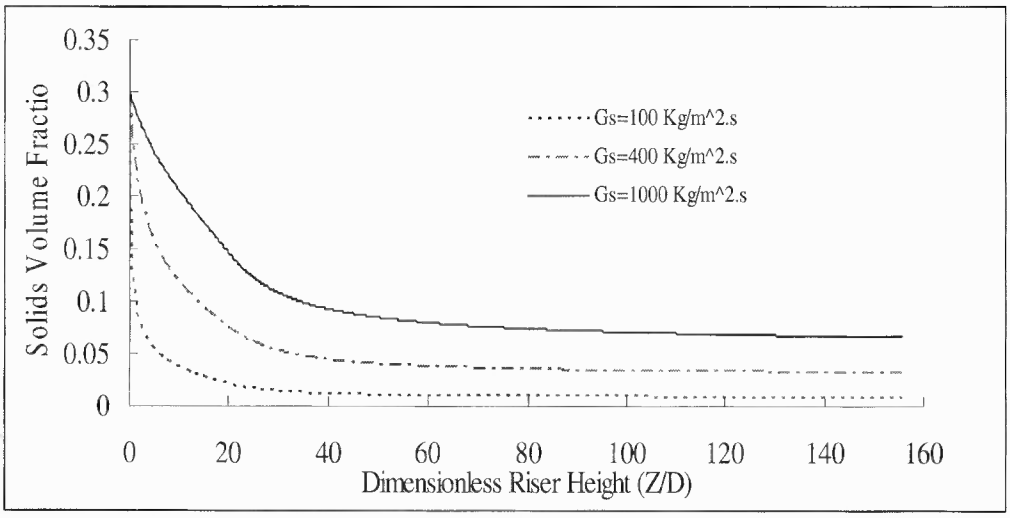

(b) Solid volume fraction

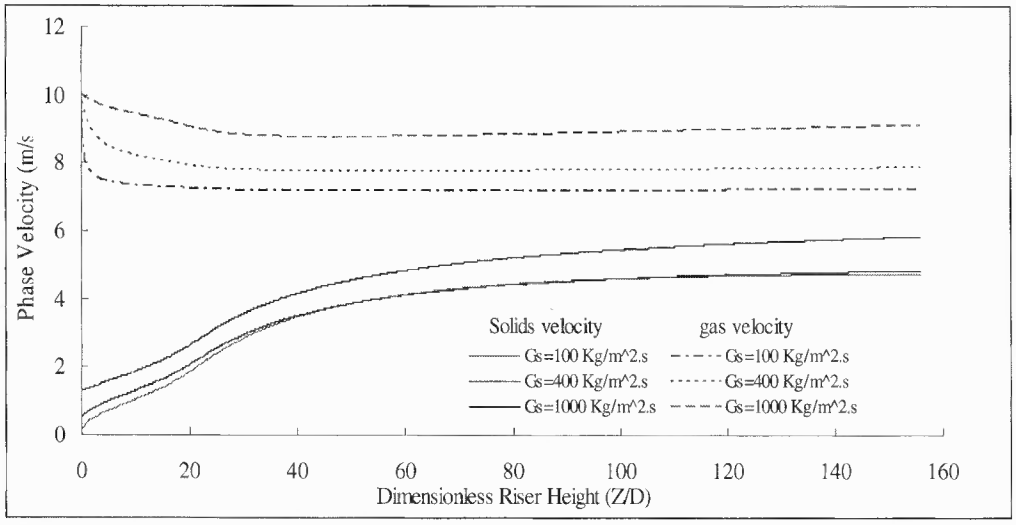

(c) Gas and Solid velocity

Figure 2.9 Effect of Solid mass flux variation on flow pattern (Ug = 7 m/s).

Figure 2.9 shows the effect of solid mass flux variation on flow patterns. The gas velocity is kept at 7 m/s and the solid mass flux are at 100, 400 and 1000 kg/m2s respectively. It reveals that, increasing in the solids mass flux causes higher pressure drop in the dense and acceleration regime if other parameters are kept unchanged, which is because of more intensive inter-particle collision. Regarding with the solid volume

fraction and solid velocity, both of them still present the same S-shape as shown in Fig. 2.9(b) and 2.9(c). The solid volume fraction decreases very fast with decrease of solids mass flux in the dense phase region. The solid volume fraction in the dilute phase regime remains constant but decreases with decrease in solids mass flux, which is shown in figure 2.9 (b).

2.5 Conclusion

In this chapter, the role of the inter-particle collision on the flow structure of gas-solids riser is detailedly analyzed and discussed. We first analyzed the role of inter-phase collision on the energy dissipation and momentum transfer of gas-solids riser flow. The existence of an axially non-balanced collision force is proved by the analysis of kinetic energy balance and momentum equation of solids phase. We then showed that the collision force should be of the same order of magnitude as that of the drag force in the dense and acceleration region, which is far more than solids gravitational force. A simple formulation of the collision force is thus proposed to bear a similar format of drag force. The mechanisms are then applied to a coupled 1-D hydrodynamic model of gas-solids riser flow to solve for the axial distribution of pressure, gas velocity, solids volume fraction and velocity along the riser. With the inclusion of the proposed correlation of collision force in the solids momentum equation, our model can yield phase distributions of gas-solid flows, which can be reasonably validated, in a bulk range, against available measurements of solids volume fraction and axial gradient of pressure.

CHAPTER 3

FLOW HETEROGENITY IN BOTH RADIAL AND AXIAL DIRECTIONS

The flow in gas-solids riser exhibits strong heterogeneous characteristics in both axial and radial directions. It is well known that, there is a S-Shape distribution of solids volume fraction and velocity along the riser, which typically presents a 3 regime evolution, namely dense-phase regime, acceleration regime and dilute-phase regime. In the radial direction, it presents a typical core-annulus (wall) flow structure with a dilute core upward flow and a solids film near the wall where solids are flowing downwards [Herb et al., 1992], or a double ring "core-annulus-wall" three-zone flow structure under some operational conditions [Du et al., 2004]. The axial heterogeneous structure is normally caused by the gas-solids interfacial interactions and particle-particle collisions. The radial distribution is aroused by wall effects of boundary effect and wall friction, collisional diffusive mass transfer and turbulent mass transfer of solids phases.

It is also noticed that, due to the radial heterogeneous structure, the one-dimensional approach may not be adequate to describe the hydrodynamics of gas-solids riser flow. The hydrodynamic characteristics of core and annulus (wall) areas are so different that it is not suitable to combine these two regions into a uniform region. Although there are some efforts on investigation of radial solids concentration, the effects of this non-uniform distribution on radial mass and momentum transfer, area of upward flow, back-mixing ratio of solids phase, and thus the performance of riser are not investigated.

This chapter is aimed to investigate the flow structure heterogeneity of gas-solids risers both radial and axial directions by presenting a continuous modeling approach with intrinsic mass transfer mechanism to characterize the formation mechanisms of heterogeneous structure and to reveal the effects of radial and axial non-uniformities on the performance of riser flow.

3.1 General Modeling Methodology

Consider a steady, isothermal gas-solids riser as given in Figure 3.1. If we ignore solids deceleration region due to end effects near the top end of the riser and the intensive mixing regime at the bottom of the riser due to the effect of asymmetric geometry of solids inlet, the riser could be treated asymmetric with hydrodynamic evolutions in both axial and radial directions. Along the riser, the flow structure could be divided into three regimes, namely dense regime, acceleration regime and dilute regime, based on the hydrodynamics of solids phase, with continuous solids acceleration and dilution due to gas-solids interaction. In the radial direction, normally there is a relatively higher solids velocity in the core region and a gradually decreasing trend towards the wall until the solids move downwards near the riser wall. For the simplification, the wall frictions on the gas and solids phases are also ignored.

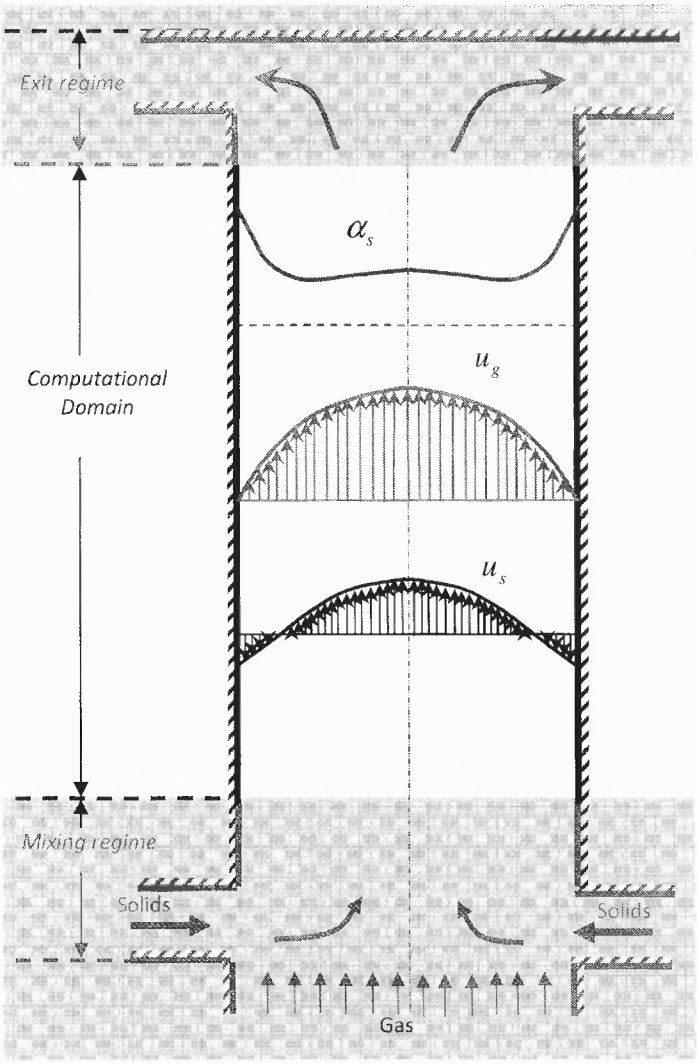

Figure3.1 Heterogeneous flow Structure in a gas-solids riser.

Following the governing equations based on the mass and momentum conservations of each phase, the hydrodynamic characteristics of riser flow could be described by

$$\frac{d}{dz}(\int_A \alpha_g \rho_g u_g dA) = 0 \tag{3.1}$$

$$\frac{d}{dz}(\int_A \alpha_s \rho_s u_s dA) = 0 \tag{3.2}$$

$$-\frac{d(\int_A \alpha_g P dA)}{dz} = \int_A \alpha_g \rho_g g dA + \frac{d(\int_A \alpha_g \rho_g u_g^2 dA)}{dz} + \int_A F_D dA \tag{3.3}$$

$$\frac{d(\int_A \alpha_s \rho_s u_s^2 dA)}{dz} = -\frac{d\left(\int_A \alpha_s P dA\right)}{dz} \int_A f_D dA - \int_A \alpha_s \rho_s g dA - \int_A f_c dA \tag{3.4}$$

where, α_g, ρ_g, ug and α_s, ρ_s, u_s are the local volume fraction, density and velocity of gas phase and solids phase respectively with the volumetric fraction relations of gas and solids phase and the equation of state of gas phase: $\alpha_g + \alpha_s = 1$ and $\rho_g = \frac{P}{RT}$; A is the area of the cross-section of riser, z is the height of the riser; P is the pressure; f_D is the drag force between gas and solids phase; f_C is the collision force due to inter-particle collision effect.

For radically uniform flow or 1-D modeling approaches, the local values (say volume fractions, velocities and pressure) in above equations can be replaced by cross-sectional averaged values and the integrals in above equation could be expressed as explicit functions of these averaged values; the closure of the problem for axially heterogeneous flow structure is fulfilled as long as the drag force and collision force are formulated. For the heterogeneous flow structure in both radial and axial directions, the integrals in above equations can be integrated only when the radial distributions are explicitly expressed and the closure of the problem by above governing equations can be fulfilled only when there are no more than 4 variables totally in these explicit expressions. Otherwise, additional intrinsic mechanisms shall be provided.

3.2 Continuous Modeling of Hydrodynamics

It shall be noticed that the flow structure in the riser reactor is highly heterogeneous in both radial and axial directions, thus the one-dimensional approach may not be adequate to describe the hydrodynamics of gas-solids riser flow, especially in radial direction. A better way for describing the flow characteristics may be providing more flow mechanisms in radial directions together with the general governing equations shown in chapter 3.1.

Noticing that the polynomial forms of transport parameters ϕ (e.g. α_g, u_g and α_s, $u_{s)}$ as following,

$$\phi(r,z)=\sum_{i=0}^{n} c_{\phi i}(z)\cdot r^{i} \tag{3.5}$$

where $c_{\Phi i}$ are the coefficients to determine the detailed distribution of the parameter along the radial direction and can be the function of cross-section height z along the riser, we can express the above governing equation as differentials of these coefficients.

For simplifying of the problem without losing the characteristics of the flow in the riser, it is safe to select 3rd order polynomials to approximate the distribution,

$$\phi(r,z)=c_{\phi 3}(z)r^{3}+c_{\phi 2}(z)r^{2}+c_{\phi 1}(z)r+c_{\phi 0}(z) \tag{3.6}$$

here, ϕ could be $\alpha(r,z)$ and $u(r,z)$ for either gas or solids phase.

It is noted that although there may have slight fluctuation of pressure in an arbitrary cross-section, the pressure gradient in radial direction is much less than that

along the riser. Thus, it is safe to assume the pressure distribution is uniform at any cross-section of the riser. From this assumption, a uniform gas density at any cross-section can easily be obtained.

To determine the four coefficients in equation (3.6), at least 4 characteristic values of concerned parameter at a cross-section shall be provided. Firstly, according to the axi-symmetricity of the riser, the gradient of the parameter at the center line shall be zero, which gives $c_{\phi 1} = 0$; The other three characteristic values are selected as value at wall boundary ϕ_w, value at the centerline of the riser ϕ_0, and the cross-sectional averaged value $\bar{\phi}$ which is defined as

$$\bar{\phi} = \frac{\int_0^R \phi(r) \cdot 2\pi r dr}{\pi R^2} \tag{3.7}$$

With above characteristic values, the coefficients of 3rd polynomial form of radial distribution of the parameter could be determined as,

$$\begin{cases} c_{\phi 0} = \phi_0 \\ c_{\phi 1} = 0 \\ c_{\phi 2} = \dfrac{10\bar{\phi} - 4\phi_w - 6\phi_0}{R^2} \\ c_{\phi 3} = \dfrac{5(\phi_w + \phi_0 - 2\bar{\phi})}{R^3} \end{cases} \tag{3.8}$$

Put the polynomials of solids concentration, solids velocity and gas velocity with above form into governing equations (3.1)-(3.4), and with the assumption of uniform

pressure across any cross-section of the riser, the integrals in the governing equations can be solved. The following series of governing equations, which are the ordinary differential equations purely about axial directions as the functions of characteristic values of any cross-section, can be obtained,

$$[C]_{4\times 10}\cdot\frac{d}{dz}\left(\alpha_{s0},\alpha_{sw},\bar{\alpha}_s,u_{g0},u_{gw},\bar{u}_g,u_{s0},u_{sw},\bar{u}_s,P\right)^T=\begin{pmatrix}0\\0\\-\dfrac{\int_A\left(f_d+\alpha_g\rho_g g\right)dA}{A}\\\dfrac{\int_A\left(f_d-f_c-\alpha_s\rho_s g\right)dA}{A}\end{pmatrix} \qquad (3.9\text{-}3.12)$$

where $C_{i,j}$ are coefficients explicitly expressed by terms of α_{s0}, α_{sw}, $\bar{\alpha}_s$, u_{g0}, u_{gw}, $\bar{u}_g$, U_{s0}, U_{sw} and $\bar{u}_s$.

We have ten unknowns (α_{s0}, α_{sw}, $\bar{\alpha}_s$, u_{s0}, u_{sw}, $\bar{u}_s$, u_{g0}, u_{gw}, $\bar{u}_g$, P) and 4 governing equations ((3.9-3.12)). These 4 governing equations describe the axial heterogeneous flow structure along the riser and could only be used to represent the change of averaged flow structure parameters $\bar{\alpha}_s$, $\bar{u}_g$, $\bar{u}_s$ and P. To close the problem of heterogeneous flow structure in both radial and axial directions, 6 additional intrinsic correlations (in radial direction) are needed. These 6 correlations shall quantify the radial transport of phases in terms of $\phi_0(z),\phi_w(z),\bar{\phi}(z)$, which link the transport properties of centerline to those at the wall and shall cover the flow structure of concentrations and velocities of both gas and solids phases across any cross-section of the riser. They shall

reveal the radial mass transport caused by the turbulence and collisional diffusion as well as the effect of wall boundary constraint on the flow structure.

Based on the non-slip condition of gas phase at the wall boundary, the gas velocity at the wall shall be zero. Thus, we have

$$u_{gw}(z) = 0 \tag{3.13}$$

The profile of gas velocity distribution in radial direction can be explained by boundary layer theory as an inner region of inviscid flow unaffected by viscosity (the majority of the flow), and a region close to the surface where viscosity is important (the boundary layer). The relationship of cross-sectional averaged gas velocity and the boundary layer thickness could be expressed as

$$u_g\Big|_{\frac{r}{R}=1-\frac{\delta}{R}} = \overline{u}_g \tag{3.14}$$

The formation mechanism of radial heterogeneous flow structure is the radial solids transport due to turbulent convection mass transfer and collisional diffusive mass transfer of solids particles. The intensity of turbulent mass transfer is dependent on the local turbulent intensity and the velocity gradient of solids and is from high velocity to low velocity. The intensity of mass transfer is dependent on the local solids concentration and the concentration gradient of solids phase, the direction is from high concentration to

low concentration. The net value of these two mass transfers gives the local solids transport.

$$J_{net} = J_{T.C.} + J_{C.D.} \tag{3.15}$$

where J_{net} is the net radial mass transfer rate of solids, while $J_{T.C.}$ and $J_{C.D.}$ are those due to turbulent convection and collisional diffusion respectively.

Assuming the turbulent convective and collisional diffusive mass transfer rates are respectively proportional to the local solids velocity and solids volume fraction gradients, we have

$$J_{T.C.} = -C_{turb}\frac{\partial u_s}{\partial r}; \qquad J_{C.D.} = -C_{diff}\frac{\partial \alpha_s}{\partial r} \tag{3.16}$$

where C_{turb} and C_{diff} are coefficients of turbulent convective and collisional diffusive mass transfer rates.

The mass balance equation of solids phase at the wall is written as

$$\frac{d}{dz}(\alpha_{sw}u_{sw}) = \left[-C_{turb}\frac{\partial u_s}{\partial r} - C_{diff}\frac{\partial \alpha_s}{\partial r}\right]_{r=R} \tag{3.17}$$

As the gas velocity near the wall is zero and the solids velocity shall be very low, the turbulence of the solids phase is much damped. It is safe to assume the solids particles at the wall are moving downwards with particle terminal velocity.

$$u_{sw} = -\frac{u_{pt}}{(1-\alpha_s)^n} \tag{3.18}$$

Noticing that due to the axi-symetricity of the riser flow, the radial gradients of solids velocity and solids volume fraction are zero. We shall have following governing equations based on the mass balance and momentum balance of solids phase at the centerline

$$\frac{d}{dz}(\alpha_{s0}u_{s0}) = 0 \tag{3.19}$$

$$\frac{d}{dz}(\alpha_{s0}u_{s0}^2) = f_{d0} - f_{c0} - \alpha_{s0}\rho_s g \tag{3.20}$$

where, f_{d0} and f_{c0} are the drag force and collisional force at the centerline of the riser.

Putting the characteristic values expressed by equation (3.13), (3.14) and (3.18) into radial profile expressions, the number of independent variables decreases to 7 (α_{s0}, α_{sw}, $\bar{\alpha}_s$, $\bar{u}_g$, u_{s0}, $\bar{u}_s$, P). They can be solved by the above coupled governing equations (equation (3.9)-(3.12), (3.17), (3.19) and (3.20)) in following simplified forms

$$[D]_{7\times7}\times\frac{d}{dz}\left(\alpha_{s0},\alpha_{sw},\bar{\alpha}_s,\bar{u}_g,u_{s0},\bar{u}_s,P\right)^T=[F]_{7\times1} \tag{3.21}$$

where **D** and **F** are coefficient matrixes explicitly expressed by terms of α_{s0}, α_{sw}, $\bar{\alpha}_s$, $\bar{u}_g$, u_{s0}, $\bar{u}_s$, P.

3.3 Results and Discussion

The model is validated by comparing the predictions with available experimental data previously published by different research groups for both axial evolution of hydrodynamics, including cross-sectional averaged solids volume fraction and pressure gradient along the riser, and the radial distributions of them in cross-sections of riser. After the validation, the model is then adopted for the prediction on heterogeneous flow structure evolutions in both radial and axial directions. The typical solids volume fraction, velocity and gas velocity are presented. The profiles are then be analyzed for the discussion of upwards core flow boundaries and the back-mixing solids mass flux.

The major experimental parameters for the experimental measurements of pressure gradient, cross-sectional solids volume fraction and radial profiles of solids volume fraction and velocity from published papers [Arena et al., 1985; Pugsley and Beruti, 1996] are listed in Table 3.1. The experimental data are specially selected for a wide range of operational conditions.

Table 3.1 Major Experimental Parameters

Case	Partilce type	d_p μm	G_s kg/m^{2}s	U_g m/s	ρ_s kg/m^3
1[1]	Glass beads	88	600	7	2600

2[1]	Glass beads	88	199	7	2600
4[3]	sand	208	400	8.5	2580
5[3]	sand	208	240	8.5	2580
6[3]	sand	208	700	8.5	2580

The prediction of solids volume fraction distribution along the riser was firstly compared with those of experimental measurements. Figure 3.2 shows the comparison of model predictions and experimental results of cross-sectional averaged solids volume fraction distribution along a CFB riser of 0.041m ID and 6.4m high with glass beads of three different solids mass flux [Arena et al, 1985]. The model prediction clearly shows a rapidly decreasing trend of solids volume fraction at the bottom of the riser and a relatively gentle slope of solids volume fraction gradient at the upper region of the riser. The model prediction fits the experimental data very well.

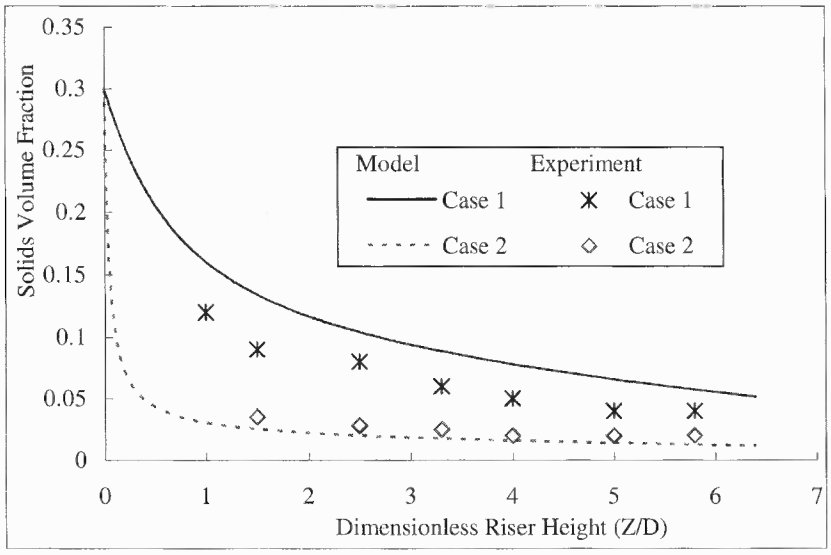

Figure 3.2 Solids volume fraction distribution of glass beads (Arena et al., 1985).

Figure 3.3 shows the comparison of model predictions and experimental results on the pressure drop along the riser under different conditions. Sand particles with a

diameter of 208 μm were used in a CFB riser of 0.041 m ID and 14.0 m high [Pugsley and Beruti, 1996]. The gas velocity in the riser is set to be fixed at 8.5 m/s under all operational conditions and the mass flux is variable at 240,400 and 700 kg/m^{2}s (case 4, 5 and 6), respectively. The pressure drop is very high at the bottom of the riser and tends to be constant near the top of the riser. The model gives a correct trend and a prediction in a bulk range on axial pressure gradient under all these conditions.

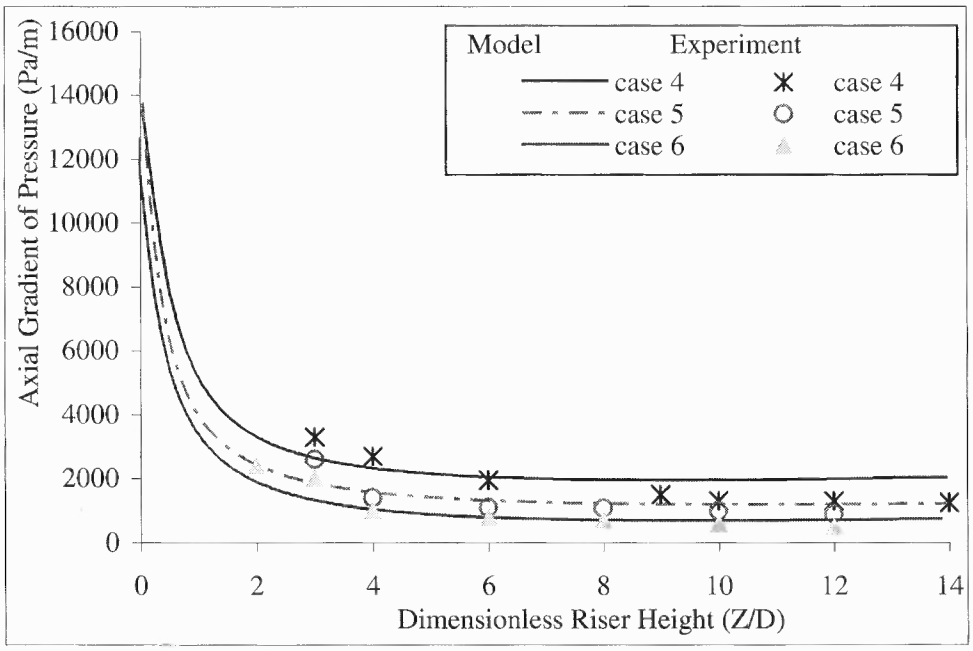

Figure 3.3 Pressure drop in the riser for sand (Pugsley and Beruti, 1996).

The modeling predictions on the radial profiles of hydrodynamics of riser flows are then be validated with different experimental measurements of solids volume fractions and solids velocities for different riser flows. The model predictions of radial profile of solids velocity in the cross-section are compared with experimental data [Yang et al., 1992] as shown in Figure 3.4. The experiments were conducted on a FCC riser with a diameter of 0.14 m. At a constant gas velocity of 4.33 m/s, the solids mass fluxes are changed from 21.9, 44.2 to 91.7 kg/m^2-s for different operational conditions. The model

accurately predicts the upward solids velocity at the center of the riser as well as the downwards solids mass fluxes near the wall for all cases.

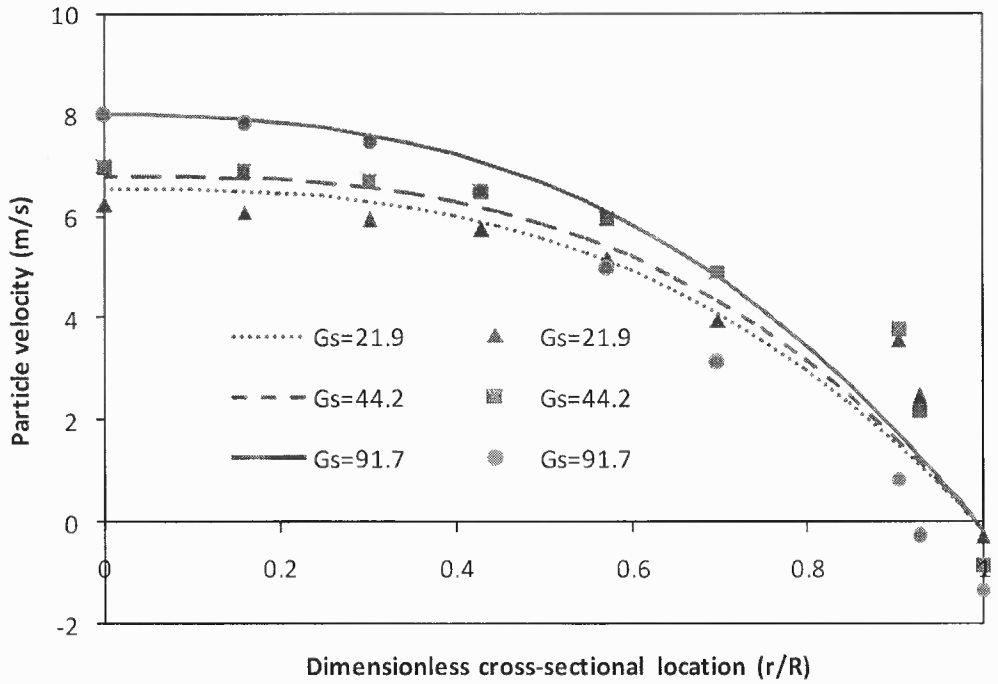

Figure 3.4 Radial solids velocity distribution (Yang et al., 1992).

The radial profile of solids volume fraction in a cross-section is shown in Figure 3.5. The experimental data [Herb et al., 1989] are collected from a 0.15 m diameter riser with a height of 10 m. The particle has a diameter of 68 mm and density of 1600 kg/m^3. The solids mass flux is 26 kg/m^2 and the gas velocity is 3.8 m/s. The model correctly predicts the denser distribution of solids volume fraction near the wall region and relatively lean distribution at the center.

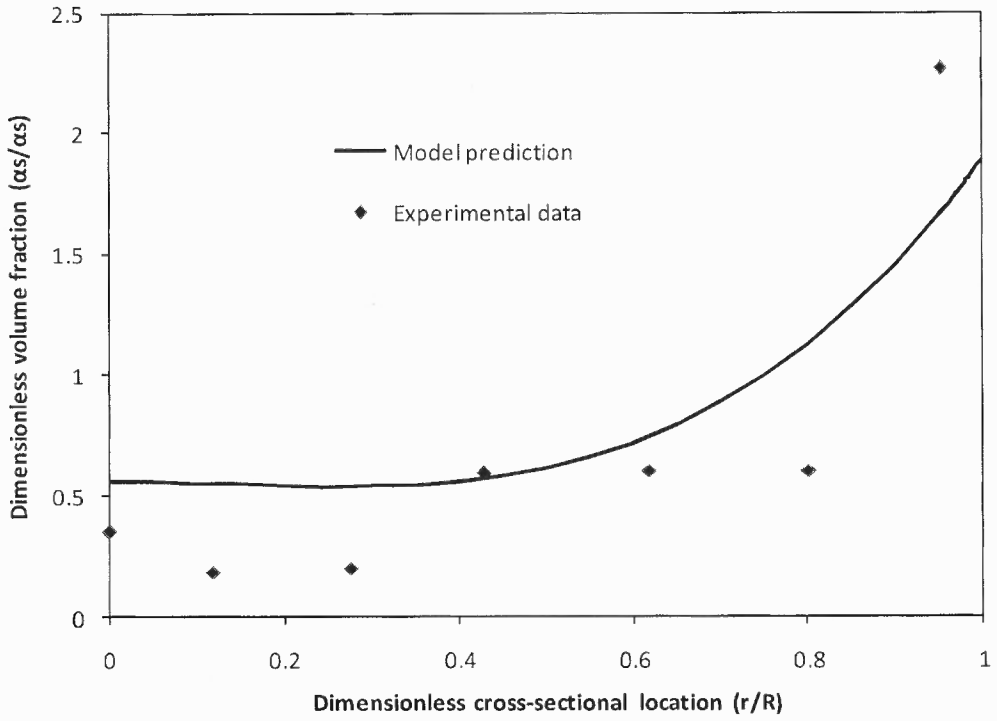

Figure 3.5 Radial profile of dimensionless solids volume fraction (Herb et al., 1989).

In order to investigate the evolution of heterogeneous structure of riser flow, the changing of radial profiles of solids velocity, volume fraction and gas velocity along the riser shall be analyzed in detail. A typical example of these evolutions is given below. The calculation is set to be in a CFB riser of 0.04m ID and 7m high. The particle diameter is set to be 100 μm with a density of 2500 kg/m^3. The cross-sectional averaged solids mass flux is 600 kg/m^{2}s with the gas velocity is 7 m/s.

Figure 3.6 shows the radial profiles of solids volume fraction at different height of the riser. At the bottom of the riser, a dense regime of solids exits. With the effect of inter-phase drag force, the solids are accelerated rapidly. The solids volume fraction decreases rapidly. In a height about 1 m, the solids phase transformed into a dilute regime. With the evolution of solids volume fraction in axial direction, the radial profile is also changed which is better presented in a dimensionless way (ratio to cross-sectional

averaged solids volume fraction) in Figure 3.7. At the bottom dense regime, the radial profile of solids volume fraction is relatively uniform. The difference between the wall and the center of the riser is not obvious. While, with the diluting of solids phase along the riser, the solids in the core region of the riser are accelerated much faster than those in the wall region. As a result, the solids volume fraction near the wall decreases much slower than that in the core region.

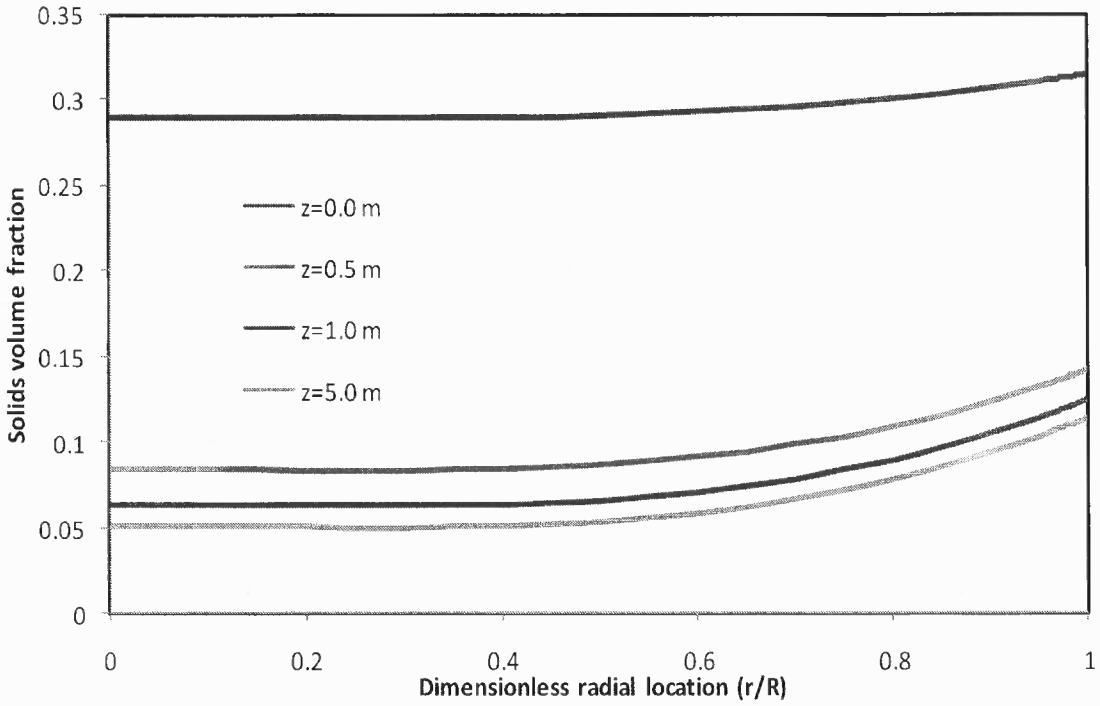

Figure 3.6 Solids volume fractions at different height of riser.

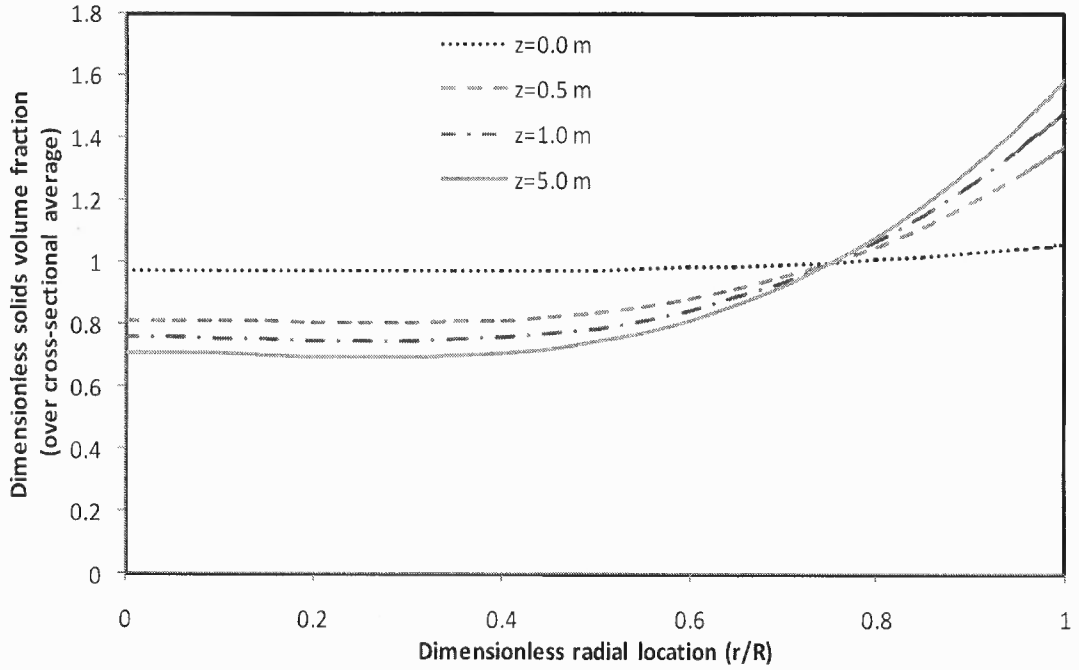

Figure 3.7 Dimensionless solids volume fractions at different height of riser.

The evolution of solids velocity distribution in radial direction is shown in Figure 3.8. The solids phase is gradually accelerated by the inter-phase interaction with gas phase. In all the profiles, the solids phase presents an upwards core flow region and a downwards wall flow region. With the increase of solids velocity, the area of downwards wall flow region decreases gradually. The downwards wall flow region in the model always exists even at the outlet of the riser. This is mainly due to our assumption of constant downwards solids velocity, which is set to be equal to the particle terminal velocity.

The gas velocity profile is also presented in Figure 3.9. The profiles always show a higher gas velocity near the core region and less gas velocity near the wall. As the power for accelerating and lifting up the solids particles is mainly supplied by the

pressure drop of gas phase, there is only slight change of gas velocity profile along the riser.

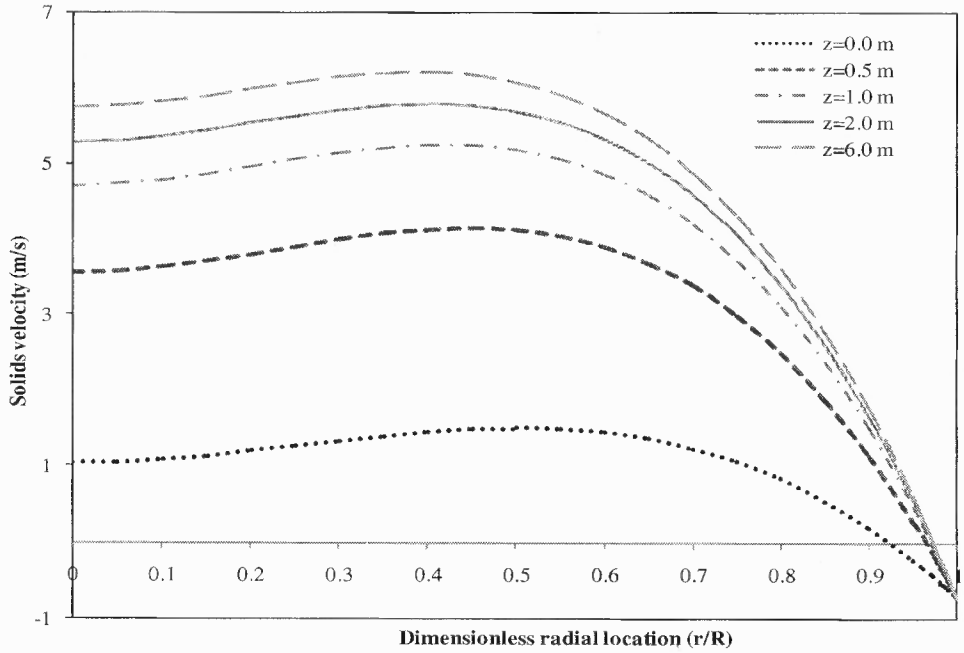

Figure 3.8 Radial profile of solids velocity at different height of riser.

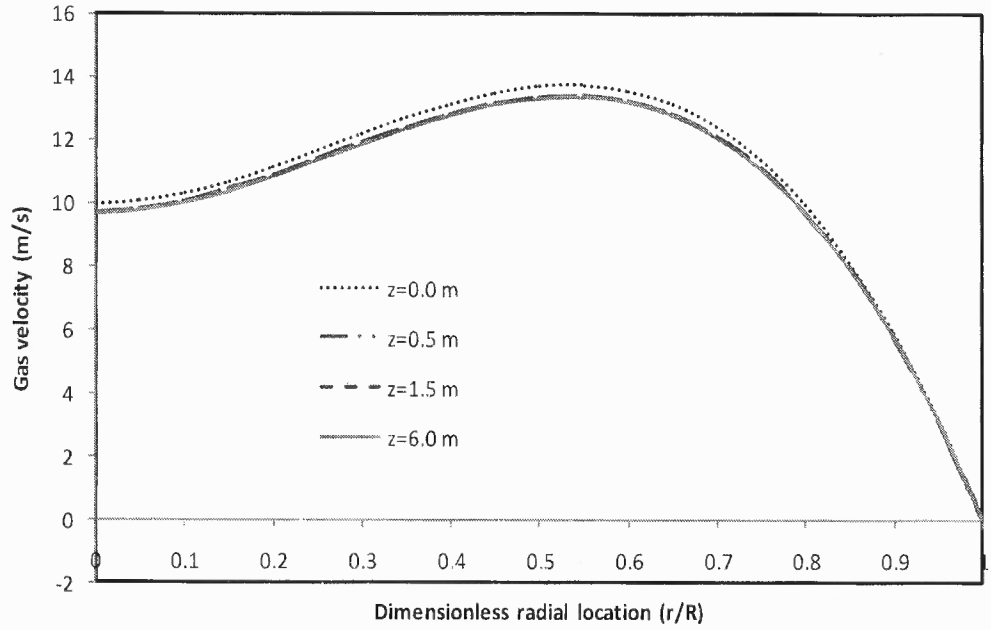

Figure 3.9 Radial profile of gas velocity at different height of riser

There is a special concern on the thickness of downwards wall flow region and the downwards solids mass flow rate as it is commonly accepted that most of chemical reactions of riser reactors take place in the core region of the riser while the solids in downwards wall flow are spent. The thickness of the wall region or the radius of core region is defined as distance from the wall or the centerline of the riser, divided by the point where the solids mass flux changes from upwards to downwards or the particle velocity is zero. Figure 3.10 gives the profile of the upwards solids flow boundary along the riser and the corresponding upwards flow area. It is shown that at the bottom of the riser where the solids volume fraction is high, the wall thickness is relatively large. With the acceleration of solids phase, this thickness the decreases dramatically and tends to be stabilized at the upper part of the riser where the solids phase is dilute.

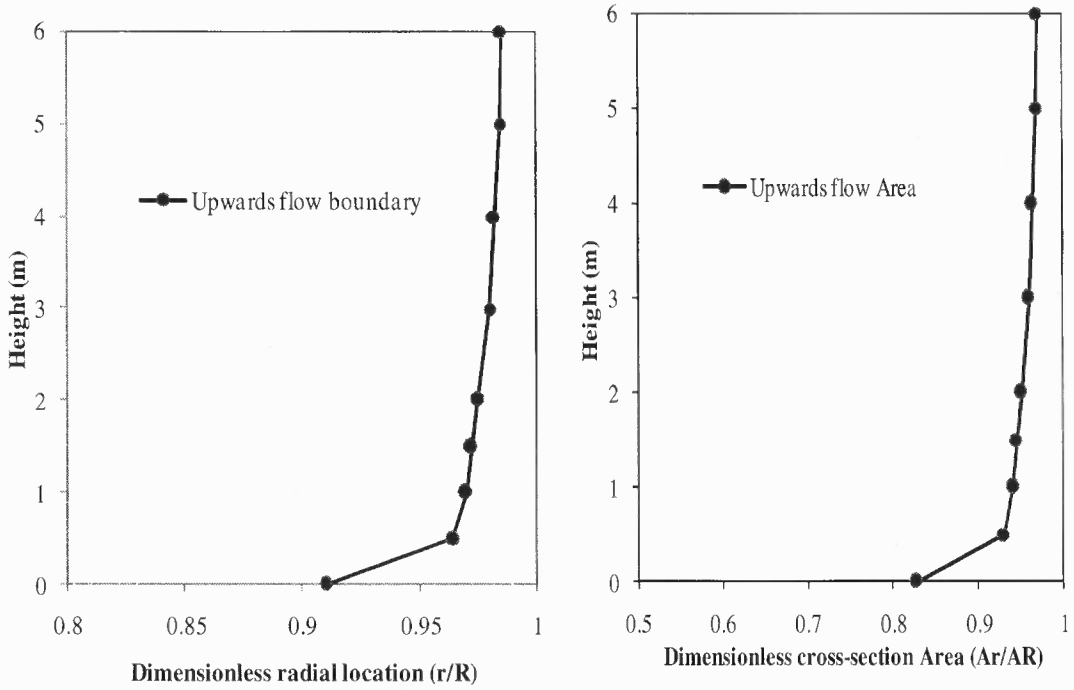

Figure 3.10 dimensionless upwards flow boundary and area along the riser.

Together with the area of core region, the upwards solids mass flow rate in the core region is also essential for the understanding of riser transportation. Based on the mass conservation of solids phase, the profile of upwards solids mass flow rate can be obtained from net solids circulating rate and downwards solids mass flow rate along the riser which is normally expressed by back-mixing ratio defined as downwards solids mass flow rate divided by net mass flow rate. Figure 3.11 shows the typical profile of back mixing ratio along the riser. At the bottom of riser where the solids velocity is low, the back-mixing is mostly severe. With the continuously accelerating of solids, the back-mixing weakens gradually. When the solids velocity tends to be stabilized, the back-mixing is fixed. Together with the gradually increased upwards flow area along the riser, it can easily be drawn that the upwards solids mass flux at the bottom of riser is much higher than that at the top of riser.

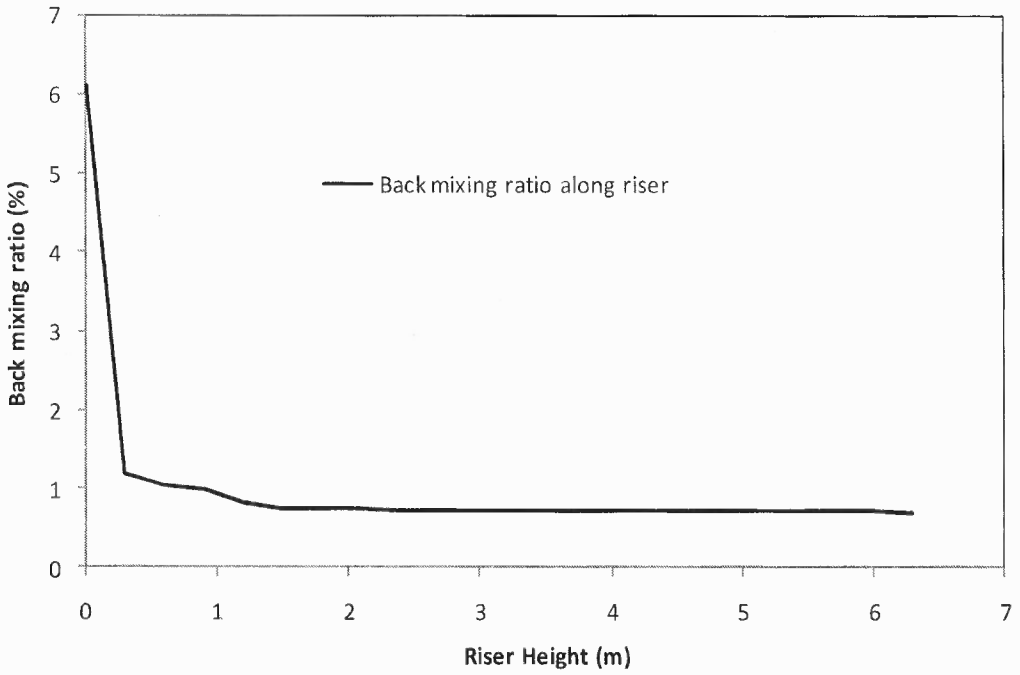

Figure 3.11 Back-mixing ratio of solids along the riser.

3.4 Conclusion

In this paper, a continuous model was developed to describe the heterogeneous structure of gas-solids riser flow in both radial and axial directions. The model adopted integral-differential form of governing equations based on mass and momentum conservations of gas and solids phases. The 3rd order polynomials are used to represent the radial profiles of hydrodynamic parameters of riser flow. Some radial transport mechanisms are proposed for the closure of the problem. The model predictions on the radial and axial profiles of key hydrodynamic parameters such as pressure drop, solids volume fraction and velocity are validated with previously published experimental data. A typical example is then analyzed for the radial and axial evolution of heterogeneous structure of riser flow. Some key parameters such as upwards flow boundary, back-mixing ratio are then analyzed and discussed.

CHAPTER 4

HYDRODYNAMICS AND REACTION COUPLING OF RISER REACTOR

Fluid catalytic cracking (FCC) riser reactors convert heavy petroleum oils into light hydrocarbon products. The conversion rates, in principle, are dependent upon the coupling of hydrodynamics and reaction kinetics in the gas-solids transport process. According to the rate law of reaction, the reaction rates are directly related to the local hydrodynamic properties, such as catalyst-to-oil ratio (CTO), temperature, concentrations of oil vapor components, pressure, and velocity or local residence time. The catalysts in a riser, on the other hand, undergo an accelerating transport process or a continuously diluting process, which is heavily influenced by the non-uniform cracking characteristics along the riser reactor. The yield of the riser reactor, which is determined by the mechanisms of catalytic chemical reaction, shall be modeled by the correct coupling of catalytic reaction model and the hydrodynamic characteristics of the riser. In the process of the riser reactor, the chemical reaction will change the components of gas phase, the local temperature and pressure, which will influence the evolution of hydrodynamics of riser flow. In turn, the evolution of hydrodynamics, which means the change of local phase volume fractions, velocities, temperatures and pressures, will influence the chemical reaction rate in the riser.

Most models on FCC in riser reactors use a simplified and de-coupled approach, namely, the hydrodynamics model of single-phase flow and reaction model that is based on the overall CTO of the entire riser. Such an approach not only neglects the non-uniform characteristics of hydrodynamics and reactions along the riser but also oversimplifies the intrinsic coupling of multiphase flow hydrodynamics and the cracking kinetics.

This chapter presents a one-dimensional steady-state modeling approach that is focused on the axial distributions and mechanistic coupling of local transport and reaction characteristics of catalysts and oils along the FCC risers. In both hydrodynamics and reaction models all variables are locally averaged over riser cross-sections. Reactions are assumed to be one-step and complete. A simple four-lump reaction scheme is adopted to simulate the cracking reactions. Modeling predictions are satisfactorily compared with the yield pattern and exit temperature of industrial scale plant data. Comparison against single-phase flow based modeling approach indicates that, the traditional methods tend to underestimate the vacuum gas oil (VGO) conversion percentage and gasoline yield in the lower part of the riser, while it overestimates these in the upper part of the riser. The axial distributions of the hydrodynamic properties of the gas-oil and catalyst are studied to exemplify the effects of reaction kinetics on the axial distributions of the flow properties. Some parametric effects on axial distributions of transport properties and yield characteristics are also demonstrated and discussed. In this study, we propose a one-dimensional steady-state modeling approach, which is focused on the axial distributions and mechanistic coupling of local transport and reaction characteristics of catalysts and oils along the FCC risers. In both hydrodynamics and reaction model all variables are locally averaged over riser cross-sections. For simplicity, the entrance and end effects of the riser are excluded in this model. It is assumed that, at the riser inlet, feed oil instantly vaporizes by the immediate contact with the hot catalysts from the regenerator. For the convenience of calculating the total energy inside the riser reactor, it is further assumed that the vapor and the catalyst are always in local thermal equilibrium. The wall of

the riser is assumed to be adiabatic. Hence, due to the endothermic cracking reactions, the local temperature of the vapor and catalysts decreases monotonically along the riser.

4.1 Chemical Reaction Scheme in Riser Reactor

The chemical reactions take place in the components of gaseous phase, which is influenced by the local solids volume fraction. Reactions are assumed to be one-step and complete. A simple four-lump reaction scheme (Lee *et al.*, 1989) is adopted to simulate the cracking reactions, as shown in Figure 4.1. It is assumed that the vacuum gas oil (VGO) is cracked into the most desired gasoline, by-products of gases, and coke. Since a FCC riser reactor is normally operated at high temperatures (e.g., in a range of 700 - 900 K), there occurs a secondary cracking reaction in which some gasoline further cracks into coke and gases. The gas oil and gasoline cracking reactions are assumed to be of the second and first order, respectively, in both single-phase flow and two-phase flow (riser flow) models. The inter-reaction between coke and gases is neglected. The small amount of steam and by-product H_2 are also neglected in the vapor mixture. All gas components are assumed to obey the ideal gas law. In addition, the coke is assumed to attach on the catalyst surface which will directly change the catalyst activity on cracking, however, the change in catalyst size is neglected. We also assume identical catalyst activity decay function for all the reactions among lumps.

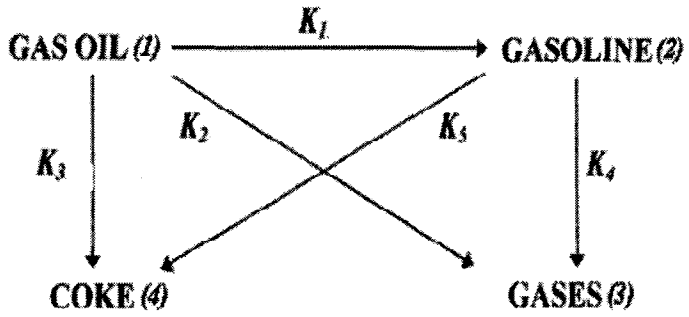

Figure 4.1 Four-lump model for gas oil cracking reactions (Lee et al., 1989).

4.1.1 Single-phase (gas) Flow Model

The reaction scheme of single-phase (gas) flow model adopted in this study is developed from the one which is originally proposed by Ali *et al.* (1997). As the reactions continuously proceed along the riser, the composition of gas phase changes and the vapor moles expand, resulting in a typical 3-4 fold increase in the gas superficial velocity. While, in their model, only the change in gas superficial velocity was considered, the effect of molar expansion was simply ignored. In our study, in order to make a direct and intuitive modeling, the vapor molar expansion are considered with the expression of gas species as weight fraction of hydrocarbons. The mass and energy balance for lumps in the single-phase flow model can thus be given as:

Gas oil:

$$\frac{dy_1}{dz} + \frac{\Phi_s A \alpha_g \rho_g}{F_g}\left[k_1 + k_2 + k_3\right] y_1^2 \rho_g \alpha_g = 0 \qquad (4.1)$$

Gasoline:

$$\frac{dy_2}{dz}+\frac{\Phi_s A\alpha_g\rho_g}{F_g}\left[\left(k_5+k_4\right)y_2-k_1{y_1}^2\rho_g\alpha_g\right]=0 \tag{4.2}$$

Light Hydrocarbon Gases:

$$\frac{dy_3}{dz}+\frac{\Phi_s A\alpha_g\rho_g}{F_g}\left[k_4y_2+k_2{y_1}^2\rho_g\alpha_g\right]=0 \tag{4.3}$$

Coke:

$$\frac{dy_4}{dz}+\frac{\Phi_s A\alpha_g\rho_g}{F_g}\left[k_5y_2+k_3{y_1}^2\rho_g\alpha_g\right]=0 \tag{4.4}$$

Energy balance:

$$\frac{dT}{dz}+\frac{A\alpha_g\rho_g}{\left(G_sc_{ps}+G_gc_{pg}\right)}\left[{y_1}^2\rho_g\alpha_g\sum_{i=1}^{3}k_i\Delta H_i+y_2\sum_{j=4}^{5}k_i\Delta H_i\right]=0 \tag{4.5}$$

Two inlet conditions, the inlet gas volume fraction and the temperature of gas and solids, must be independently determined. As noted, most of the plug flow reaction models just simply assume the inlet gas volume fraction to be unity or there is no clear method to determine the gas void fraction at the riser inlet. While, a suitable way to determine the inlet gas void fraction of a plug flow riser would be via the total pressure drop across the reactor since the gas volume fraction along the reactor is constant and the flow could be

treated as a flow through the porous media. The relationship of gas volume fraction and the total pressure drop in the fixed or moving bed can be estimated by Ergun equation as (Fan & Zhu, 1998):

$$-\frac{dp}{dz}=150\frac{\left(1-\alpha_g\right)^2}{\alpha_g^3}\frac{\mu.U}{\varphi^2 d_p{}^2}+1.75\frac{\left(1-\alpha_g\right)}{\alpha_g^3}\frac{\rho U^2}{\varphi d_p}+\left(1-\alpha_g\right)\rho_s g \tag{4.6}$$

An energy balance between hot regenerated catalyst and gas oil feed at inlet is use to determine the temperature of the hydrocarbon mixture and catalyst at the riser inlet. Under the steady state condition, the inlet temperature of the riser is given by:

$$T_0=\frac{G_g.c_{pg}.T_B+G_s.c_{ps}.T_{s0}-G_g.\left(\Delta H_{fg}+m_g.c_{pl}\left(T_B-T_{l0}\right)\right)}{G_s.c_{ps}+G_g.c_{pg}} \tag{4.7}$$

4.1.2 Two-Phase Flow (Riser Flow) Model

Based on the reaction scheme shown in Fig. 4.1, the reaction equation for each component of reactant is given by:

Gas-oil:

$$U_g\frac{dC_1}{dz}+C_1\frac{dU_g}{dz}=-\Phi_s\left(k_1+k_2+k_3\right)C_1^2 \tag{4.8}$$

Gasoline:

$$U_g \frac{dC_2}{dz} + C_2 \frac{dU_g}{dz} = \Phi_s \left(\frac{M_1}{M_2} k_1 C_1^2 - (k_4 + k_5) C_2 \right) \tag{4.9}$$

Light Gases:

$$U_g \frac{dC_3}{dz} + C_3 \frac{dU_g}{dz} = \Phi_s \left(\frac{M_1}{M_3} k_2 C_1^2 + \frac{M_2}{M_3} k_4 C_2 \right) \tag{4.10}$$

Coke:

$$U_g \frac{dC_4}{dz} + C_4 \frac{dU_g}{dz} = \Phi_s \left(\frac{M_1}{M_4} k_3 C_1^2 + \frac{M_2}{M_4} k_5 C_2 \right) \tag{4.11}$$

The rate equation of the i^{th} conversion can be described using the Arrhenius type expression:

$$k_i = k_{i0R} \lambda \exp\left(-\frac{E_{ai}}{RT_i} \right) \tag{4.12}$$

where k_{i0R} is pre-exponential factor for two-phase flow, which is derived from the single-phase flow model. It is noted that the pre-exponential function in the single-phase flow, k_{i0}, is mass-based with the assumption of inlet as gas volume fraction to be unity. The pre-exponential factor for two-phase flow is molar-based, which is expressed as:

$$K_{i0R} = \left(\frac{M_i}{\alpha_g \rho_g} \right) K_{i0} \tag{4.13}$$

The distribution of catalyst is non-uniform along reactor height, which is presented by typical S-shape. In the dense phase region, the catalyst concentration is very high, with high slip velocity between gas and solids phase. The catalysts are gradually accelerated under the interaction with gas phase, and finally reach the relatively steady and dilute regime at the upper part of riser. The non-uniform distribution of the catalyst in the FCC reactor has significant influence on the reaction rates. Most of the modeling work on FCC reactor, so far used single-phase flow hydrodynamic modeling and reaction model that is based on the overall CTO of the entire riser, which assumes uniform catalyst volume fraction along riser height and ignored the effect of the non-uniform distributions of solids on reaction kinetics. The effects of the local hydrodynamics on the kinetic reactions can be coupled by introducing local catalyst-to-oil ratio instead of overall catalyst-to-oil ratio (CTO). λ represents the local catalyst to oil ratio, which was related to the overall mass flow ratio of catalyst to oil (CTO) or the feeding mass flow rate ratio of catalyst over hydrocarbon gases by:

$$\lambda = \left(\frac{\alpha_s}{\alpha_{s,avg}} \right)^n \cdot \left(\frac{C}{O} \right)_{overall} \tag{4.14}$$

where $\alpha_{s,avg}$ represents the average solid volume fraction along entire riser, which was calculated for overall CTO for riser reactor. The average solid volume fraction can be expresses as:

$$\alpha_{s,avg} = \frac{1}{L}\int_0^L \alpha_s .dz \tag{4.15}$$

The power index 'n' in the above Eq. (17-c) is introduced to obtain the S-shape of catalyst volume fraction along the reactor. The power index 'n' is selected as 0.25 in this study, which is obtained from data match against industrial plant measurements. Replacing the overall catalyst to oil ratio with the localized ratio, the cracking reaction rate can be directly related to local mass ratio of catalyst and oil instead of phase velocities only, because this localized mass ratio of catalyst and gas oil is independent of local phase velocities and only related to local phase concentration in any control volume.

The parameter Φ_s represents the catalyst decay of activity due to coke deposition. In the present work, we used catalyst deactivation function proposed by Pitault *et al.* (1994)

$$\Phi_s = \frac{X+1}{X+\exp(Y.C_c)} \tag{4.16}$$

where X and Y are deactivation constants, taken as 4.29 and 10.4, respectively and C_c is the weight percent of coke on catalyst.

The energy balance between the hot catalyst and gas oil feed during the reaction is given by;

$$\left(\alpha_s \rho_s u_s c_{ps} + \alpha_g \rho_g u_g c_{pg}\right)\frac{dT}{dz} + \left(r_3 + r_5\right)\left(c_{ps} - c_{pg}\right)T = -\sum_{i=1}^{5} r_i . \Delta H_i \qquad (4.17)$$

where ΔH_i is reaction heat for the i^{th} endothermic cracking reaction.

4.2 Equations of Hydrodynamics

In the radial direction, a core-annulus (wall) flow structure is typical, with a dilute core upward gas-solids flow and a downward flow of dense solids near the wall [Herb et al., 1992]. We shall also notice that the hydrodynamic characteristics of core flow and wall boundary flow are quite different [Zhou et al., 1994]. The solids in the core region are accelerated by the carrying gas flow, while those transported to the wall region by turbulent diffusion and collision move downwards under gravity and the wall friction. A two-regional averaged approach may be possible yet involve more complexity in both modeling mechanisms and mathematic treatment on the interaction of the two regions. A simple approach is to construct the hydrodynamic models solely on the core region whereas the effect of the wall flow is reflected through the continuous area change and inter-regional phase transfer along the core boundary. In this section, the development of a one-dimensional model on the hydrodynamics of upward flow in the core region of gas-solids riser is presented. The core cross-sectional area and effective solids mass flux

from the wall region are formulated using published correlations [Harris et al., 2002; Johansson et al., 2007].

The main part of the riser would consist of three regimes, namely, the dense regime, acceleration regime and dilute regime. The classification of these regimes is based on the hydrodynamic characteristics of solids flow. The solids in the core region are continuously accelerated and diluted by the carrying gas, whereas the core solids flow is enhanced by solids gained from the wall in the dense phase transport regime and weakened by solids lost to the wall in the dilute transport regime. The radial distributions of solids and gas phases are more or less uniform in the core region, which provides some justifications to the simple one-dimensional modeling approach in this study. The schematic diagram of two zone one-dimensional flow structure is shown in Figure 4.2.

When the governing equations only in the core region depicted in Figure 4.3 are considered, all phase variables in the previous general governing equations in chapter 3.1 shall be replaced by pre-averaged values over the cross-section of the core region, hence, are functions of axial coordinate only.

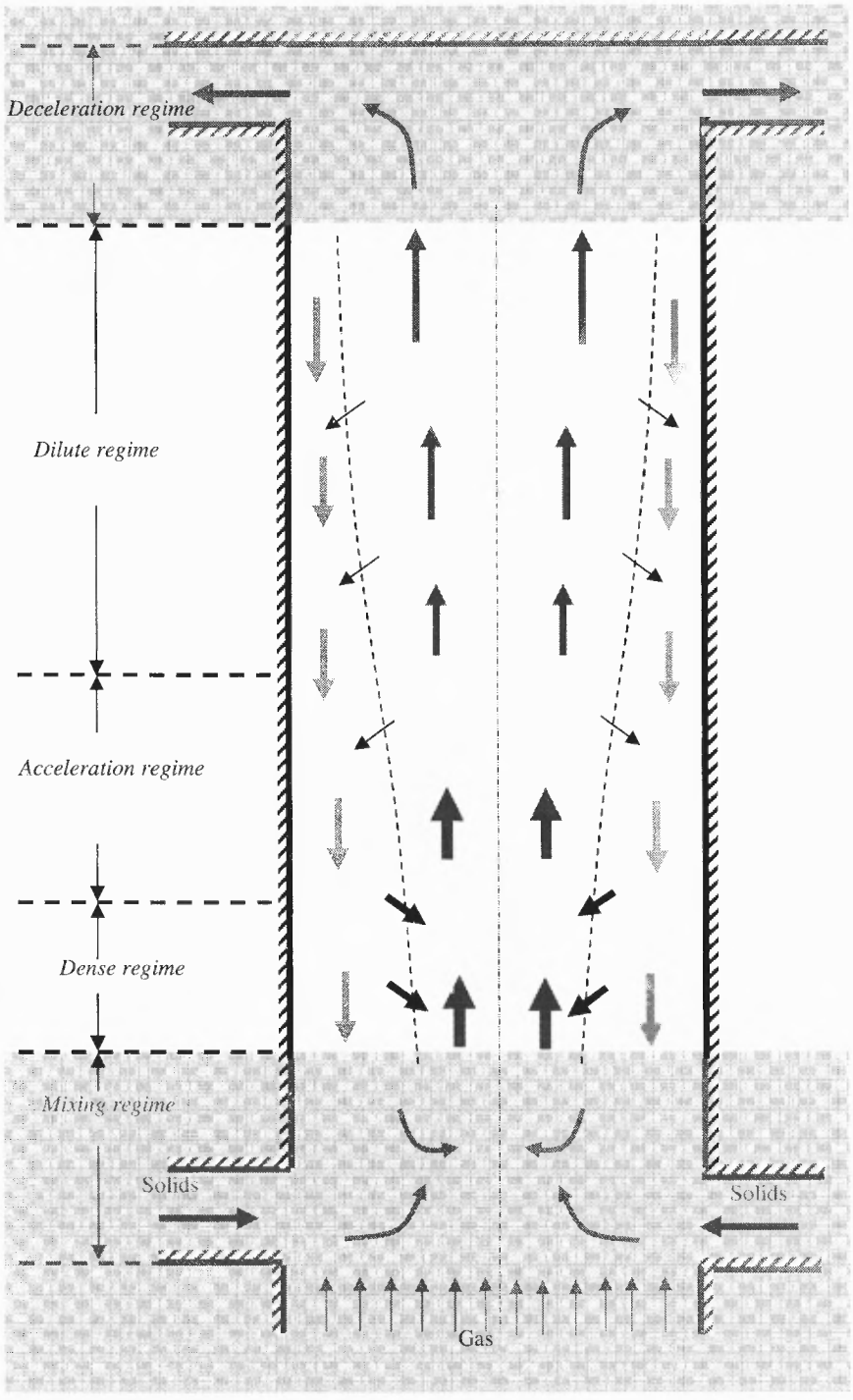

Figure 4.2 Flow structure in a gas-solids riser.

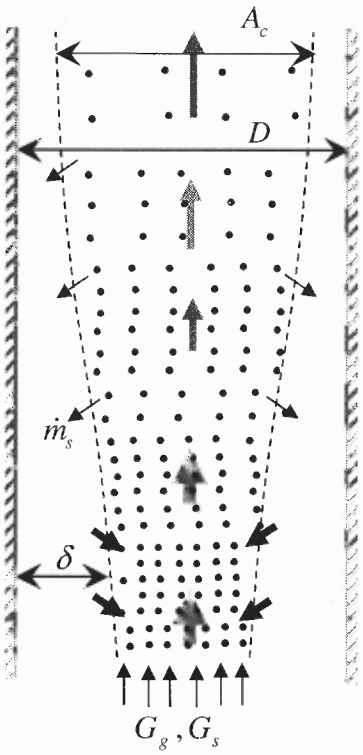

Figure 4.3 Computational domain of core-flow model.

Assuming the gas in the wall boundary is stagnant, the mass continuity equations of gas and solids phases in the core region can be expressed, respectively, by

$$\frac{d}{dz}(\alpha_g \rho_g u_g A_c) = 0 \tag{4.18}$$

$$\frac{d}{dz}(\alpha_s \rho_s u_s A_c) = \dot{m}_s \tag{4.19}$$

where α_g and α_s are the volume fractions of gas and solids phases, A_c is the cross-sectional area of core region, $\dot{m}_s$ is the mass transfer rate of solids across the core boundary.

The momentum equation of gas phase can be obtained as

$$-\alpha_g \frac{dP}{dz} = \frac{1}{A_c}\frac{d}{dz}(\alpha_g \rho_g u_g^2 A_c) + \alpha_g \rho_g g + F_D \tag{4.20}$$

where the four terms on the right hand side represent, respectively, the gas shearing force on core boundary, gas acceleration, gravitational force, and inter-phase momentum transfer between gas and solids (commonly known as drag force). The momentum equation of solids phase is given by

$$-\alpha_s \frac{dP}{dz} + F_D = \frac{\tau_{sc} l_c}{A_c} + \frac{1}{A_c}\frac{d}{dz}(\alpha_s \rho_s u_s^2 A_c) + \alpha_s \rho_s g + F_c \tag{4.21}$$

The area of core region, A_c, in above governing equations could be determined by investigating the wall boundary thickness, δ, along the riser. According to the measurements [e.g., Patience & Chaouki, 1993; Rhodes & Laussman, 1992], the wall boundary is originated from the mixing regime and the thickness is gradually reduced towards the top exit of a riser.

There is a strong phase transfer (especially mass transfer of solids) across the core-wall regional boundary. The solids flow rate across the core boundary, $\dot{m}_s$, can be determined in terms of the back-mixing ratio defined as the ratio of the solids flow rate in the wall region to the overall net solids mass flow rate:

$$R_b = \frac{\dot{m}_{sw}}{G_{s,net} A_R} \tag{4.22}$$

where $\dot{m}_{sw}$ is the solids mass flow rate in the wall region; and $G_{s,net}$ is the net mass flux of solids of the riser. Therefore, by solids mass balance along the riser, the solids mass flux in any cross-section of the core region can be expressed as

$$G_{sc} = (1 + R_b) G_{s,net} \frac{A_R}{A_c} \tag{4.23}$$

The above two parameters can be obtained from the results of continuous model described in Chapter 3. The wall boundary thickness is defined by the distance from the wall to where the solids velocity reaches to zero. The net solids mass flow rate in wall region, $\dot{m}_{sw}$, can be obtained by simply making following integration,

$$\dot{m}_{sw} = \int_{R-\delta}^{R} \alpha_s \rho_s u_s 2\pi r dr \tag{4.24}$$

Put the parameters of core region area and solids mass flux in the core region into above hydrodynamic model, the above 6 governing equations for chemical reactions together with the 4 hydrodynamic equations can solve for 10 independent variables (α_s, U_s, U_g, C_1, C_2, C_3, C_4, ρ_g, P, T). The problem is closed.

By solving coupled equations of hydrodynamics and reaction kinetics, our model can predict not only the yield pattern but also various axial profiles of transport parameters, such as temperature, pressure, phase velocities and phase concentrations, along a riser. We can also study the effect of reaction kinetics on hydrodynamic properties of gas-solid phase vice versa.

4.3 Inlet Conditions

The proposed model is based on a simplified one-dimensional approach, namely, all variables are averaged over the cross-section of a riser. In order to solve the coupled governing equations outlined in above section, appropriate inlet boundary conditions as well as inlet location must be predetermined, especially when comparing with measurement data from actual industrial or laboratory systems. Since our model excludes the vaporization and initial liquid/vapor/catalyst mixing effects, the starting location of our model simulation conceptually should be somewhere above the locations of feed nozzles. The length of mixing region (from initial location of complete vaporization to where one-dimensional flow begins in the core) can be roughly estimated by a recent study of You et al. (2009a), which shows that the length is typically much less than that of acceleration, dilution and other flow regimes in the riser. Hence, in this study, the model inlet is approximated at the immediate downstream of oil feeding locations assuming an instant vaporization and mixing.

At the given inlet pressure P_0, the inlet catalyst volume fraction α_{s0} is estimated in a way so that the resulted pressure at the riser exit will reasonably agree with the measurement or common sense. Based on the catalyst mass flow rate and catalyst volume fraction α_{s0}, the catalyst initial velocity U_{s0} is thus calculated. Due to the simple assumptions of an instant evaporation and thermal equilibrium at feed inlet, the temperature of the catalyst is adjusted to a value so that, using the plug flow model, the gasoline yield and VGO conversion at the riser exit can match the measured ones. The average density of gas oil ρ_{g0} is determined from the ideal gas law, and consequently, the gas initial velocity U_{g0} is obtained. The initial mole concentrations for C_2, C_3 and C_4 are

null, assuming no cracking occurs before the model inlet. Thus, all ten inlet boundary conditions are determined from feeding and operation conditions. In the riser flow model, the determination of power index 'n' in Eq. (17-c) is based on the best match to the published industrial plant data (e.g., Derouin et al., 1997).

4.4 Model Validation and Comparisons

The model predictions are validated against two sets of FCC plant data (Ali et al., 1997; Derouin et al., 1997). Table 4.1 lists the operation parameters and physical properties of catalyst and lump components, whereas Table 4.2 lists the reaction constants and heat of reaction for the four-lump reaction. It must be pointed that the FCC reaction properties, namely, the pre-exponential factors, activation energies, and reaction heats in the four-lump model are the same in both cases, indicating a possibility of finding a common set of properties for general modeling predictions.

Table 4.1 Operation Parameters and FCC Properties of Riser Reactors

Operation parameters & FCC properties	**Case 1** (Ali & Rohani, 1997)	**Case 2** (Derouin et al., 1997)
Catalyst feed rate (kg/s)	144	470
VGO feed rate (kg/s)/CTO	20/7.2	85/5.5
Inlet temperature of VGO feed (K)	496	650
Inlet temperature of catalyst (K)	960	960
Riser diameter (m)	0.8	1
Riser height (m)	33	35
Catalyst diameter (μm)	70	75
Inlet riser pressure (atm)	2.9	3.15
Catalyst density (kg/m^3)	1800	1800

Specific heat of lumps -Gas(J/kg-K)		3299	3299
Specific heat of lumps –Liquid(J/kg-K)		2671	2671
Catalyst specific heat (J/kg-K)		1150	
Molecular weight (kg/kmol)	VGO	400	
	Gasoline	100	
	Gas	50	
	Coke	400	

Table 4.2 Pre-exponential Factor, Activation Energy, and Reaction Heat

Cracking Reaction	ΔH_i kJ/kg	K_{i0} s^{-1}	E_a kJ/kmol
VGO → Gasoline	195	1457.5	57359
VGO → Light Gases	670	127.59	52754
VGO → Coke	745	1.98	31830
Gasoline → Light Gases	530	256.81	65733
Gasoline → Coke	690	0.022	66570

Figure 4.4 shows a comparison between two-phase flow model predictions with single-phase flow model and reported plant data (Ali et al., 1997 and Derouin et al., 1997) on yield and conversion distributions along the risers. It shows a fairly good agreement in comparison between two-phase flow model predictions and reported plant data (Ali et al., 1997 and Derouin et al., 1997) on yield and conversion distributions along the risers.

The gradient of yield of each lump predicted by two-phase flow model is higher in dense phase region of reactor than the rest of the riser regions as shown in Fig. 4.4 (b), showing that most of the cracking reactions occur in the dense phase transport. In addition, the gradient of each lump gradually decreases along the riser, showing a gradual slowdown

of cracking reaction in the dilute phase transport region. A quantitative analysis can be illustrated in Fig. 4.4 (a). For FCC plant data of Ali et al. (1997), the overall unconverted VGO is about 32.1% whereas the gasoline yield is about 53.5% at the exit of riser. It is noted that at the riser height of 5 m (15% of the total riser height), the unconverted VGO has already reached about 54.5% and gasoline yield is about 36.7%, which are about two third of the total conversion and yield. This clearly demonstrates that the bottom of the riser is the place where most cracking reactions occur and VGO cracks down to lighter molecules. The model prediction for the conversion rate is underestimated by about 16% at the riser exit in comparison with the plant data of both Ali et al.(1997), and Derouin et al.(1997), which may be due to the simplifications in both hydrodynamic and reaction models as well as the uncertainties in measurements.

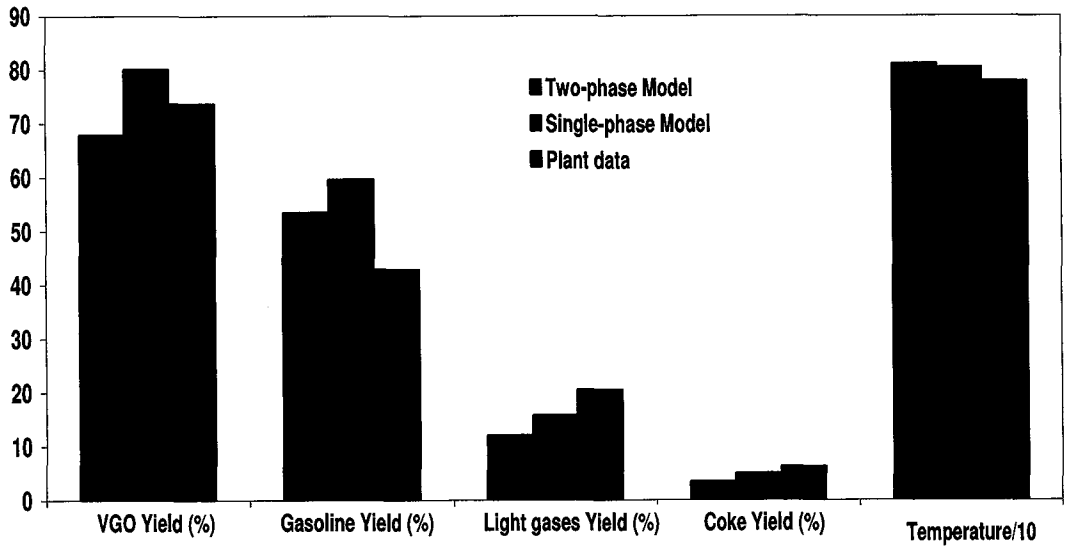

(a) Conversion or yield (at riser exit) of two models against plant data from Ali et al., 1997

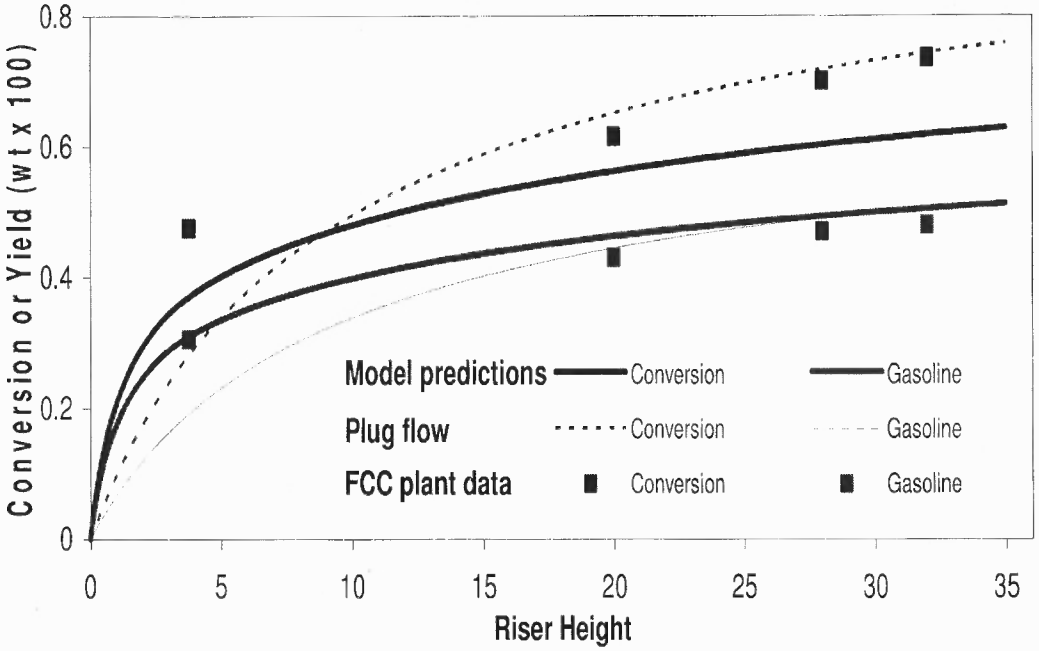

(b) Conversion or yield of two models against plant data from Derouin et al., 1997

Figure 4.4 Comparisons of models predictions with FCC plat data.

The comparison of two-phase model predictions and single-phase flow model predictions on yields and conversions against the FCC plant data of Ali et al. (1997) and Derouin et al. (1997) are also shown in figure 4.4. Figure 4.4(a) shows that both models predictions of various yields reasonably agree with the plant data at the exit of riser. However, as shown in Fig. 5.2(b), in the dense transport regime, our model predictions shows a better agreement than those of the single-phase flow reaction model, indication a better prediction of the intensive cracking in that regime. This may be partly attributed to the very high local catalyst-to-oil ratio in bottom of riser. In the dilute phase transport regime, our two-phase flow riser model shows a more asymptotic trend of the gasoline yield, which agrees with the trend of reported plant data. We may conclude that the implementation of local catalyst-to-oil ratio and better hydrodynamics model (especially in

the dense transport regime) yields better predictions of the reaction characteristics of FCC riser reactors.

The typical parameters in FCC riser reactors include phase velocities of gas and catalysts, riser temperature, riser pressure, and molar concentrations. The axial distributions of these parameters are exemplified in Figure 4.5 to Figure 4.8, using operation conditions of Case 2 in Table 4.1.

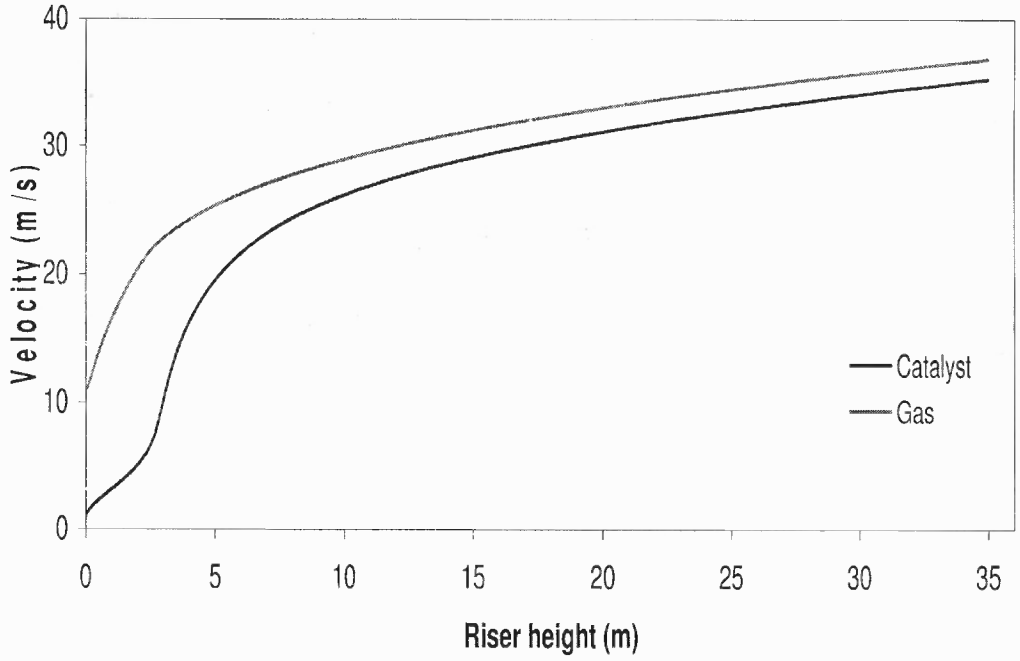

Figure 4.5 Model predictions of phase velocity.

Figure 4.5 shows the model predictions of gas and solid phase velocities along the riser reactor. The gas phase velocity is increasing along the reactor height, which is due to the reaction-induced vapor moles expansion. It is interesting to notice that in the lower part of the riser, the increase in gas phase velocity is much larger than the rest of the riser; this is attributed to the intensive cracking reactions in bottom of riser. In the dilute region, the increase in gas velocity is very gradual due to the slower reaction rate and decreasing

pressure. The velocity of solids phase follows the same trend of gas phase velocity, as the solids are carried by gas phase. However in dense phase region the slip velocity is very high, this is because of more intensive energy dissipation due to inter-particle collisions.

Figure 4.6 shows the axial profile of temperature with the assumption of local equilibrium between gas feed and catalyst. Due to the endothermic cracking reaction, the temperature drops monotonically along the riser. Since the reaction rates are strongly dependant upon temperature, the decrease in temperature slows down the cracking reactions and hence the gradient of temperature along the reactor height.

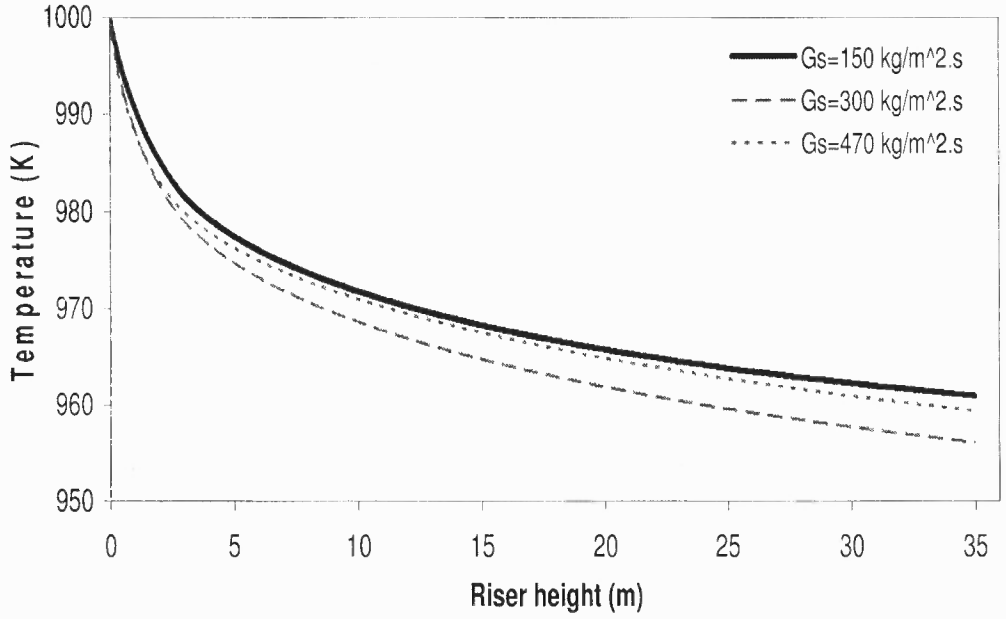

Figure 4.6 Model prediction of riser temperature.

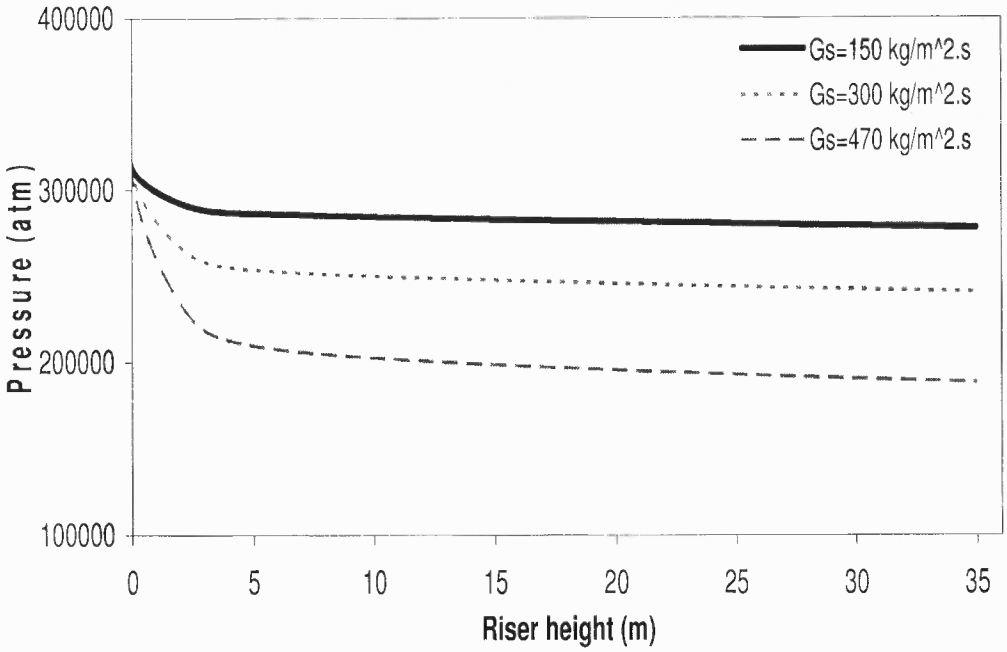

Figure 4.7 Model prediction of riser pressure.

Figure 4.7 shows the model prediction of axial distribution of pressure along the riser reactor, with a reasonable trend. The pressure decreases very fast in the dense phase region, partly due to the intensive inter-particle collisions induced energy dissipation, temperature drop due to endothermic cracking reaction, and kinetic energy for catalysts acceleration and dense phase transport. In the dilute phase region of riser, the slow pressure decrease is mainly due to the catalyst transport and friction loss between gas/solids and wall. It is should be pointed that the effect of back mixing in the riser flow can be significant, which would render a sever increase in catalysts transport in the core region and hence an increase pressure drop along the riser. However, in the current hydrodynamics model, the effect of back mixing from the wall region is ignored for the simplicity of the model. This effect will be accounted for in the future modeling.

Figure 4.8 shows the model predictions of molar fraction of different species of riser reactor during cracking process. The VGO cracks to form the gasoline, light gases and coke whereas the gasoline is further cracked into light gases and coke, as shown in Fig. 1. The mole concentration of VGO decreases very fast in the dense phase transport and acceleration regime of reactor due to the intensive cracking reactions, which results in the rapid increase in gasoline, gases and coke molar concentration in this region. In the dilute phase region, the reaction rates are very low, so the molar concentrations of VGO and other lumps approach to asymptotic values in this region.

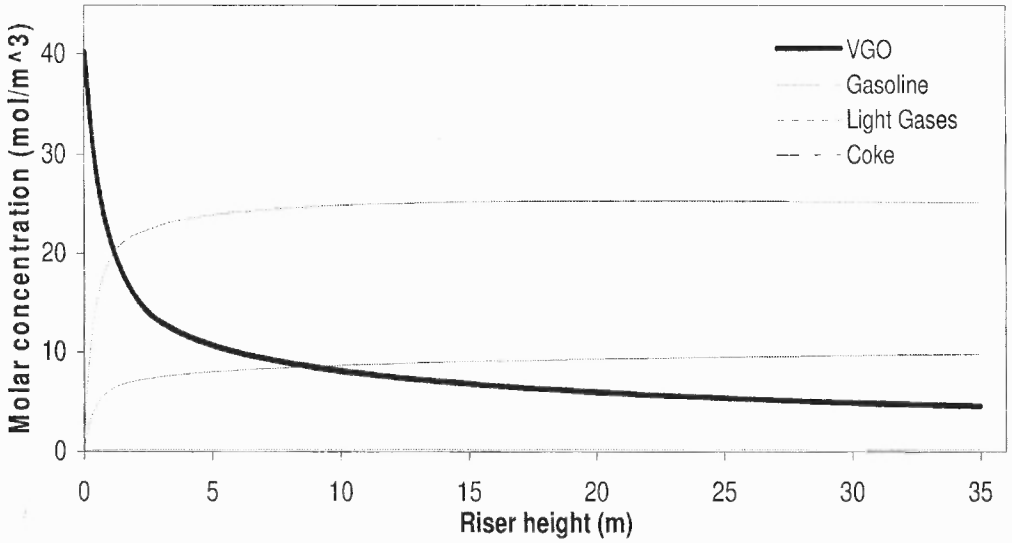

Figure 4.8 Model prediction of lump molar concentration.

We also extend our discussion into the parametric effect of power index "n", catalyst-to-oil ratio and inlet temperature on the reaction yields, which may be beneficial to the optimization of reactor design and operation.

Figure4.9 shows the sensitivity of the index "n" on the gasoline yield from our riser model (for Case-2 in Table 4.1) against the plant data of Derouin et al. (1997). The index

varies from 0 to 0.75. It is shown that the curves of gasoline yield with index 'n' of 0.25 and 0.5 best match against the measured gasoline yields. Further investigation on the conversion of VGO shows the index 'n' of 0.25 better matches the measurements than that from 'n' of 0.50. Therefore, the index n of 0.25 is selected for both cases of study.

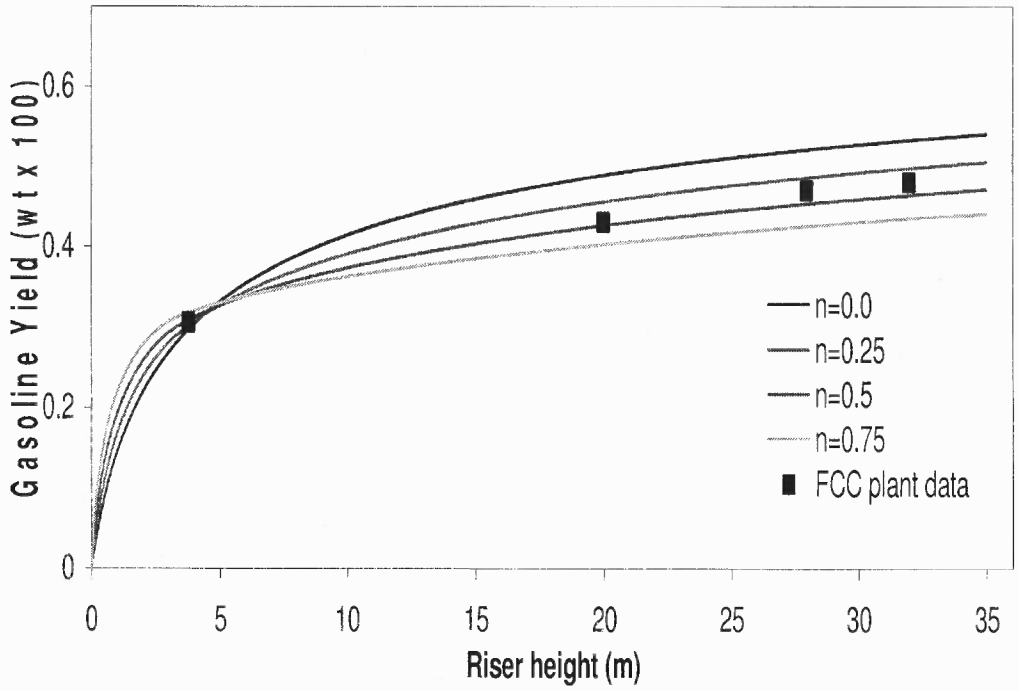

Figure 4.9 Parametrical study of power index "n".

Figure 4.10 shows the effect of catalyst-to-oil ratio on final yields of lumps, with CTO from 5.0 to 9.0. All other parameters are from Case-1 in Table 4.1. The change in CTO from 5.0 to 9.0 is equivalent to the change in catalyst mass flux rate from 100 to 180 kg/m^2 s at a fixed feed rate of VGO.

As shown in Figure 4.10, with the increase in CTO from 7.2 to 9.0 (increased by 25%), the gasoline yields increases about by 7.3% and the unconverted VGO drops by 17% at riser exit. The effect of CTO on product yield is quite significant in the dense phase

region, where the catalyst volume fraction is very high compare to other portion of riser and hence higher cracking reactions. It is noted that, with the same increase in CTO, at a riser height of 5 m (about 15% of total height), the increase in gasoline yield is about 40.5% and decrease in unconverted VGO is about 33%. Similarly, the decrease in CTO from 7.2 to 5.0 (about 30%) leads to the decrease of gasoline yield by 14% and the increase in unconverted VGO by 31% at riser exit. Above examples suggest that the effect of CTO is strong on yields and their axial distributions in the FCC riser reactor.

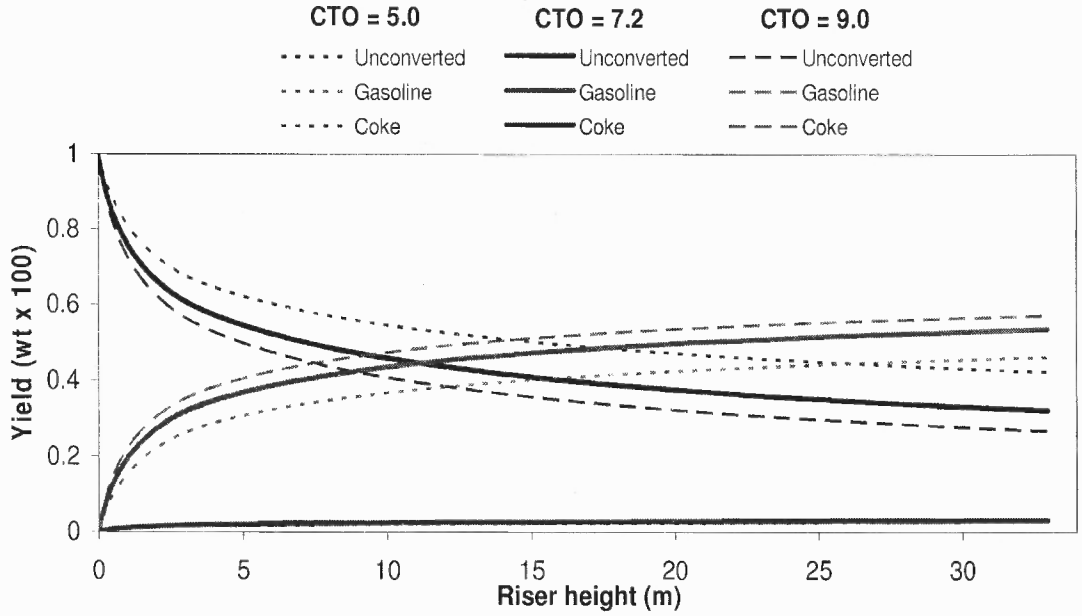

Figure 4.10 Parametric study of catalyst to oil ratio.

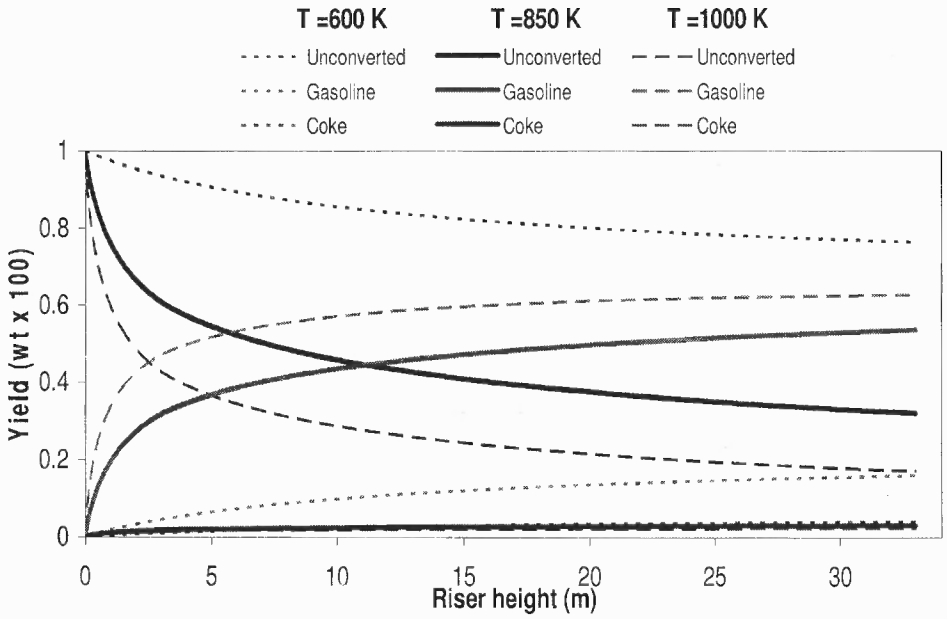

Figure 4.11 Parametric study of inlet temperature.

The reactor inlet temperature is a key parameter in governing the reaction rates. The increase in riser inlet temperature results in significant increase in the reaction rates and hence the yields of products, as shown in Figure 5.9. For the parametric study, the temperature is changed from 600K to 1000K whereas the other parameters are kept the same as those of Case-1 in Table 1. With the temperature increased from 850K to 1000K (increased by 17.6%), the gasoline yield increases by 17% and the unconverted VGO drops by 46.7% at reactor exit, whereas at a riser height of 5 m (about 15% of total height), the increase in gasoline yield is 40.5% and decrease in unconverted VGO is about 33%.

The selectivity of the gasoline for single-phase and two-phase flow model is studied at riser exit by changing the inlet temperature to the riser for reactor operating conditions of both Ali et al., 1997 and Derouin et al., 1997.

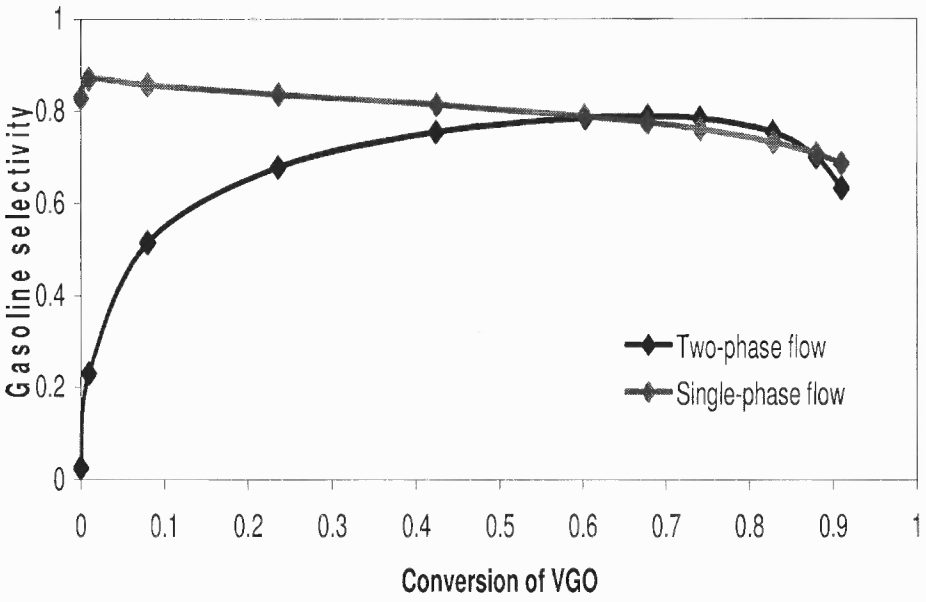

(a) Plant data of Ali et al., 1997

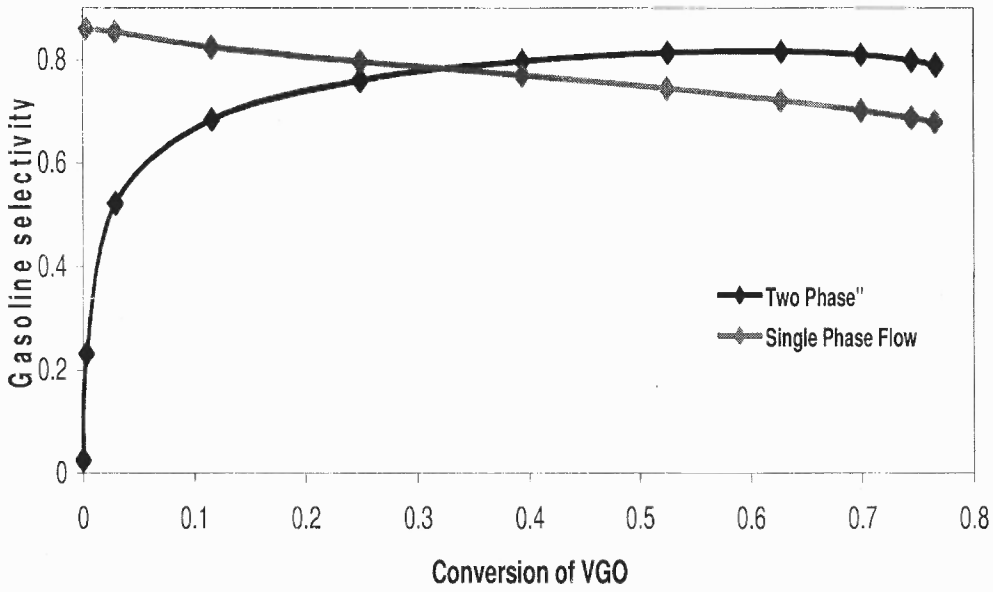

(b) Plant data of Derouin et al., 1997

Fig.4. 12 Comparison of gasoline selectivity between two-phase and single-phase flow models at riser exit.

The gasoline selectivity for two-phase flow model increases initially, reaches to the maximum and then decreases with increase in VGO conversion, while that of the

single-phase model shows decrease in gasoline selectivity with increase in VGO conversion for reactor operating conditions of both Ali et al., and Derouin et al. For VGO conversion above 55%, both two-phase and single phase flow model shows almost identical gasoline selectivity for riser operating conditions of Ali et al., but for operating conditions of Derouin et al., two-phase flow model shows higher gasoline selectivity than single-phase flow model as shown in Figure 4.12. The maximum gasoline selectivity for two-phase flow model is 80% for Ali's and Derouin's data for VGO conversion of 70% and 60% respectively, as shown in Figure 4.2 (a) & (b) respectively.

4.5 Conclusion

A comprehensive mechanistic model is proposed in this paper, which describes the mechanism to consider the inter-coupling between gas-solid flow hydrodynamic and cracking reaction kinetics. The emphasis of this model is to develop a framework, to simultaneously simulate the multiphase flow hydrodynamics, cracking reaction and their inter-coupling characteristics in riser reactors. The predictions from the proposed riser model have been reasonably validated against the two different sets of published FCC plant data. The FCC reaction properties, namely, the pre-exponential factors, activation energies, and reaction heats in the four-lump model are the same in both cases, indicating a possibility of finding a common set of properties for general modeling predictions. The model predictions are also compared with traditional reaction model whose hydrodynamics is based on plug flow. It shows that flow hydrodynamics has significant influence on reaction cracking kinetics, which has not evoked enough attention in the past. In order to test model robustness and extend model applications, a series of parametric

CHAPTER 5

EVAPORATION AND REACTION OF SPRAY FEED REACTANT

Due to its advantage over gaseous phase on the transportation, storage, big specific volume and easy handling, most of important industrial applications use industrial reactant in liquid phase. The reactants are injected at the bottom of riser reactor in the form of gas-droplet spray. The sprays of gas-droplet which has a relatively high momentum then interact with the gas and particles entrained from the environmental fluidized bed, heated up and evaporated. During the process of evaporation, some reactions of gasified reactants will take place with the inter-action of catalytic solids particles. The resulting gas and solids characteristics after the evaporation of all the liquid reactants are the components for the transport of main body of riser reactor discussed in previous chapter. Thus, the understanding the hydrodynamic and reaction characteristics of spray jet of feed reactant into bottom of riser reactor is essential for the understanding the performance and flow structure in the main body.

During the spray, evaporating and reacting process of the spray jet into fluidized bed, mass, momentum, heat and energy transfers among phases present and are coupled with each other complicatedly. To investigate the characteristics of spray of feed reactant into the bottom of riser reactor, the hydrodynamics, evaporation process and chemical reaction mechanisms shall all be modeled. In this chapter, the characteristics of spray jet of feed reactant into bottom of riser are investigated by a modeling approach that couples the hydrodynamics of spray jet with its reaction characteristics. The profiles of spray jet,

of cracking reaction in the dilute phase transport region. A quantitative analysis can be illustrated in Fig. 4.4 (a). For FCC plant data of Ali et al. (1997), the overall unconverted VGO is about 32.1% whereas the gasoline yield is about 53.5% at the exit of riser. It is noted that at the riser height of 5 m (15% of the total riser height), the unconverted VGO has already reached about 54.5% and gasoline yield is about 36.7%, which are about two third of the total conversion and yield. This clearly demonstrates that the bottom of the riser is the place where most cracking reactions occur and VGO cracks down to lighter molecules. The model prediction for the conversion rate is underestimated by about 16% at the riser exit in comparison with the plant data of both Ali et al.(1997), and Derouin et al.(1997), which may be due to the simplifications in both hydrodynamic and reaction models as well as the uncertainties in measurements.

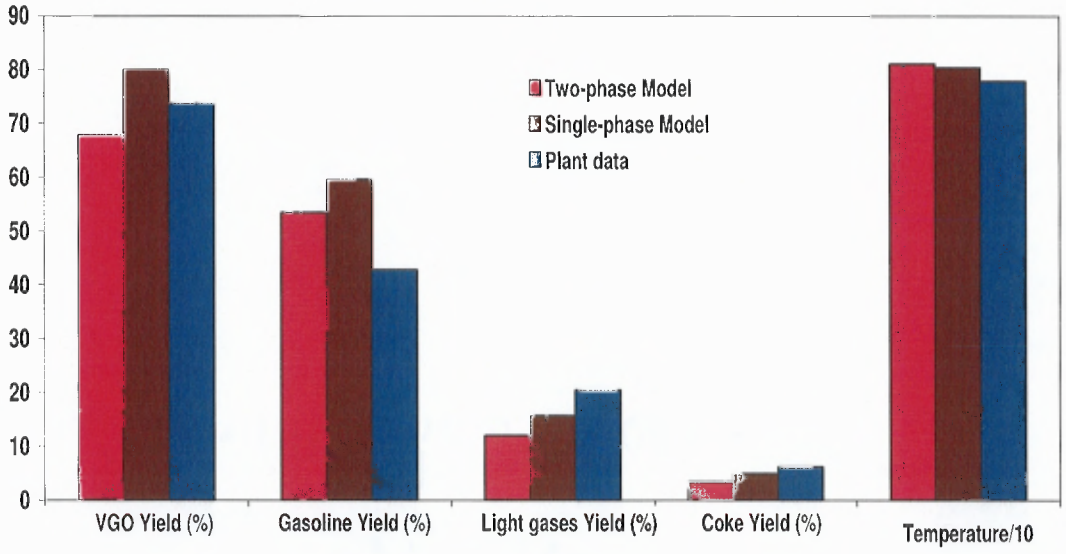

(a) Conversion or yield (at riser exit) of two models against plant data from Ali et al., 1997

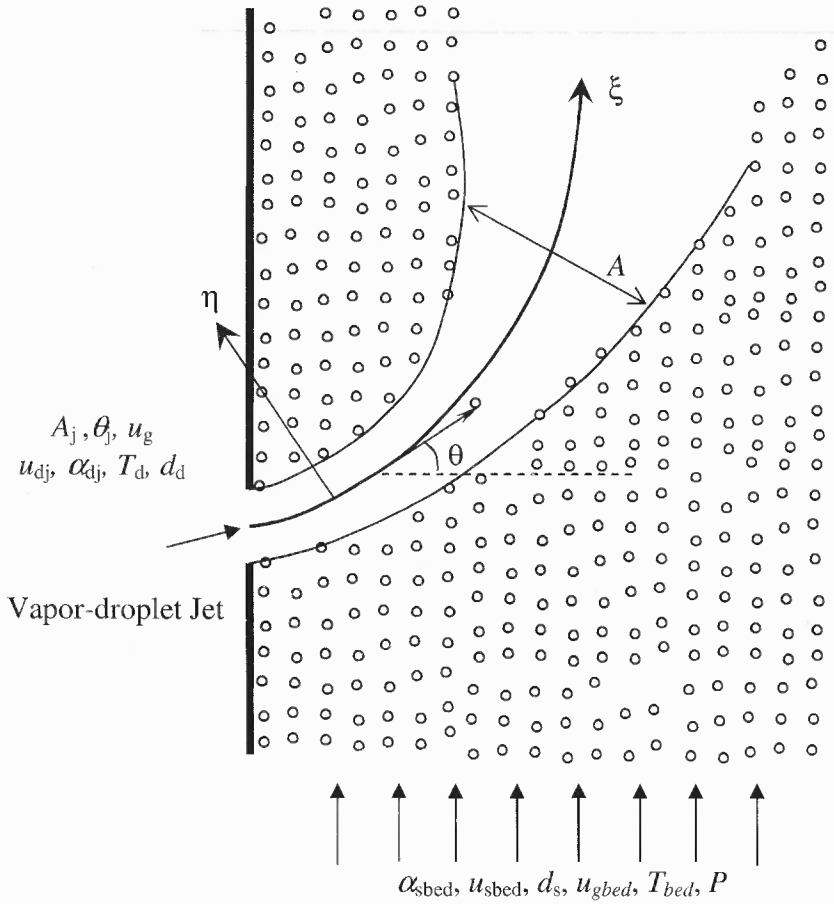

Figure 5.1 Schematic diagram of spray jet into gas-solids riser flow.

5.1.1 Hydrodynamic Equations

Governing equations of the flow mixing involves dynamic interactions among gas-solid-liquid three phases via the strong coupling of momentum, heat and mass transfer. The phase trajectory and mixing characteristics in the jet region can be readily described using the deterministic Lagrangian trajectory approach in a coordinate system (ξ, η) attached to the centerline of the jet, as shown in Figure 5.1. All phases are assumed to be moving along the ξ direction only within the jet mixing region while the ambient gas and solids are engulfed into the mixing stream by jet entrainment. The jet mixing region is

bended due to the convective as well as the collision momentum transfer from flowing round gas-solid flow.

Based on the mass, momentum, and energy balance over a control volume in the (ξ, η) coordinates, as shown in Figure 5.2, general governing equations of each phase can be constructed in differential forms. It is noted that, due to the assumption of the identical flow centerline of each phase in the mixing region, only one momentum equation in the η direction is independent. The most representative η-momentum equation should be selected from the phase whose inertia effect is the minimum among the three phases. Hence, in the following, the η-momentum equation of gas-vapor mixture is used to define the bending of the centerline.

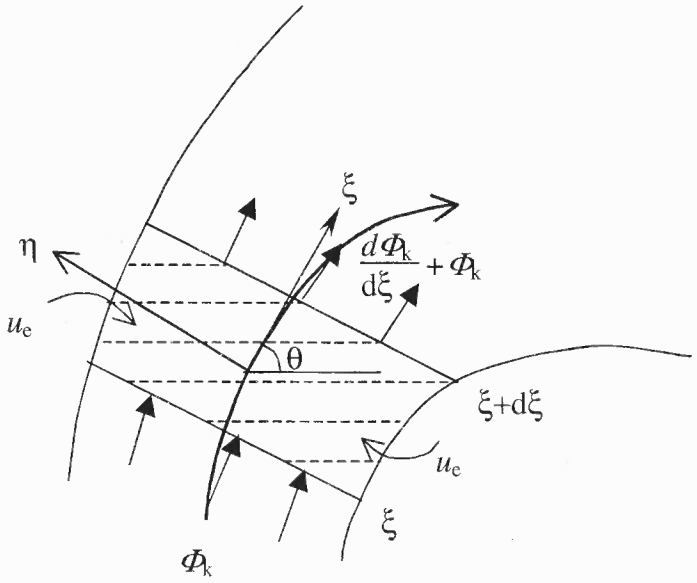

Figure 5.2 Schematic diagram of control volume.

(1) Deflection angle of spray jet

The deflection of the spray jet is due to the increasing in its η-component momentum by ambient gas-solids entrainment, penetration as well as drag forces from gas-solids flow

around the jet; its rate can be expressed by a ratio of η-component momentum increasing rate to its total momentum in ξ direction as

$$\frac{d\theta}{d\xi}=\frac{\left[\dot{m}_{ge}l_e u_{ge}+\left(\dot{m}_{se}l_e+\dot{m}_{sp}D_d\right)u_{se}\right]\sin\theta}{\left(\alpha_g\rho_g u_g^2+\alpha_d\rho_d u_d^2+\alpha_s\rho_s u_s^2\right)A}+\frac{F_r}{\left(\alpha_g\rho_g u_g^3+\alpha_d\rho_d u_d^3+\alpha_s\rho_s u_s^3\right)A} \tag{5.1}$$

where the first term of right hand side represents the η-component momentum increasing due to gas-solids entrainment and diffusive penetration; the second term represents the effect of drag force on jet trajectory due to gas-solids flow around the jet. In the equation, θ is the spray jet angle; ξ is the jet trajectory; $\dot{m}_{ge}$ $\dot{m}_{se}$ and $\dot{m}_{sp}$ are gas entrainment rate, solids entrainment rate and solids penetration rate, respectively; l_e, D_d and A are circumference, diameter and cross-sectional area of jet; F_r is the drag force due to gas-solids flow around jet; α, u, ρ are volume fraction, velocity and density with subscripts g, d, s represent gas, droplet and solids, respectively.

(2) Vapor-gas Phase

The continuity equation is derived based on a mass balance among the increase rate of mass flow along ξ, gas entrainment rate across the jet boundary, gas diffusion rate from jet area due to convection and vapor generation rate by droplet evaporation, which yields

$$\frac{d}{d\xi}\left(\alpha_g\rho_g u_g A\right)=\dot{m}_{ge}l_e+\dot{m}_v A-\gamma\alpha_g\rho_g u_g A \tag{5.2}$$

where the first term of right is the contribution of entrainment; the second term is the total droplet evaporation rate; and the third term is the total gas diffusion rate from jet area which is expressed as a portion function, γ, of the total gas mass flow rate.

The ξ-component momentum equation is obtained based on a ξ-component momentum balance among the increase rate of momentum flow, momentum entrainment carried by the gas entrainment across the jet boundary, momentum generation due to droplet evaporation, and interfacial momentum transfer between the mixture and droplets as well as between the mixture and solids. Hence the ξ-component momentum equation is given by

$$\frac{d}{d\xi}\left(\alpha_g \rho_g u_g^2 A\right) = \dot{m}_v u_d A + \dot{m}_{ge} u_{ge} l_e \cos\theta - \gamma \alpha_g \rho_g u_g^2 A - \left(F_{Dd} + F_{Ds}\right) A \tag{5.3}$$

where the four terms in the right hand side represent the momentum change due to evaporation, gas entrainment, gas diffusion from jet and drag forces on droplets and solids which are denoted with F_{Dd} and F_{Ds}, respectively.

The conservation of thermal energy is obtained based on the energy balance among the increase rate of flow enthalpy, the energy entrainment from the ambient gas stream, heat generation due to phase change, heat generation due to chemical reaction, heat transfer between droplets and the mixture as well as the heat transfer between solids and the mixture, which is given by

$$\begin{aligned}\frac{d}{d\xi}(\alpha_g \rho_g u_g C_{pg} T_g A) = {} & \dot{m}_{ge} l_e C_{pg} T_{bed} - \gamma \alpha_g \rho_g u_g C_{pg} T_g A \\ & + \dot{m}_v (L + h_{dd}) A + \left(E_{Cs} - E_{Cd}\right) A - E_R\end{aligned} \tag{5.4}$$

where the terms in right hand side are the heat change due to gas entrainment, gas diffusion from jet area, droplet evaporation, convective heat transfer with solids and droplet, E_{cs} and E_{cd}, and reactive heat generation, E_R. In the equation, c_{pg} is the thermal capacity of gas-vapor mixing phase; T_g and T_{bed} are temperatures of the gas phase and gas-solids fluidized bed; L and h_{dd} stand for the latent heat and enthalpy of droplet at saturated temperature.

(3) Droplet phase

Spray of fast evaporating liquids typically evaporates within the jet mixing region. The continuity equation is based on the fact that the decrease rate of mass flow along ξ is due to the droplet evaporation, which gives

$$\frac{d}{d\xi}(\alpha_d \rho_d u_d A) = -\dot{m}_v A \tag{5.5}$$

The ξ-component momentum equation is generated from a ξ-component momentum balance among the increase rate of droplet momentum flow, interfacial forces between droplets and the gaseous mixture, solids-droplets collision, and the momentum transfer due to droplet evaporation, which leads to

$$\frac{d}{d\xi}\left(\alpha_d \rho_d u_d^2 A\right) = -\dot{m}_v u_d A + \left(F_{Dd} - F_{Cds}\right) A \tag{5.6}$$

where F_{cds} is the solids-droplets collisional force.

An energy balance is established among the increase rate of flow enthalpy of droplets, heat convection from the gaseous mixture, heat transfer from solids by collision, radiative heat transfer from ambient hot solids and the latent heat transfer due to droplet evaporation. Thus the energy equation of droplets is obtained by

$$\frac{d}{d\xi}(\alpha_d \rho_d u_d C_{pd} T_d A) = E_{Cds} + E_{Cd} - \dot{m}_v (L + h_{dd}) A + E_{Rad} \tag{5.7}$$

Where C_{pd} is the heat capacity of droplet, E_{Cds} is heat transfer between solids and droplets due to collision and E_{rad} is the radiative heat transfer rate from ambient hot solids in fluidized bed.

(4) Solids phase

It is assumed that solids enter the mixing region only by jet entrainment and penetration due to solids diffusion, all entrained solids flow along the ξ-direction only. Thus the mass balance equations is obtained by

$$\frac{d}{d\xi}(\alpha_s u_s \rho_s A) = \dot{m}_{se} l_e + \dot{m}_{sp} D_d \tag{5.8}$$

The momentum equation is obtained based a momentum balance among the increase rate of solids momentum flow, momentum transfer by solids entrainment, interfacial forces from the gaseous mixture, and momentum changes due to solids-droplets collision, which is expressed by

$$\frac{d}{d\xi}\left(\alpha_s \rho_s u_s^2 A\right) = (\dot{m}_{se} l_e + \dot{m}_{sp} D_d) u_{se} \cos\theta + \left(F_{Ds} + F_{Cds}\right) A \tag{5.9}$$

The energy equation of solids phase is based on an energy balance among the increase rate of flow enthalpy of solids, heat transfer from the solids entrainment, heat transfer by droplets-solids collision, and heat transfer between solids and gaseous mixture, which gives

$$\frac{d}{d\xi}(\alpha_s \rho_s u_s C_{ps} T_s A) = -E_{Cds} - E_{cs} + (\dot{m}_{se} l_e + \dot{m}_{sp} D_d) C_{ps} T_{bed} \tag{5.10}$$

where C_{ps} is solids heat capacity.

5.1.2 Reaction Equations

The chemical reactions take place in the components of gaseous phase as long as the reactant evaporated from droplet phase. Reactions are assumed to be one-step and complete. Here, we still adopt the simple four-lump reaction scheme described in chapter 4 to simulate the cracking reactions in spray jet region. The only difference is that besides the four reactive components, i.e. VGO, gasoline, light gases and coke, there is another non-reactive spice, steam, which comes from the carrying media of spray jet and gas entrainment from ambient fluidized bed which uses steam as the lubricating media of solids. Based on the characteristics of reactions among each reactive component and the mass conservation, the governing equations of the components can be expressed as,

VGO:

$$\frac{d}{d\xi}(C_1 u_g A) = -\Phi_s \left(k_1 + k_2 + k_3\right) C_1^{\,2} A + \frac{\dot{m}_v A}{M_1} - \gamma C_1 u_g A \tag{5.11}$$

Gasoline:

$$\frac{d}{d\xi}(C_2 u_g A) = \Phi_s \left(\frac{M_1}{M_2} k_1 C_1^{\,2} - (k_4 + k_5) C_2 \right) A - \gamma C_2 u_g A \tag{5.12}$$

Light Gases:

$$\frac{d}{d\xi}(C_3 u_g A) = \Phi_s \left(\frac{M_1}{M_3} k_2 C_1^{\,2} + \frac{M_2}{M_3} k_4 C_2 \right) A - \gamma C_3 u_g A \tag{5.13}$$

Coke:

$$\frac{d}{d\xi}(C_4 u_g A) = \Phi_s \left(\frac{M_1}{M_4} k_3 C_1^{\,2} + \frac{M_2}{M_4} k_5 C_2 \right) A - \gamma C_4 u_g A \tag{5.14}$$

Steam:

$$\frac{d}{d\xi}(C_5 u_g A) = \frac{\dot{m}_{ge} l_e}{M_5} - \gamma C_5 u_g A \tag{5.15}$$

5.2 Intrinsic Correlations

In order to solve the governing equations, additional intrinsic correlations on the flow entrainment velocity, particle collision frequency and collision efficiency must be provided. Although the presence of particles and droplets in the jet flow does affect the flow entrainment, there is no simple correlation to quantify this effect. The equation of jet entrainment velocity in single-phase flows was used in this model, which was

proposed by Platten and Keffer (1968), as the first-order approximation. Hence, the flow entrainment velocity is estimated by

$$u_{Ge} = 0.06(u_g - u_{gbed}\cos\theta) + 0.3u_{gbed}(\cos\theta - \cos\theta_j) \tag{5.16}$$

A similar equation is extended to estimate the jet entrainment of particle phase so that

$$u_{se} = 0.06(u_s - u_{sbed}\cos\theta) + 0.3u_{sbed}(\cos\theta - \cos\theta_j) \tag{5.17}$$

Although the above entrainment velocity was originally obtained from the study of oblique jets, the extension of this equation to a co-current case reveals a close resembling of the equations directly derived from co-current jet studies, for example, $u_e = 0.026(u - u_\infty)$ from Rajaratnam (1976). For simplicity and generality of the mechanistic modeling, Equation (5.16) was adopted as a general one to cover all injection angles.

The mass of solids penetrated into the spray jet region is dependent on the ratio of environmental solids momentum perpendicular to the jet and the jet momentum

$$\dot{m}_{sp} = \alpha_{se}\rho_s u_{se}\exp\left(-\frac{\alpha_{se}\rho_{se}u_{se}^2\sin\theta}{\alpha_s\rho_s u_s^2 + \alpha_g\rho_g u_g^2 + a_d\rho_d u_d^2}\right) \tag{5.18}$$

The jet expansion rate can be expressed as a function of momentum ratio between ambient gas-solids fluidized bed and gas-droplet spray, which is written as

$$R = R_j + 0.11\left(1 + \frac{\alpha_{gbed}\rho_{gbed} + \alpha_{sbed}\rho_s}{\alpha_{gj}\rho_g + \alpha_{dj}\rho_d}\right)\xi \tag{5.19}$$

The drag forces of solids and droplet phases inside the spray jet region can be expressed as,

$$F_{Di} = n_i c_{di} \frac{\pi}{8} d_i^2 \rho_g \left|u_g - u_i\right| (u_g - u_i) \quad i = d, s \tag{5.20}$$

where

$$C_d = \begin{cases} \dfrac{24}{\mathrm{Re}} & \mathrm{Re} < 2 \\ \dfrac{18.5}{\mathrm{Re}^{0.6}} & 2 < \mathrm{Re} < 500 \\ 0.44 & 500 < \mathrm{Re} < 2\times10^5 \end{cases} \tag{5.21}$$

The *Re* in above equation is based on the relative velocity between gas and solids or droplet phase, respectively for solids and droplets drag forces.

Collision frequency among droplets and solid particles can be calculated by Fan and Zhu (1998)

$$f_{ds} = \eta_{co} n_d n_s \frac{\pi\left(d_s + d_d\right)^2}{4}\left|u_s - u_d\right| \tag{5.21}$$

where the collision efficiency, η_{co}, is given from an analytical approximation, which is derived based on the rigid sphere collisions in Stokesian flows (Zhu, 2000)

$$\eta_{co} = \left(1 + 34 \frac{d_d}{d_s} \frac{\rho}{\rho_s} \frac{1}{\mathrm{Re}_{sd}}\right)^{-2} \tag{5.22}$$

where Re_{pd} is the particle Reynolds number based on the relative velocity of particle and droplet.

The total reactive heat generation can be expressed as

$$E_R = -\sum_{i=1}^{5} r_i . \Delta H_i \tag{5.23}$$

where the minus sign in the right hand side represents the reactions are heat absorptive; r_i are the mass change rates due to chemical reactions, H_i are corresponding reaction heats.

Total convective heat received by a droplet can be obtained as

$$E_{cd} = n_d \pi d_d^2 h_d (T_g - T_d) A \tag{5.24}$$

where h_d is the convective heat transfer coefficient which can be obtained from

$$h_d = \frac{Nu_d K}{d_d} \tag{5.25}$$

in which

$$Nu_d = \frac{2 + 0.6 \mathrm{Re}_d^{*0.5} \mathrm{Pr}^{0.333}}{\left[1 + \frac{C_p (T - T_d)}{L}\right]^{0.7}} \tag{5.26}$$

where the relative Reynolds number of droplets in a gas-solids mixture is defined by

$$\mathrm{Re}_d^* = \frac{(\rho_d \alpha_d + \rho_g)(u_d - u_g)d_d}{\mu} \tag{5.27}$$

The convective heat transfer between gas and solids can be obtained by

$$E_{cs} = n_s \pi d_s^2 h_s (T_g - T_s) A \tag{5.28}$$

where

$$h_s = \frac{Nu_s K}{d_s} \tag{5.29}$$

and the Nusselt number for the heat transfer coefficient of a single particle can be expressed by the Ranz-Marshall equation

$$Nu_s = 2 + 0.6\,\mathrm{Re}_s^{0.5}\,\mathrm{Pr}^{0.333} \tag{5.30}$$

5.3 Problem Closure

The linkage among the mole concentrations of components in gas phase obtained from reaction equations and the gas density can be written based on the ideal gas law, which gives

$$\rho_g = \frac{P}{RT_g} \frac{\sum_{i=1}^{5} (C_i . M_i)}{\sum_{i=1}^{5} C_i} \tag{5.31}$$

Another additional equation which is used to make the problem closed is the volumetric relationship among gas-solids-droplet phases, which is

$$\alpha_s + \alpha_g + \alpha_d = 1 \tag{5.32}$$

So far there are 17 coupled independent equations (equation 5.1 - 5.15, 5.31, 5.32) for solving 17 independent variables (θ, u_g, α_g, T_g, u_d, α_d, T_d, u_s, α_s, T_s, C_1, C_2, C_3, C_4, C_5, ρ_g, γ). The problem in principle is closed. Hence, with the given or presumed cross-sectional distributions for variables of interest, the coupled differential equations become solvable.

5.4 Results and Discussion

The model can be used to predict the hydrodynamic characteristics of evaporative and reactive gas-droplet spray jet into hot gas-solids riser reactor. The predicted parameters can be classified into three catalogues, i.e. 1) jet properties such as jet penetration length, trajectory and spray angle; 2) hydrodynamics in spray region include the velocities, volume fractions, temperatures of gas, solids and droplet phases; 3) reactant characteristics such as the mole and mass concentrations of each component of the gas phase.

In this section, a calculation example is provided and its results are analyzed and discussed. The calculation uses the typical working parameters for the real FCC unit. The major input parameters are listed in Table 5.1.

Table 5.1 Major Input Parameters

Name	Symbol	Unit	Value
Gas velocity	u_g	m/s	53
Droplet volume fraction	α_d	-	0.11
Droplet velocity	u_d	m/s	53
Droplet size	d_d	μm	300
Droplet density	ρ_d	kg/m^3	900
Nozzle radius	R_J	Inch	0.5
Droplet temperature	T_d	K	350
Jet penetration angle	θ	o	30
Bed steam velocity	u_{gbed}	m/s	5.726
Fluidized bed solids volume fraction	α_{sbed}	-	0.4
Bed solids velocity	u_{sbed}	m/s	1
Solids density	ρ_s	Kg/m^3	1400
Solids size	d_s	μm	75
Bed temperature	T_{bed}	K	715
Droplet saturated temperature	T_{dd}	K	425
Droplet latent heat	L	J/kg	220160
Gas thermal conductivity	K	w/m·K	0.0415
Gas viscosity	μ_g		5e-5
Gas thermal capacity	C_{pg}	J/kg·K	2250
Droplet thermal capacity	C_{pd}	J/kg·K	2093
Solids thermal capacity	C_{ps}	J/kg·K	1214
Crude oil molecular weight	M_1	Kg/Kmol	280
Gasoline molecular weight	M_2	Kg/Kmol	108
Light gases molecular weight	M_3	Kg/Kmol	28
Coke molecular weight	M_4	Kg/Kmol	32
Steam molecular weight	M_5	Kg/Kmol	18

Figure 5.3 shows the spray jet trajectory when the feed reactant sprayed into the bottom of the riser reactor with an initial jet angle of 30°. During its penetration, the jet continuously bends towards the downstream direction of ambient gas-solids riser flow due to convective momentum transfer by the ambient gas-solids riser flow. When it reaches to the end of its penetration, where the droplet mass flow rate close to zero, the jet direction nearly reaches to the riser axial direction.

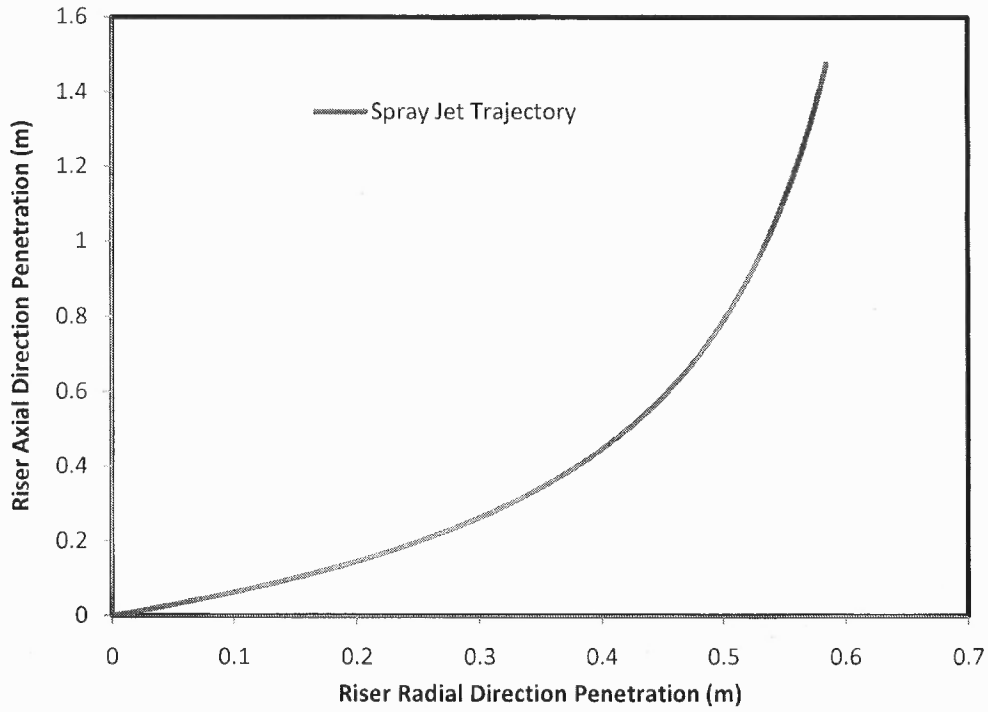

Figure 5.3 Spray jet trajectory in fluidized bed.

Figure 5.4-5.6 represents the hydrodynamic characteristics of spray jet, which include the temperatures, volume fractions and velocities of gas, solids and droplet phases. Figure 5.4 shows the temperature profiles of gas, solids and droplet phases along the trajectory of the spray jet. It can be seen that the droplet temperature keeps at its saturated temperature except for the initial stage of the jet spray. This is due to the

intensive heat transfer among the phases. Before the droplet reaches to its saturated temperature, part of the heat absorbed by it is used for the heating up effect. When it reaches to the saturated temperature, all the heat absorbed will be adopted for the evaporation. The gas temperature continuously increases until the equilibrium between gas and solids phases are established. During the course, the temperature of solids phase decreases due to intensive heat transfer to gas phase for the chemical reaction and droplet phase for the evaporation.

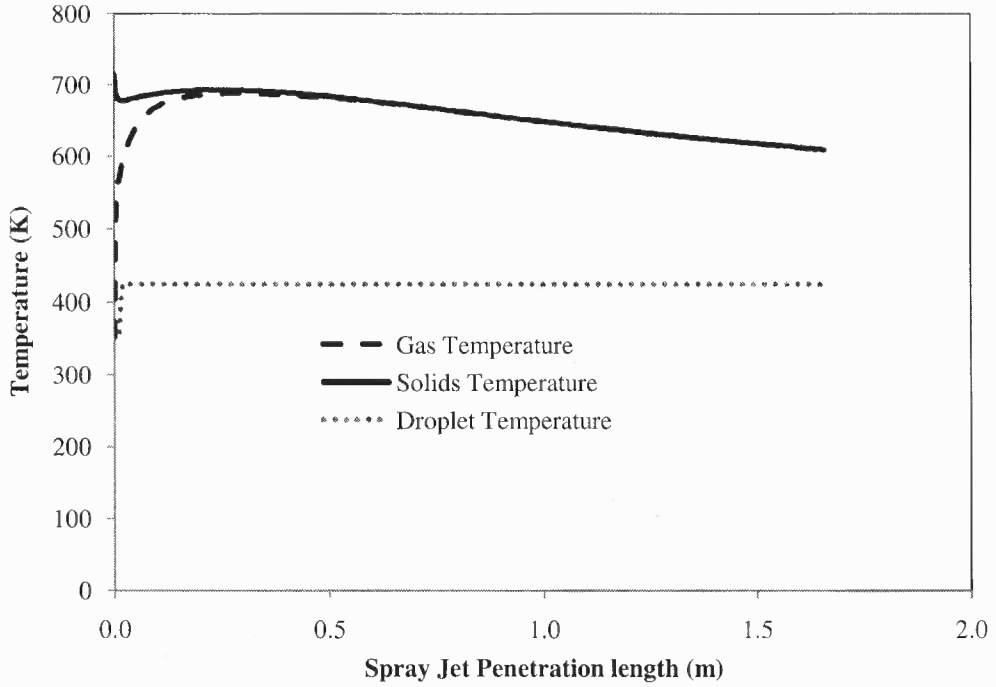

Figure 5.4 Temperatures of phases in spray region.

The velocity profiles for the phases are shown in Figure 5.5. With the gas-solids entrainment from the ambient fluidized bed, the velocities are keeping decreasing along the trajectory. Due to the fricitional drag force and chemical reaction, the momentum of gas phase is transferred to the added gas and solids rapidly. Thus, the velocity of the gas decreases much faster than that of droplet, while it is always larger than the solids

velocity. The droplet velocity shall also decrease due to the drag with gas phase and collisional momentum transfer with solids phase.

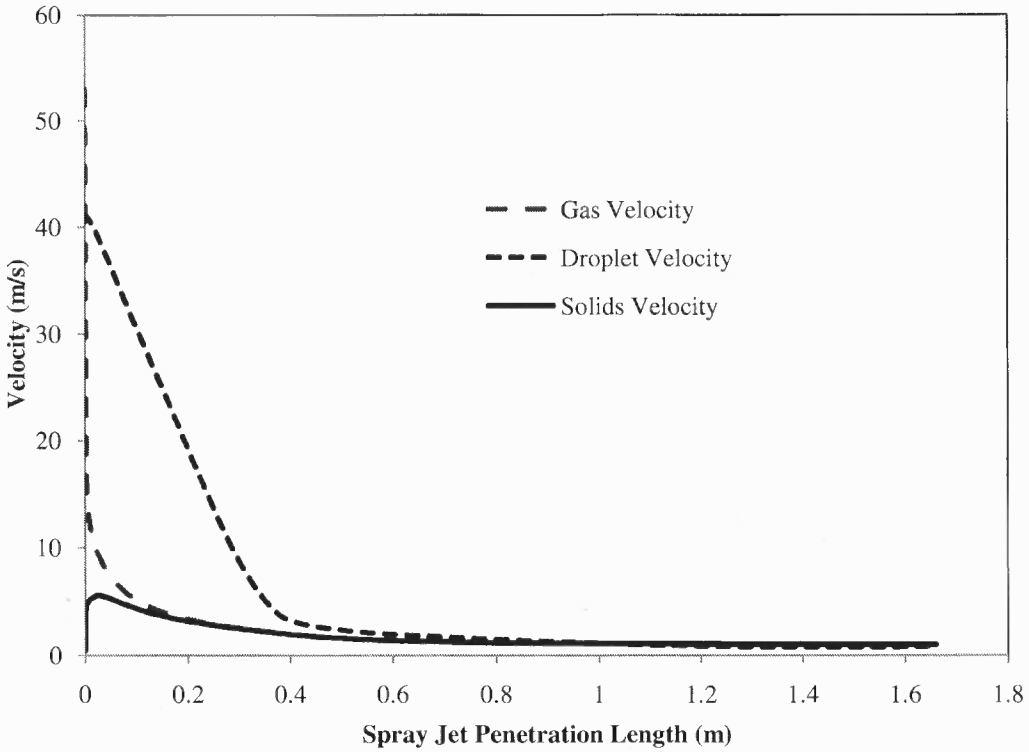

Figure 5.5 Velocity profiles in spray region.

Figure 5.6 gives the volume fractions of phases along the spray trajectory. With the intensive evaporation and jet expansion, the volume fraction of droplet phase decreases dramatically along the spray trajectory. During the course, the solids volume fraction increases with the continuous entrainment and diffusive penetration across the jet boundary. The gas volume friction changes with the gas entrainment and chemical cracking of the reactant.

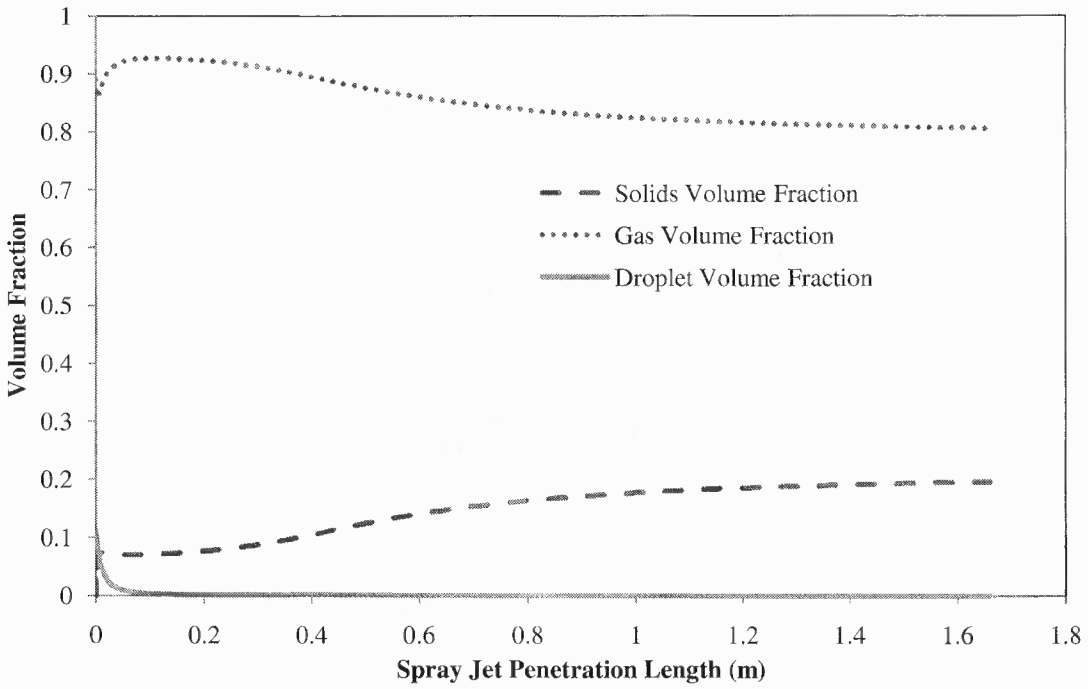

Figure 5.6 Volume fractions of phases in spray region.

Along the spray trajectory, the content of the gas phase keeps changing. At the beginning of the spray jet, all the gas phase consists of the steam which served as carried gas of the spray jet. The concentration of crude oil increases dramatically with the continuous evaporation of droplets. During the course, the steam concentration tends to decrease due to dilution effect. As long as there is vapor occurs, the chemical reactions take place, thus the components of gasoline, light gases and coke appear. With the spray penetration, the concentrations of components keep changing. Near the end of the jet, the gasoline takes an important portion of the vapor phase, while the concentrations of light gases and coke keep in a lower level. The concentrations of these reactants will directly influence the content of gas phase at the inlet of the downstream riser flow. The hydrodynamic and chemical reaction characteristics at the end of the jet shall be further analyzed and translated as the inlet condition of the models for downstream riser reactor.

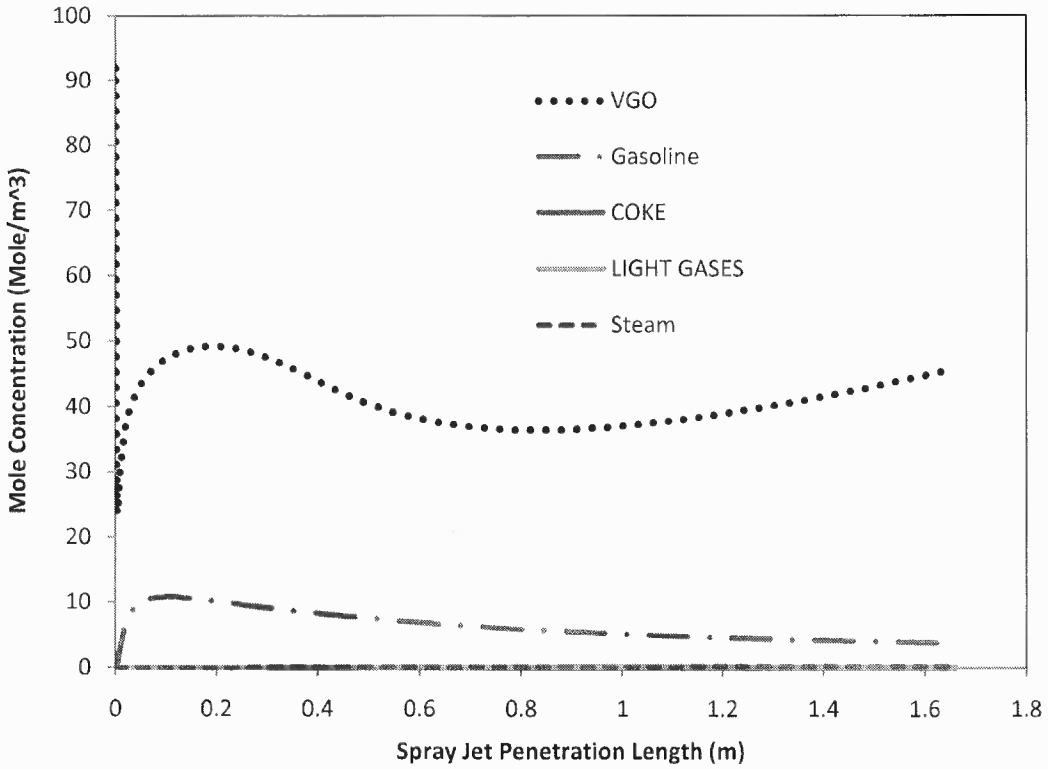

Figure 5.7 Mass concentrations of components of gas phase in spray region.

5.5 Conclusion

To investigate the characteristics of spray of feed reactant into the bottom of riser reactor, the hydrodynamics, evaporation process and chemical reaction mechanisms are modeled in this chapter. The characteristics of spray jet of feed reactant into bottom of riser are investigated by a modeling approach that couples the hydrodynamics of spray jet with its reaction characteristics. The profiles of spray jet, including the velocities, volume fractions, temperatures as well as gas species along the spray jet trajectory are obtained and analyzed.

CHAPTER 6

SUMMARY AND PROPOSED FUTURE STUDY

6.1 Summary

This dissertation is aimed at the development of mechanism-based parametric model that yields reliable prediction in transport and reaction characteristics in general catalytic riser reactors. The study was developed with three integrated parts: 1) governing mechanisms and modeling of gas-solids transport in a riser; 2) coupling mechanisms between hydrodynamics and catalytic reactions in riser reactors; 3) modeling of reaction in the spray mixing and vaporization process.

On the hydrodynamic modeling part, we discovered several new control mechanisms that govern the gas-solids transport in riser reactors. The role of inter-particle collision on the kinetic energy dissipation and solids acceleration were analyzed. An additional force due to inter-solids collision in the acceleration regime was added to the momentum equation of solids. The new developed model successfully predicted the axial profiles of transport properties throughout the entire transport domain, including dense phase, acceleration, and dilute phase regimes. To further explore the flow heterogeneity in both radial and axial directions, an integral-differential hydrodynamics model with a general third-order polynomial across any riser cross-sections has been developed. The model not only predicts the radial and axial phase transport but also yields the much-needed information of the wall boundary layer and backflow mixing for the popular core-annulus models.

The coupling mechanisms of hydrodynamics and catalytic reaction were established. A new correlation has been proposed to link the local reaction rate to the local transport properties (such as concentrations of catalyst and reactants, reaction temperature, and transport velocities). The resulted model not only predicts the correct reaction characteristics against the plant data but also demonstrates the feasibility of adopting the same reaction properties of the same type of catalytic reactions in different riser reactors.

The coupling of hydrodynamics and catalytic reaction has also been extended to investigate the catalytic reaction in the spray region. The resulted changes in transport properties provide the inlet conditions for the follow-up reactions in the riser reactor.

The major contributions and findings on the hydrodynamic modeling of gas-solids riser flow are:

1) The formulation of frictional drag force was re-formulated and corrected based on the mechanisms of gas-solids inter-phase interaction;
2) The role of inter-particle collision on the kinetic energy dissipation and solids acceleration was analyzed. The newly-found collisional force was added into solids momentum equation;
3) The model is able to correctly predict the pressure gradient and solids volume friction simultaneously;
4) Proposed a continuous approach to simulate the radial heterogeneity of gas-solids riser flow;
5) The model successfully predicts the profiles of phase transport in both radial and axial directions;

6) The model can yield generic information on the wall boundary layer and backflow mixing instead of empirical correlations.

The major contributions and findings on the coupling of hydrodynamics and reactions in the riser reactor are:

1) Established a coupling model between hydrodynamics and chemical reaction;
2) Developed new mechanisms to link the local reaction rate to the local transport properties;
3) Predicted the correct reaction characteristics against the plant data;
4) Demonstrated the feasibility of adopting the same reaction properties of the same type of catalytic reactions in different riser reactors.

The major contributions and findings on the modeling of reaction in the spray mixing and vaporization process are:

1) Established a coupling model among spray evaporation, vapor-catalyst mixing and chemical reaction;
2) Yielded predictions for both hydrodynamic and chemical reaction characteristics;
3) Yielded realistic inlet condition for riser reactor;
4) Demonstrated the impact of chemical reaction in spray region on the performance of the riser reactor.

6.2 Suggested Future Study

The research on the transport mechanisms of riser reactors is far from completion for characteristics in both main transport region and spray region. Here, several research topics are suggested to further understand the mechanisms of the riser reactor.

(1) Coupling of reaction and hydrodynamics in wall region of riser

As we stated in chapter 4, the hydrodynamics and chemical reaction characteristics in the core and annulus regions of the riser reactor are totally different and closely coupled. The fully understanding of the transport of riser reactor needs the information of both regions. In the present model, only the characteristics in the core upward flow region are investigated with the linkage to wall region with wall thickness and back-mixing ratio. While, the hydrodynamics and chemical reactions in wall region are not yet revealed.

In the wall region, the solids are moving downwards with a relatively higher volume fraction. Most catalyst particles in this region are spent particles with decreased catalytic activities. Its chemical reaction intensity shall be less than that in the core region. This non-equilibrium in turn will cause intensive mass, momentum and energy transfers between these two regions. A detailed investigation on the characteristics in wall region shall be built up on the coupling of chemical reaction and hydrodynamics in this region. The mass, momentum and energy transfers with core region shall be based on the characteristics of both region and shall be balanced accordingly.

(2) Multiple jet overlapping in confined riser bottom region

In the real industry, the feed reactants are normally feed into the reactor from multiple nozzles around the riser diameter. Sometimes, there are multiple layers of nozzles distributed along the riser axial direction. When multiple jets sprayed into the confined

region, the available space, solids particles, thermal energy are extremely limited. Thus, the profiles and characteristics of each spray may alter very much. This in turn, will cause the big difference at the end of the spray region. The overlapping effect would not be a simply adding effect.

For the space overlapping, a possible way is to consider the boundaries among the jets as a mirror which makes the mass flow bounces back to its original region. The other available solids and thermal energy may be modeled using coefficients due to overlapping effects.

(3) Multiple droplet size and velocity distribution from nozzle

Another challenge in investigating the spray characteristics is that the gas-droplet flow from complex industrial nozzles is always not uniform. There is always a wide range of droplet size distribution and velocity distribution across the cross-section of the jet from nozzle. A further investigation on this topic may be based on the grouping methodology which divides the nozzle cross-section into multiply sub-regions in each of which the droplet size and velocity are treated as uniform.

REFERENCES

1. U. Arena, A. Cammarota, L. Pistone, High Velocity Fluidization Behavior of Solids in a Laboratory Scale Circulating Bed. Circulating Fluidized Bed Technol., Halifax, Nova Scotia, Canada, 1985.
2. Ariyapadi, S., Holdsworth, D.W., Norley, C.J.D., Berruti, F., Briens, C., Digital X-ray imaging technique to study the horizontal injection of gas–liquid jets into fluidized beds. International Journal of Chemical Reactor Engineering 1, A56, 2003a.
3. Ariyapadi, S., Berruti, F., Briens, C., Griffith, P., Hulet, C., Modeling the injection of gas–liquid jets into fluidized beds of fine particles. Canadian Journal of Chemical Engineering 81,pp. 891–899, 2003b.
4. Siva Ariyapadi, Franco Berruti, Cedric Briens, Jennifer McMillan, David Zhou, Horizontal Penetration of Gas-Liquid Spray jets in Gas-Solid Fluidized Beds, 2004.
5. Siva Ariyapadi, Jennifer McMillan, David Zhou, Franco Berruti, Cedric Briens, Edward Chan, Modeling the mixing of a gas-liquid spray jet injected in a gas-solid fluidized bed: The effect of the draft tube. Chemical Engineering Science 2005, pp. 5738-5750, 2005.
6. R. Bader, J. Findlay, T.M. Knwlton, Gas-solid flow patterns in a 30.5 cm diameter circulating fluidized bed, in: P. Basu, J.F. Large (Ed.). Circulating Fluidized Bed Technology, vol. II, Pergamon Press, New York, pp. 123-137, 1988.
7. Becher RD, Schlu¨nder EU. Fluidized bed granulation: Gas flow, particle motion and moisture distribution. Chem. Eng. Process., 36, pp. 261-269, 1997.
8. Benjelloun, F., R. Liegeois and J. Vanderschuren, Penetration Length of Horizontal Gas Jets into Atmospheric Fluidized Beds in "Proc. Fluidization-VIII". J-F. Large and C. Laguerie, Eds., Engineering Foundation, N.Y. , pp. 239–246, 1995.
9. Berry, T., McKeen, T., Pugsley, T., Dalai, A., Two-dimensional reaction engineering model of the riser section of a fluid catalytic cracking unit. Indus. & Eng. Chemistry Research, 43, pp. 5571-5581, 2004.
10. Buchanan, J.S., Analysis of heating and vaporization of feed droplet in fluidized catalytic cracking risers. Indus. & Eng. Chemistry Research, 33, pp. 3104-3111, 1994.
11. W. Büssing, and L. Reh, On viscous momentum transfer by solids in gas–solids flow through risers, Chemical Engineering Science, 56, pp. 3803–3813, 2001.
12. Cleaver, M. Ghadiri, V. G. Tuponogov, J. G. Yates and D. J. Cheesman, Measurement of Jet Angles in Fluidized Beds. Powder Technol. 85, pp. 221–226, 1995.
13. Matthew Dawe, Deric Briens and Franco Berruti, study of horizontal sonic gas jets in gas-solid fluidized beds. The Canadian Journal of Chemical Engineering, Volume 86, pp. 506-513, 2008.

14. B. Du, W. Warsito and L.S. Fan, ECT studies of the choking phenomenon in a gas-solid circulating fluidized bed. AIChE J., 50(7), pp.1387, 2004.

15. Farag, H., Gianetto, A., Blasetti, A., de Lasa, H., FCC catalyst for reformulated gasolines. Kinetic modeling. Indust. & Eng. Chemistry Res., 33,pp. 3053, 1994.

16. Fan, L. S., Zhu, C., Principles of Gas-Solids flow, Cambridge University press, 1998.

17. Fan LS, Lau R, Zhu C, Voung K, Warsito W, Wang X, Liu G., Evaporative liquid jets in gas–liquid–solid flow system. Chem. Eng. Sci. 56, pp. 5871-5891, 2001.

18. Filla, M., L. Massimilla and S. Vaccaro, Gas Jets in Fluidized Beds: The Influence of Particle Size, Shape and Density on Gas and Solids Entrainment. Int. J. Multiphase Flow 9, pp. 259–267, 1983.

19. Felli, V., Solids entrainment from a fluidized bed into a gas–liquid jet: effect of the draft tube. Master's Thesis, The University of Western Ontario, London, Ontario, Canada, 2002.

20. Gao, J., Xu, C., Lin, S., Yang, G., Simulation of gas–Liquid–solid 3 phase flow and reaction in FCC Riser Reactors. AIChE. Journal,47, pp. 677- 692, 2001.

21. D. Geldart, M. J. Rhodes, From minimum fluidization to pneumatic transport: a critical review of the hydrodynamics, in: P. Basu (Ed.). Circulating Fluidized Bed Technology, Pergamon Press, Oxford, pp. 193-200,1986.

22. Gu W, Tuzla K, Chen J. C., Measurement of liquid spray evaporation in fast fluidized beds. AIChE Symp. Ser. 92, pp. 153-154, 1996.

23. A.T. Harris, R.B. Thorpe, J.F. Davidson, Characterization of the annular film thickness in circulating fluidized-bed risers. Chemical Engineering Science, 57, pp. 2579-2587, 2002.

24. B. Herb, S. Dou, K. Tuzla, & J.C. Chen, Solid mass fluxes in circulating fluidized beds. Powder Technology, 70, pp. 197-205, 1992.

25. Y. He and V. Rudolph, The volume-average voidage in the riser of a circulating fluidized bed. Powder Technology, 89, pp.79-82, 1996.

26. Heinrich S, Mo¨rl L. Fluidized bed spray granulation—A new model for the description of particle wetting and of temperature and concentration distribution. Chem. Eng. Process, 38, 635-663, 1999.

27. Hinze, J. O., Turbulence. McGraw-Hill, New York, 1975.

28. Hong, R., H. Li, H. Li and Y. Wang, Studies on Inclined Jet Penetration Length in a Gas-Solid Fluidized Bed. Powder Technology 92, pp. 205–212 , 1997.

29. Jacob, S. M., Gross, B., Voltz, S. E., & Weekman, V. W., A lumping and reaction scheme for catalytic cracking. AIChE J. 22, pp. 701-713, 1976.

30. D. S.J. Jones and P. P. Pujado, Handbook of Petroleum Processing , Springer, 2006.

31. A. Johansson, F. Johnsson, B. Leckner, Solids back-mixing in CFB boilers. Chemical Engineering Science, 62, pp. 561-573, 2007.

32. S.W. Kim, G. Kirbas, H. Bi, C.J. Lim, J.R. Grace, Flow structure and thickness of annular downflow layer in a circulating fluidized bed riser. Powder Technology, 142, pp. 48-58, 2004.

33. T.M. Knowlton, Modeling benchmark exercise. Workshop at the eighth engineering foundation conference on fluidization, Tours, France, 1995.

34. Guangliang Liu, Evaporating crossflow sprays in gas-solid flows. PhD thesis, New Jersey Institute of Technology, 2003.

35. M. Louge and H. Chang, Pressure and voidage gradients in vertical gas-solid risers. Powder Technology, 60, pp. 197-201, 1990.

36. M.Y. Louge , E. Mastorakos and J.T, Jenkins, The role of particle collisions pneumatic transport, J. Fluid Mechanics, 231, pp.345-359, 1991.

37. Maronga SJ, Wnukowski P., Establishing temperature and humidity profiles in fluidized bed particulate coating. Powder Technology, 94, pp. 181-185, 1997.

38. Merry, J.M.D., Penetration of horizontal gas jet into a fluidized bed. Transactions of the Institute of Chemical Engineers, 49, 1971.

39. Merry, J. M. D., Penetration of Vertical Jets into Fluidized Beds. AIChE J. 21, pp. 507–510, 1975.

40. A. Miller and D. Gidaspow, Dense, vertical gas-solid flow in a pipe. AIChE J., 38, pp.1801, 1992.

41. Musmarra, D., Influence of Particle Size and Density on the Jet Penetration Length in Gas Fluidized Beds. Ind. Eng. Chem. Res. 39, pp. 2612–2617, 2000.

42. Newton D, Fiorentino M, Smith GB., The application of X-ray imaging to the develop-ments of fluidized bed processes. Powder Technology, 120, pp. 70-75, 2001.

43. G.S. Patience, J. Chaoki, Gas phase hydrodynamics in the riser of a circulating fluidized bed. Chemical Engineering Science, 48, pp. 3195-3205, 1993.

44. Pitault, I., Nevicato, D., Blasetti, A. P., Delasa, H. I., Fluid catalytic cracking catalyst for reformulated gasolines-kinetic modeling. Ind. & Eng. Chem. Res, 33, pp. 3053-3062, 1994.

45. M. M. Rafique Qureshi, Flow characteristics and phase interactions of evaporating sprays in gas-solid suspensions. PhD thesis, New Jersey Institute of Technology, 2006.

46. T. S. Pugsley and F. Berruti, A predictive hydrodynamic model for circulating fluidized bed risers. Powder Technology, 89, pp.57-69, 1996.

47. M.J. Rhodes, P. Laussman, Characterizing non uniformities in gas-particle flow in the riser of a circulating fluidized bed. Powder Technology, 72, pp. 277-284, 1992.

48. J. F. Richardson and W. N. Zaki, Sedimentation and fluidisation part I. Trans. Inst. Chem. Eng., 32, pp. 35-53, 1954.

49. Rader, Mari Lyn, Worldwide Refining. Oil & Gas Journal, pp.52, 1996.

50. A. Rautiainen, G. Stewart, V. Poikolainen, P. Sarkomaa, An experimental study of vertical pneumatic conveying. Powder Technology, 104, pp.139-150, 1999.

51. Roach, P. E., The Penetration of Jets into Fluidized Beds. Fluid Dyn. Res., 11, 197–216, 1993.

52. Reza Sadeghbeigi, Fluid Catalytic Cracking Handbook, Gulf Publishing Company, Houston, Taxas, 2002.

53. H. Sabbaghan, R.S.Gharebagh and N.Mostoufi, Modeling the acceleration zone in the riser of circulating fluidized beds. Powder Technology, 142, pp.129-135, 2004.

54. P. Schlichthaerle, and J.Werther, Axial pressure profiles and solids concentration distribustions in the CFB bottom zone. Chemical Engineering Science, 54, pp. 5485-5493, 1999.

55. Skouby DC., Hydrodynamic studies in a 0.45-m riser with liquid feed injection. AIChE Symp. Ser. 95, pp. 67-70, 1995.

56. Smith PG, Nienow AW. On atomizing a liquid into a gas fluidized bed. Chem. Eng. Sci. 1982;37:954-956.

57. J. G. Speight , The Chemistry and Technol. of Petroleum (4th ed.). CRC Press, 2006.

58. Vaccaro, S., D. Musmarra and M. Petrecca, Evaluation of the Jet Penetration Depth in Gas-Fluidized Beds by Pressure Signal Analysis. Int. J. Multiphase Flow, 23, pp. 683–698 , 1997.

59. Vaccaro, S., Analysis of the Variables Controlling Gas Jet Expansion Angles in Fluidized Beds. Powder Technology, 92, pp. 213–222, 1997.

60. Xiaohua Wang, Concurrent Evaporating Spray Jets in Dilute Gas-Solid Pipe Flows, PhD thesis, New Jersey Institute of Technology, 2002.

61. Weekman, V. W., Nace, D. M., Kinetics of catalytic cracking selectivity in fixed, moving, and fluid bed reactors. AIChE J. 16 (3), pp. 3397-3404, 1970.

62. J. Werther, Fluid mechanics of large scale CFB units In: M. Kwauk & L. Jinghai (Eds.). Circulating Fluidized Bed Technology V, pp. 1-14, 1994.

63. Yates, J. G., S. S. Cobbinah, D. J. Cheesman and S. P. Jordan, Particle Attrition in Fluidized Beds Containing Opposing Jets. AIChE Symp. Ser., 281, pp. 13–19, 1988.

64. Jun You, Heterogeneous flow structure and gas-solid transport of riser. PhD thesis, New Jersey Institute of Technology, 2009.

65. Jun You, Chao Zhu, Bing Du and Liang-Shih Fan, Heterogeneous structure in Gas-Solid Riser Flow. AIChe Journal, 1460, pp. 1459-1469, 2008.

66. B. Zhou, H. Li, Y. Xia & X. Ma, Cluster structure in a circulating fluidized bed. Powder Technology, 78, pp. 173-178, 1994.

67. Zhu C, Wang X, Fan LS., Effect of solids concentration on evaporative liquid jets in gas–solid flows. Powder Technology, 111, pp. 79-82, 2000.

68. C. Zhu, S.-C. Liang, L.-S. Fan, Particle wake effects on the drag force of an interactive particle. Int. J. Multiphase Flow, 20, pp. 117-129, 1994.

69. Chao Zhu, J. You, An energy-based model of gas-solid transport in a riser, Powder Technology, 175, pp. 33-42, 2007.